

2017

Investigation of CO₂ Sequestration for the Assessment of the Impact on Resource Storage with Co-production of Brine

Mohammad Junaid Ashfaq

Follow this and additional works at: <https://researchrepository.wvu.edu/etd>

Recommended Citation

Ashfaq, Mohammad Junaid, "Investigation of CO₂ Sequestration for the Assessment of the Impact on Resource Storage with Co-production of Brine" (2017). *Graduate Theses, Dissertations, and Problem Reports*. 5127.

<https://researchrepository.wvu.edu/etd/5127>

This Thesis is protected by copyright and/or related rights. It has been brought to you by the The Research Repository @ WVU with permission from the rights-holder(s). You are free to use this Thesis in any way that is permitted by the copyright and related rights legislation that applies to your use. For other uses you must obtain permission from the rights-holder(s) directly, unless additional rights are indicated by a Creative Commons license in the record and/ or on the work itself. This Thesis has been accepted for inclusion in WVU Graduate Theses, Dissertations, and Problem Reports collection by an authorized administrator of The Research Repository @ WVU. For more information, please contact researchrepository@mail.wvu.edu.

Investigation of CO₂ Sequestration for the Assessment of the Impact on Resource Storage with Co-production of Brine

Mohammad Junaid Ashfaq

Master's Thesis submitted
to the Statler College of Engineering and Mineral Resources
at West Virginia University

in partial fulfillment of the requirements for the degree of

Master of Science in
Petroleum and Natural Gas Engineering

Sam Ameri, M.S., Chair
Huseyin Ilkin Bilgesu, Ph.D.
Kashy Aminian, Ph.D.

Department of Petroleum and Natural Gas Engineering

Morgantown, West Virginia
2017

Keywords: CO₂, Sequestration, Brine, Aquifer, Mt. Simon, storage
Copyright 2017 Mohammad Junaid Ashfaq

ABSTRACT

Investigation of CO₂ Sequestration for the Assessment of the Impact on Resource Storage with Co-production of Brine

Mohammad Junaid Ashfaq

In order to reduce Green House Gases, Carbon-dioxide (CO₂) storage in deep saline aquifers is a viable commercial application for minimizing emissions. It is important to understand surface area needed to predict large scale CO₂ storage while fully utilizing injection capacity. This study presents results from varying Injection pressure and well spacing to find minimal-effective well spacing required to store CO₂. The study shows pressure management to manipulate hydrodynamic behavior of CO₂ in saline formations system. In conjunction, understanding the interplay of CO₂ dissolution, buoyancy flow, and capillary forces in regulating the behavior of the injected CO₂ plume are important. Pressure manipulated by changing injection pressure with selected brine co-production, a technique known as CO₂ sequestration.

A 3-D reservoir model has been utilized to model CO₂ sequestration behavior in a compositional simulator, CMG Builder. Mount Simon Sandstone (Cambrian) was selected as a 'base case model' for its recognition as an important deep saline reservoir with potential to serve as a largescale commercial CO₂ storage field in the Midwestern United States.

The study shows the impact of selected injection pressure on the utilization of brine aquifer. It is recommended to store CO₂ with 4000 – 4500 psi injection pressure range for optimum storage and production conditions.

Dedication

I want to dedicate this to my wife, parents, and siblings. I have been attending this school since 2005 and masters since 2010, and after the grace of Allah this accomplishment would not have been possible without my parents' support, in conjunction with wife and siblings. They are the only love and motivation in my life. I must express my very profound gratitude to my family for providing me with unfailing support and continuous encouragement throughout my years of study and through the process of researching and writing this thesis. Also, I want to appreciate my professors for not giving up on me, and for going out of your way to help me countless times over the decade.

Acknowledgements

I would like to thank the experts from National Energy Technology Laboratory and West Virginia University who were involved in developing the idea for this research project. Without their participation and input, this study could not have been successfully conducted. This research was supported/partially supported by West Virginia University, and Computer Modeling Group Ltd.

Table of Contents

| | | |
|-------|---|----|
| 1 | Introduction | 1 |
| 1.1 | Climate Change | 1 |
| 1.1.1 | Extreme Weather..... | 7 |
| 1.1.2 | CO ₂ in atmosphere | 8 |
| 1.1.3 | Carbon and Other Biogeochemical Cycles | 13 |
| 1.1.4 | Is CO ₂ a driver of Climate Change? | 15 |
| 1.1.5 | CO ₂ and Power plants in US | 17 |
| 1.2 | Reducing Emissions by Carbon dioxide (CO ₂) capture and sequestration (CCS) 19 | |
| 1.3 | CO ₂ sequestration application in limited space | 22 |
| 2 | Literature Review | 24 |
| 2.1 | CO ₂ plume monitoring technologies | 24 |
| 2.2 | CO ₂ absorption reduces pressure buildup..... | 25 |
| 2.3 | Long term CO ₂ storage possibility | 26 |
| 2.4 | Pressure management scheme mitigated for large scale pressure build up | 26 |
| 2.5 | Maximum injection capacity | 28 |
| 2.6 | Modelling CO ₂ plume behavior..... | 30 |
| 2.7 | Using modeling to verify feasibility of CO ₂ Storage | 30 |
| 2.8 | Mt. Simon Sandstone for CO ₂ storage | 31 |
| 2.9 | Application for a Power Plant | 35 |
| 2.9.1 | Handling Produced Brine..... | 36 |
| 2.9.2 | Permitting availability & costs and tax relief..... | 36 |
| 2.9.3 | Handling of CO ₂ | 37 |
| 2.10 | CO ₂ Behavior and it's Formulation | 37 |

| | | |
|--------|--|----|
| 2.10.1 | Brine & CO ₂ solubility behavior | 37 |
| 2.10.2 | Structural trapping | 39 |
| 2.10.3 | Residual Gas Trapping..... | 40 |
| 2.10.4 | Chemical reactions..... | 41 |
| 2.11 | Comparison with other studies..... | 43 |
| 3 | Objective:..... | 44 |
| 4 | Methodology | 46 |
| 4.1 | Model Design | 46 |
| 4.2 | Grid description | 46 |
| 4.3 | Description of the reservoir characteristics | 47 |
| 4.4 | Well location selections | 49 |
| 4.4.1 | Vertical location | 49 |
| 4.4.2 | Optimizing well location horizontally | 49 |
| 4.5 | Injection Pressures..... | 50 |
| 4.6 | Local Production Management..... | 50 |
| 5 | Discussion of Results | 52 |
| 5.1 | Run #1 | 53 |
| 5.2 | Run #2 | 54 |
| 5.3 | Run #3 | 54 |
| 5.4 | Run #4 | 56 |
| 5.5 | Run #5 | 57 |
| 5.6 | Run #6 | 58 |
| 5.7 | Run #7 | 59 |
| 5.8 | Run #8 | 60 |
| 5.9 | Run #9 | 61 |

| | | |
|------|-----------------------------|----|
| 5.10 | Run #10 | 62 |
| 5.11 | Run #11 | 63 |
| 5.12 | Run #12 | 64 |
| 5.13 | Run #13 | 65 |
| 5.14 | Run #14 | 66 |
| 5.15 | Run #15 | 67 |
| 5.16 | Run #16 | 68 |
| 5.17 | Run #17 | 69 |
| 5.18 | Run #18 | 70 |
| 5.19 | Run #19 | 71 |
| 5.20 | Additional discussion | 72 |
| 5.21 | Summary of results | 74 |
| 6 | Conclusions | 75 |
| 7 | References | 75 |

List of Tables

| | |
|---|----|
| Table 1 - Reservoir Characteristics | 48 |
| Table 2 - Summary of Runs | 52 |
| Table 3 – Optimum results for injection pressure used in this study | 75 |

List of Figures

| | |
|---|----|
| Figure 1 - Indicators for decrease in values for global warming (IPCC, 2013) | 2 |
| Figure 2 - Indicators for increase in values for global warming (IPCC, 2013)..... | 3 |
| Figure 3 - Global heat content consensus (IPCC, 2013)..... | 4 |
| Figure 4 - Heat's impact on Earth (IPCC, 2013) | 4 |
| Figure 5 - Observed Global Temperature Change (IPCC, 2013) | 6 |
| Figure 6 - Observed Global Precipitation Change (IPCC, 2013) | 7 |
| Figure 7 - Phenomenon and direction of trend (IPCC, 2013) | 8 |
| Figure 8 - Full Mauna Loa CO ₂ record (IPCC, 2013)..... | 9 |
| Figure 9 - NOAA/ESRL/GMD CCGG cooperative air sampling network (NOAA, 2015) | 10 |
| Figure 10 - Recent global CO ₂ Average (IPCC, 2013) | 10 |
| Figure 11 - CO ₂ in Air and Ocean (IPCC, 2013)..... | 12 |
| Figure 12 - Total Anthropogenic CO ₂ Emissions (IPCC, 2013) | 14 |
| Figure 13 - Radiative force by emissions and drivers (IPCC, 2013)..... | 16 |
| Figure 14 - CO ₂ Capture & Extraction Facilities and Sources (Environmental Protection Agency, 2011) | 20 |
| Figure 15 - Geologic Storage Potential in the United States (Environmental Protection Agency, 2015) | 21 |
| Figure 16 - National Mortality Effects from Existing Power plants (Clean Air Task Force, 2010) | 22 |
| Figure 17 - US Power Plant CO ₂ Emissions (Huttenbach, 2009) | 23 |
| Figure 18 - Life cycle of a storage project and monitoring requirements (Office Fossil Energy, Dept of Energy) | 24 |
| Figure 19 - Example of CO ₂ Plume in Brine Aquifer (Water Saturation) (Agarwal & Zhang, 2014)..... | 28 |
| Figure 20 - Bounded vs Open Reservoir (Anchliya, 2009) | 29 |
| Figure 21 - Mount Simon Aquifer - Contour Map (U.S. Geological Survey, 2009) | 33 |
| Figure 22 - Contour map showing dissolved-solids concentrations of St. Peter-Prairie du Chien-Jordan Aquifer (U.S. Geological Survey, 2009) | 34 |
| Figure 23 - Gas Saturation vs. Gas Relative Permeability (Shen et al. 2015)..... | 41 |
| Figure 24 - 3D Grid used in the model | 47 |

| | |
|--|----|
| Figure 25 - 5-spot spacing..... | 48 |
| Figure 26 - 2-D image of the x-y plane..... | 50 |
| Figure 27 – Cumulative production as a function of time [for production well when it gets close to the plume]..... | 51 |
| Figure 28 – Results for Run #1 | 53 |
| Figure 29 - Results for Run #2 | 54 |
| Figure 30 – Results for Run #3 | 55 |
| Figure 31 - Results for Run #4 | 56 |
| Figure 32 - Results for Run #5 | 57 |
| Figure 33 - Results for Run #6 | 58 |
| Figure 34 - Results for Run #7 | 59 |
| Figure 35 - Results for Run #8 | 60 |
| Figure 36 – Results for Run #9 | 61 |
| Figure 37 - Results for Run #10 | 62 |
| Figure 38 - Results for Run #11 | 63 |
| Figure 39 – Results for Run #12 | 64 |
| Figure 40 - Results for Run #13 | 65 |
| Figure 41 - Results for Run #14 | 66 |
| Figure 42 - Results for Run #15 | 67 |
| Figure 43 - Results for Run #16 | 68 |
| Figure 44 – Results for Run #17 | 69 |
| Figure 45 - Results for Run #18 | 70 |
| Figure 46 - Results for Run #19 | 71 |
| Figure 47 – Initial pressure distribution..... | 72 |
| Figure 48 – Pressure distribution at the end of 50 years for injection pressure of 6000 psi..... | 73 |
| Figure 49 – Gas saturations at the end of 50 years for injection pressure of 6000 psi.. | 73 |
| Figure 50 - Gas saturations at the end of 50 years for an injection pressure of 3500 psi without production well | 74 |

Page Intentionally Left Blank

1 Introduction

It is a common understanding that weather plays a role for humans in many ways. A terminology used for long term weather change is called climate change. NOAA describes this as, “One of the most vigorously debated topics on Earth is the issue of climate change”. On earth, climate has always changed and it is always changing as discussed in numerous scientific studies, media etc. One of the most common subjects in discussing or explaining the recent climate changes is increase in global temperatures also known as global warming, which is also a debated topic but majority of meteorologist community agrees to global warming exists and the increase in acceleration of the temperature is caused partly by human activity or influence (IPCC, 2013) (Stenhouse, et al., 2014).

One of the biggest and major source of Green House Gases (GHG) emissions is the energy supply sector with 17 GtCO₂eq, 35% of global GHG emissions. Some of the organizations, agencies or other entities have been asking the world governments and policy makers to take actions, against emissions responsible for contributing global warming also known as Green House Gases (GHG). Which is why the governments are now enforcing and/or looking for new ways to control or minimizing air emissions. One of the new ways of performing environmentally friendly industry practices is by looking into curtailing or stopping CO₂ production from research and development in CO₂ sequestration for the sake of storage (IPCC, 2013).

1.1 Climate Change

Today the observations conducted on the climate system are based on direct physical and biogeochemical measurements, and remote sensing from ground stations and satellites. The Overall global scale observations started in mid-19th century, and paleoclimate allowed reconstruction of records back to hundreds to millions of years. These two independent sources were synced in order define comprehensive insight in long-term changes in the atmosphere, the ocean, the cryosphere and at the land surface. In recent years there has been substantial advancements in the availability, quality, and analysis of the collected data sets as the science is matured by increase of

manpower, experience behind the science, funding data collection, and wealth of knowledge (IPCC, 2013).

When assessing the collected data for determining the changes in temperature, it is certain that average global surface temperatures has increased since the late 19th century with a continued increase into the last three decades. The global temperature averages (land and ocean) have increased by .85 Celsius based on unweighted average linear trend according to Climatic Research Unit in IPCC, over the period 1880-2012 (IPCC, 2013).

Figures 1 and 2 show data on indicators of climate variation over several decades. Each line represents an independently analyzed set of data perform by an institute or panel. The first set of graphs indicates anomalies that show decrease in pattern that indicates a warming world. The second set of graphs indicates anomalies that show increase in pattern that indicates a warming world. The data come from many different technologies including weather stations, satellites, weather balloons, ships and buoys (IPCC, 2013).

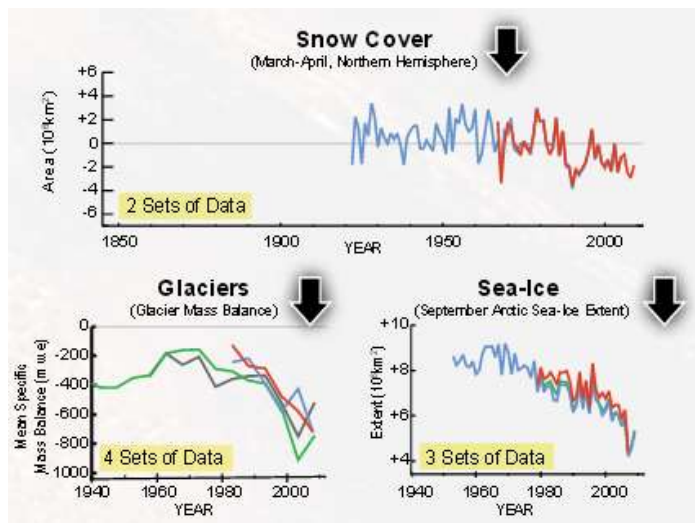


Figure 1 - Indicators for decrease in values for global warming (IPCC, 2013)

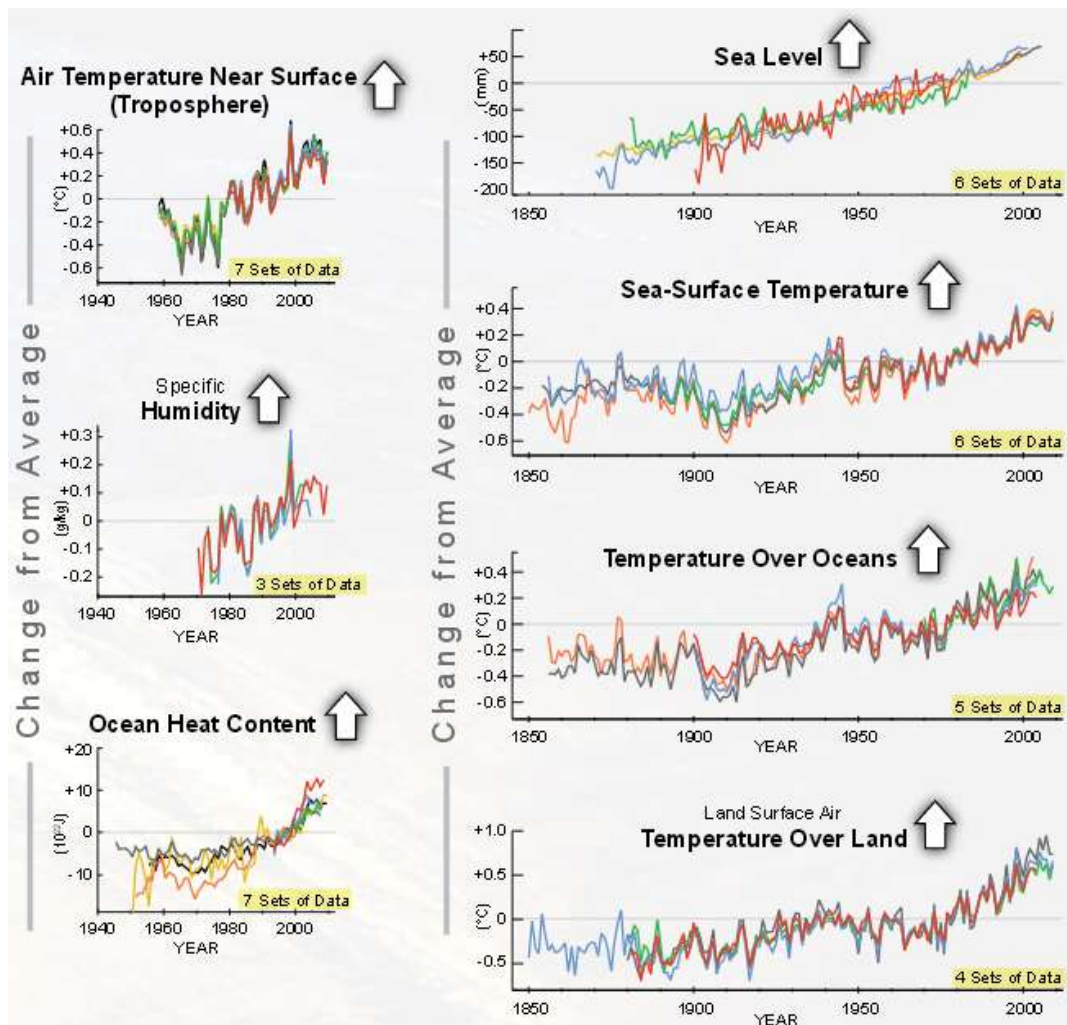


Figure 2 - Indicators for increase in values for global warming (IPCC, 2013)

While most data of the sets are indicators rather than the actual cause, one may wonder where the majority of the energy (or heat) is going. NOAA's studies shows more than 90 percent of the warming that's happened on earth during the past 50 years has gone into the oceans. This increase in temperature has been observed as far as 6,000 feet below the surface, but most of the heat is accumulating in the oceans' near-surface layers (IPCC, 2013).

First, because water expands as it warms, ocean heating is responsible for much of the sea-level rise we've observed. Melting of land-based ice is responsible for the rest. Further, the oceans will hold the heat they've accumulated because they warm and cool much more slowly than air. Just as it is quicker to heat the air in a room than the water

in a swimming pool, and how much longer the pool holds its heat. Figures 3 and 4 show the heat content and its relationship with other elements on earth (D. S. Arndt, 2010)

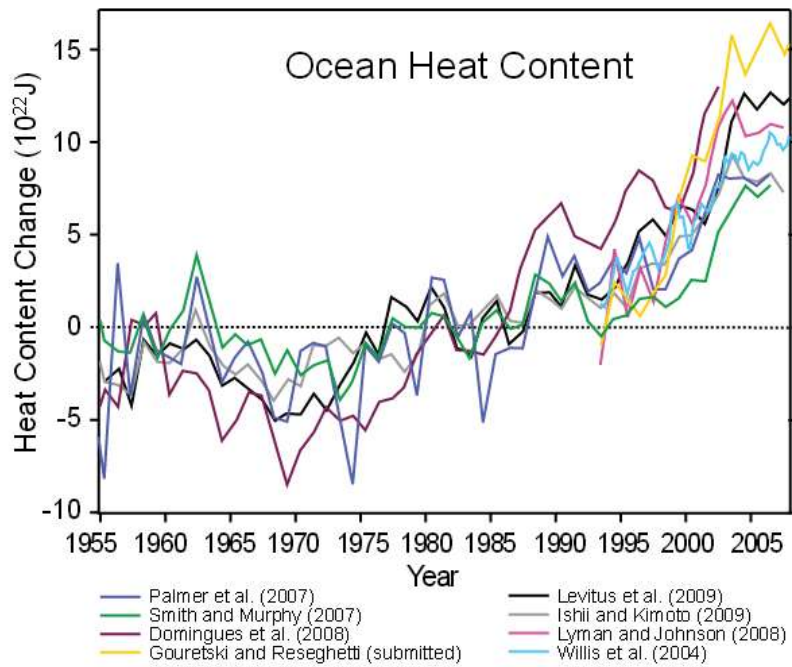


Figure 3 - Global heat content consensus (IPCC, 2013)

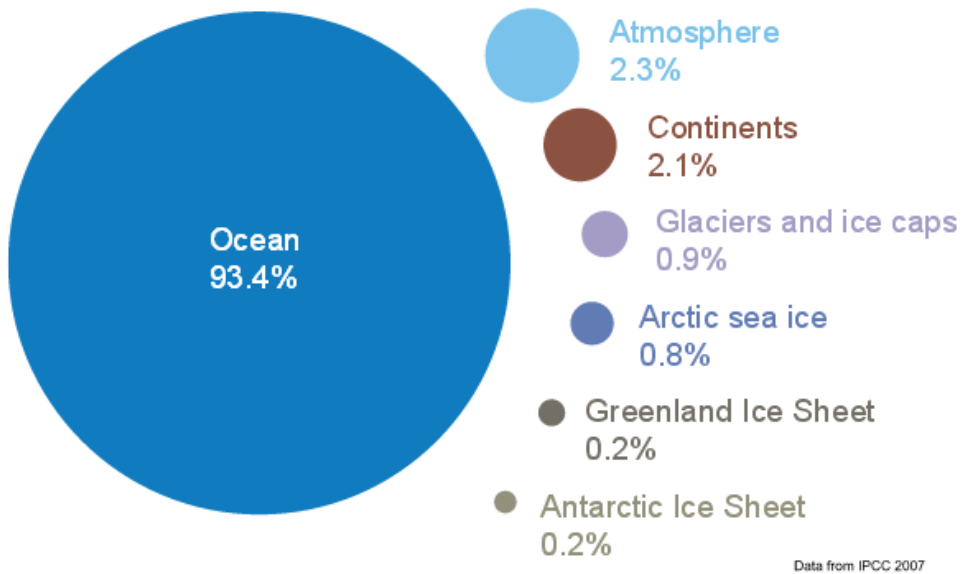


Figure 4 - Heat's impact on Earth (IPCC, 2013)

The globally averaged combined land and ocean surface temperature data as calculated by a linear trend, show a warming of ~ 0.85 °C, over the period 1880 to 2012, when multiple independently produced datasets exist (see Figure 5). The total increase between the average of the 1850–1900 period and the 2003–2012 period is ~ 0.78 °C, based on the single longest dataset available (IPCC, 2013).

For the longest period when calculation of regional trends is sufficiently complete (1901 to 2012), almost the entire globe has experienced surface warming. In addition to robust multi-decadal warming, global mean surface temperature exhibits substantial decadal and inter-annual variability. Due to natural variability, trends based on short records are very sensitive to the beginning and end dates and do not in general reflect long-term climate trends. As one example, the rate of warming over the past 15 years (1998–2012) of ~ 0.05 °C per decade, which begins with a strong El Niño, is smaller than the rate calculated since 1951 (1951–2012) of ~ 0.12 °C per decade (IPCC, 2013). Continental-scale surface temperature reconstructions show, with high confidence, multi-decadal periods during the Medieval Climate Anomaly (year 950 to 1250) that were in some regions as warm as in the late 20th century. These regional warm periods did not occur as coherently across regions as the warming in the late 20th century. More complete observations allow greater confidence in estimates of tropospheric temperature changes in the extratropical Northern Hemisphere than elsewhere (IPCC, 2013).

Overall, all data leads to conclusion that the troposphere has globally warmed since the mid-20th century. Each of the last three decades has been successively warmer at the Earth's surface than any preceding decade since 1850. In the Northern Hemisphere, 1983–2012 was probably the warmest 30-year period of the last 1400 years (IPCC, 2013).

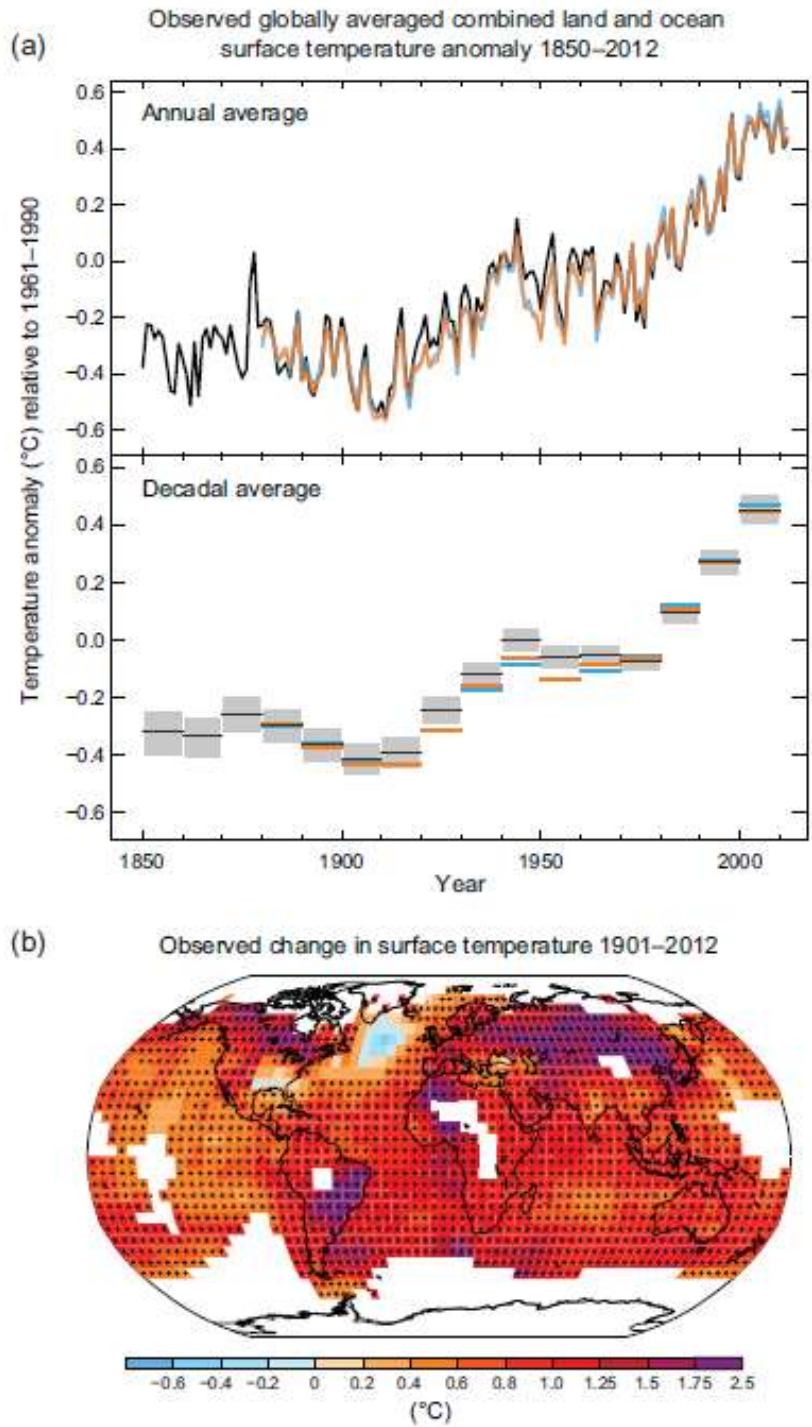


Figure 5 - Observed Global Temperature Change (IPCC, 2013)

Figure 6 shows heavy precipitation events over land has increased in more regions than it has decreased. In North America and Europe there has been increase in either the

frequency or intensity of heavy precipitation with some seasonal and regional variations. And there have been trends towards heavier precipitation events in central North America (IPCC, 2013).

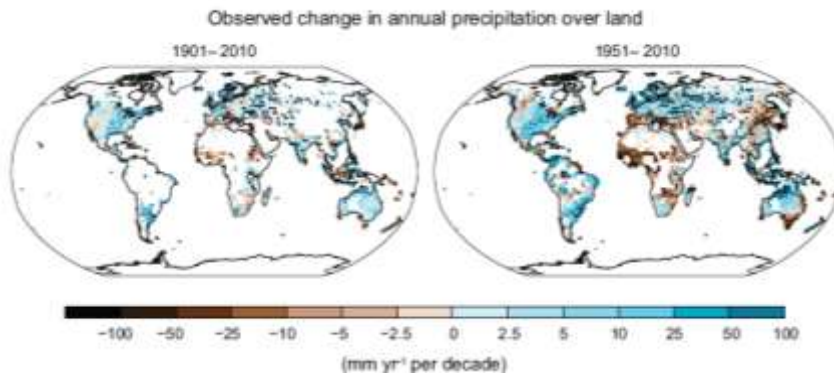


Figure 6 - Observed Global Precipitation Change (IPCC, 2013)

1.1.1 Extreme Weather

Changes in many extreme weather and climate events have been observed since about 1950, see Figure 7 for trends' likelihood. It is very likely that the number of cold days and nights has decreased and the number of warm days and nights has increased on the global scale. It is likely that the frequency of heat waves has increased in large parts of Europe, Asia and Australia. There are likely more land regions where the number of heavy precipitation events has increased than where it has decreased. The frequency or intensity of heavy precipitation events has likely increased in North America and Europe. In other continents, confidence in changes in heavy precipitation events is at most medium.

There has been increase in extreme weather and also natural weather related disasters like Hurricane Katrina, rain related floods in Pakistan, Brazil, etc., heat waves responsible for deaths in Asia.

Recent analyses of extreme events generally support the IPCC. It is very likely that the number of cold days and nights has decreased and the number of warm days and nights has increased on the global scale between 1951 and 2010. Globally, there is indications that the length and frequency of warm spells, including heat waves, has

increased since the middle of the 20th century, mostly owing to lack of data or studies in Africa and South America. However, it is likely that heat wave frequency has increased over this period in large parts of Europe, Asia and Australia (IPCC, 2013).

| Phenomenon and direction of trend | Assessment that changes occurred (typically since 1950 unless otherwise indicated) | Assessment of a human contribution to observed changes | Likelihood of further changes | |
|--|--|--|------------------------------------|--|
| | | | Early 21st century | Late 21st century |
| Warmer and/or fewer cold days and nights over most land areas | Very likely (2.4) Very likely Very likely | Very likely (10.4) Likely Likely | Likely (11.3) | Virtually certain (12.4) Virtually certain Virtually certain |
| Warmer and/or more frequent hot days and nights over most land areas | Very likely (2.4) Very likely Very likely | Very likely (10.4) Likely Likely (night only) | Likely (11.3) | Virtually certain (12.4) Virtually certain Virtually certain |
| Warm spells/heat waves. Frequency and/or duration increases over most land areas | Medium confidence on a global scale Likely in large parts of Europe, Asia and Australia (2.4) Medium confidence in many (but not all) regions Likely | Likely* (10.4) Not formally assessed More likely than not | Not formally assessed* (11.3) | Very likely (12.4) Very likely Very likely |
| Heavy precipitation events. Increase in the frequency, intensity, and/or amount of heavy precipitation | Likely more land areas with increases than decreases* (2.4) Likely more land areas with increases than decreases Likely over most land areas | Medium confidence (7.4, 10.4) Medium confidence More likely than not | Likely over many land areas (11.3) | Very likely over most of the mid-latitude land masses and over wet tropical regions (12.4) Likely over many areas Very likely over most land areas |
| Increases in intensity and/or duration of drought | Low confidence on a global scale Likely changes in some regions* (2.4) Medium confidence in some regions Likely in many regions, since 1970* | Low confidence* (10.4) Medium confidence* More likely than not | Low confidence* (11.3) | Likely (medium confidence) on a regional to global scale* (12.4) Medium confidence in some regions Likely* |
| Increases in intense tropical cyclone activity | Low confidence in long term (interdecadal) changes Virtually certain in North Atlantic since 1970 (2.4) Low confidence Likely in some regions, since 1970 | Low confidence* (10.4) Low confidence More likely than not | Low confidence (11.3) | More likely than not in the Western North Pacific and North Atlantic (14.4) More likely than not in some basins Likely |
| Increased incidence and/or magnitude of extreme high sea level | Likely since 1950 (2.2) Likely (late 20th century) Likely | Likely* (2.2) Likely* More likely than not* | Likely* (11.3) | Very likely (11.3) Very likely* Likely |

Figure 7 - Phenomenon and direction of trend (IPCC, 2013)

1.1.2 CO₂ in atmosphere

According to NOAA, carbon dioxide concentration measured at Mauna Loa Observatory, Hawaii, is 403 ppm as of July 2015. This lab serves as ideal location to provide a non-bias data due to its remoteness, which minimizes impacts from vegetation and human activity. Figure 8 shows CO₂ observed in last five decades.

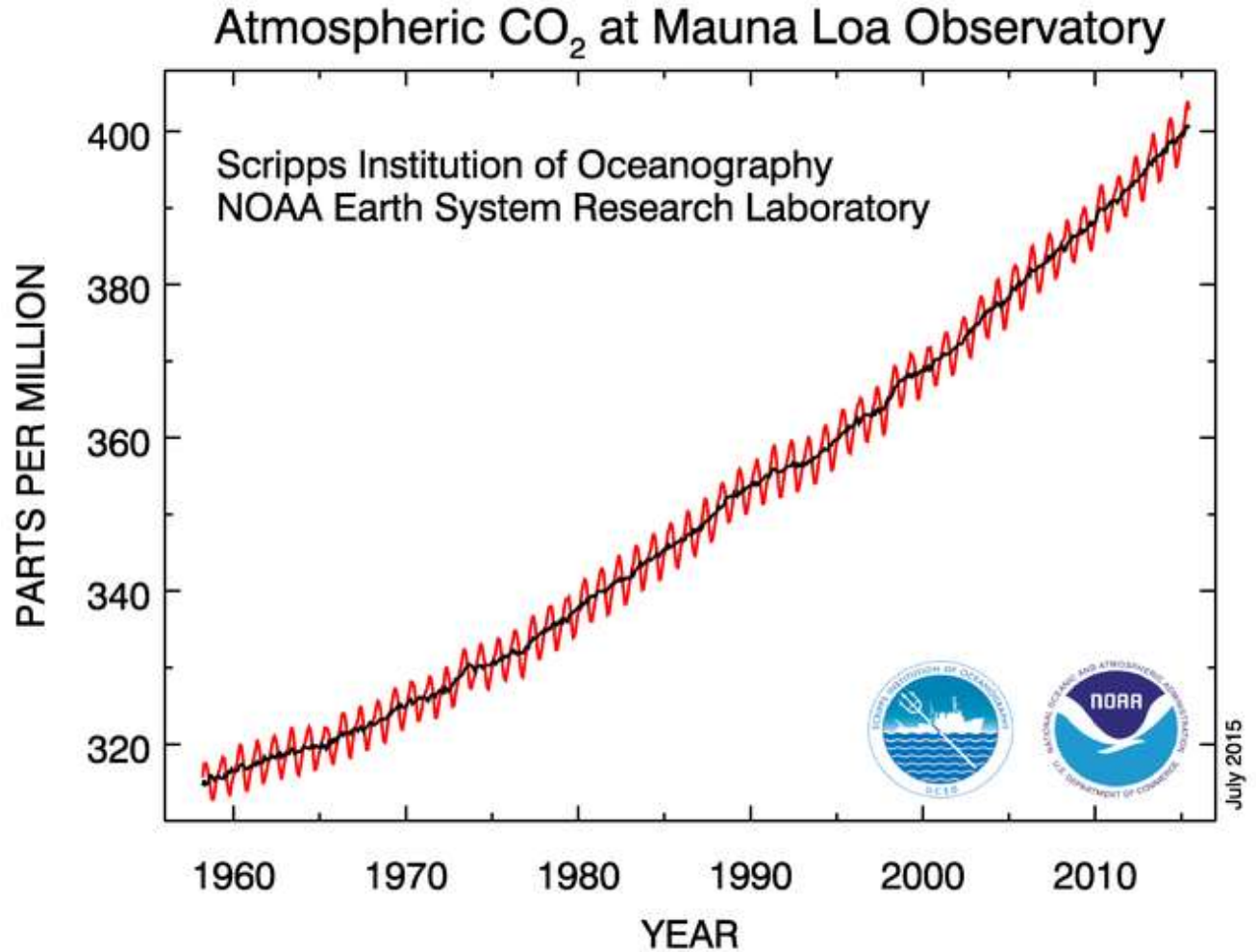


Figure 8 - Full Mauna Loa CO₂ record (IPCC, 2013)

When comparing the Mauna Loa data with the NOAA/ESRL/GMD CCGG cooperative air sampling network (Figure 9) it shows positive correlation (Figure 10). This network is an international effort which includes regular discrete samples from the NOAA ESRL/GMD baseline observatories, cooperative fixed sites, and commercial ships with air samples collected on a weekly basis. Samples are analyzed for CO₂, CH₄, CO, H₂, N₂O, and SF₆. The measured data are used to determine long-term trends, seasonal variability, and spatial distribution of carbon cycle gases (NOAA, 2015).

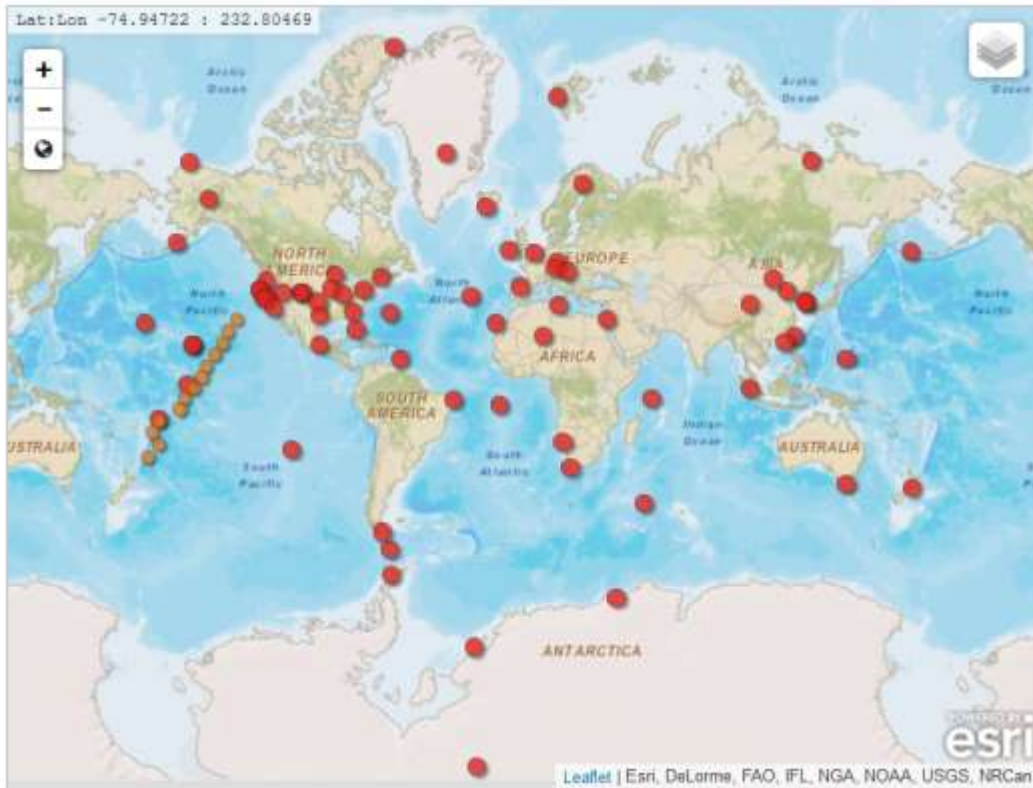


Figure 9 - NOAA/ESRL/GMD CCGG cooperative air sampling network (NOAA, 2015)

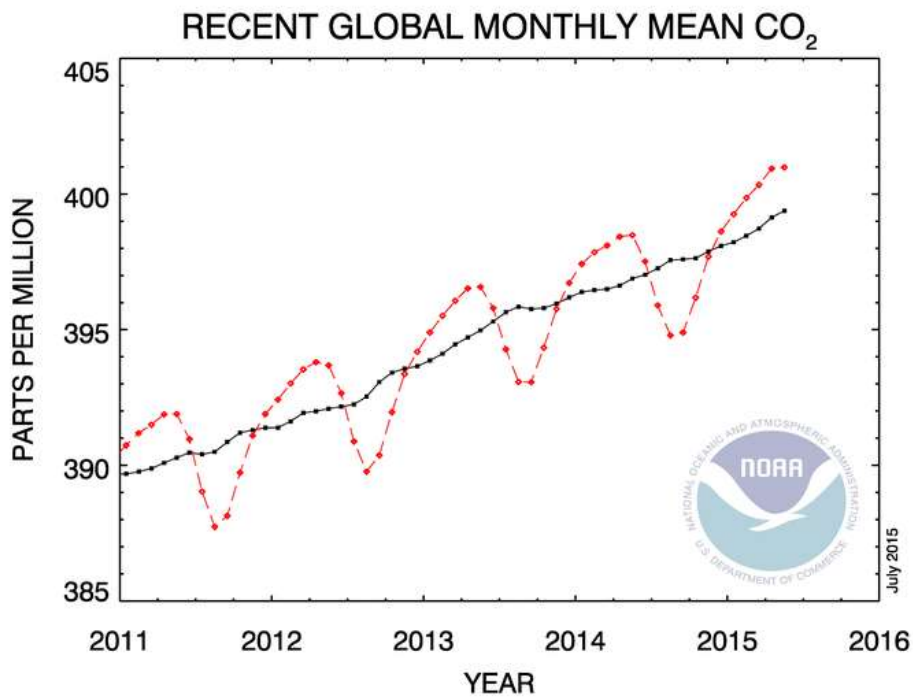


Figure 10 - Recent global CO₂ Average (IPCC, 2013)

According to IPCC atmospheric concentrations of carbon dioxide, methane, and nitrous oxide have increased to levels unprecedented in at least the last 800,000 years. Carbon dioxide concentrations have increased by 40% since pre-industrial times, primarily from fossil fuel emissions and secondarily from net land use change emissions. The ocean has absorbed about 30% of the emitted anthropogenic carbon dioxide, causing ocean acidification. The ocean acidification has the most serious concerns, but they are not covered because they are not within the scope of this thesis. Ocean acidification is quantified by decreases in pH (see Figure 11). The pH of ocean surface water has decreased by 0.1 since the beginning of the industrial era, corresponding to a 26% increase in hydrogen ion concentration. (IPCC, 2013) The ocean acidity normally fluctuates within limits as a result of natural processes, and ocean organisms where the marine life is generally well-adapted to survive the changes that they normally experience. But in the case of ocean acidification many marine life will suffer, and there will likely be extinctions. Scientists don't know this for sure, but during the last great acidification event 55 million years ago, there were mass extinctions in some species including deep sea invertebrates. A more acidic ocean won't destroy all marine life in the sea, but the rise in seawater acidity of 30 percent that we have already seen is already affecting some ocean organisms. (Bennet)

The atmospheric concentrations of the greenhouse gases like carbon dioxide (CO₂), methane (CH₄), and nitrous oxide (N₂O) have all increased since 1750 due to human activity. In 2011 the concentrations of these three greenhouse gases were 391 ppm, 1803 ppb, and 324 ppb, and exceeded the pre-industrial levels by about 40%, 150%, and 20%, respectively. Concentrations of CO₂, CH₄, and N₂O now substantially exceed the highest concentrations recorded in ice cores during the past 800,000 years. The mean rates of increase in atmospheric concentrations over the past century are, with very high confidence, unprecedented in the last 22,000 years. (IPCC, 2013)

According to IPCC, the annual CO₂ emissions from fossil fuel combustion and cement production were ~8.3 GtC/yr averaged over 2002–2011 and were ~9.5 GtC/yr in 2011, 54% above the 1990 level. Annual net CO₂ emissions from anthropogenic land use change were ~0.9 GtC/yr on average during 2002 to 2011. Additional data reveals that from 1750 to 2011, CO₂ emissions from fossil fuel combustion and cement production

have released ~375 GtC to the atmosphere, while deforestation and other land use change are estimated to have released ~180 GtC. This results in cumulative anthropogenic emissions of ~555 GtC. And of these cumulative anthropogenic CO₂ emissions, ~240 GtC have accumulated in the atmosphere, ~155 GtC have been taken up by the ocean and ~160 GtC have accumulated in natural terrestrial ecosystems (i.e., the cumulative residual land sink). (IPCC, 2013)

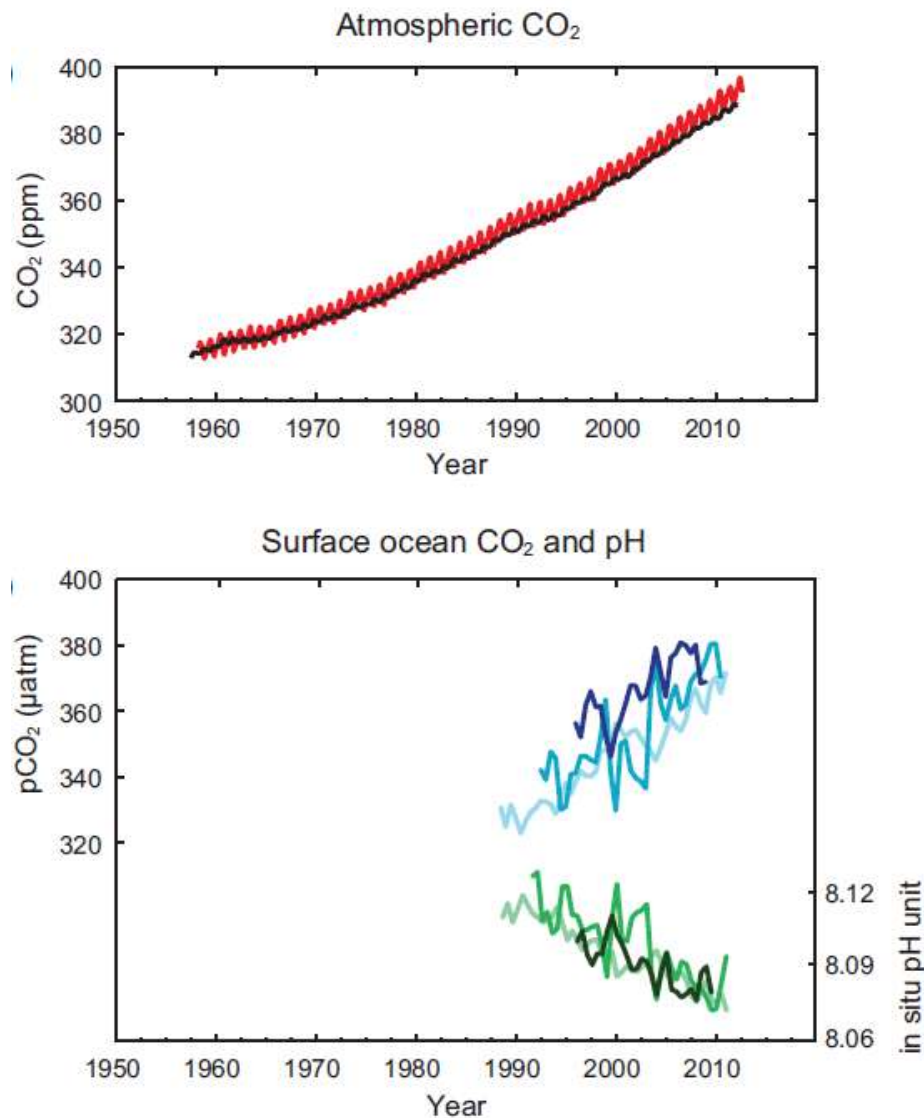


Figure 11 - CO₂ in Air and Ocean (IPCC, 2013)

1.1.3 Carbon and Other Biogeochemical Cycles

Climate change will affect carbon cycle processes in a way that will exacerbate the increase of CO₂ in the atmosphere. Further uptake of carbon by the ocean will increase ocean acidification. Ocean uptake of anthropogenic CO₂ will continue under all four RCPs through 2100s, with higher uptake for higher concentration pathways (very high confidence). The future evolution of the land carbon uptake is less certain. A majority of models project a continued land carbon uptake under all RCPs, but some models simulate a land carbon loss due to the combined effect of climate change and land use change (IPCC, 2013).

Based on Earth System Models, there is a high confidence that the feedback between climate and the carbon cycle is positive in the 21st century; that is, climate change will partially offset increases in land and ocean carbon sinks caused by rising atmospheric CO₂. As a result more of the emitted anthropogenic CO₂ will remain in the atmosphere. A positive feedback between climate and the carbon cycle on century to millennial time scales is supported by paleoclimate observations and modelling. (IPCC, 2013)

A large fraction of anthropogenic climate change resulting from CO₂ emissions is irreversible on a multi-century to millennial time scale, except in the case of a large net removal of CO₂ from the atmosphere over a sustained period. Surface temperatures will remain approximately constant at elevated levels for many centuries after a complete cessation of net anthropogenic CO₂ emissions. Due to the long time scales of heat transfer from the ocean surface to depth, ocean warming will continue for centuries. Depending on the scenario, about 15 to 40% of emitted CO₂ will remain in the atmosphere longer than 1,000 years (IPCC, 2013).

It is virtually certain that global mean sea level rise will continue beyond 2100, with sea level rise due to thermal expansion to continue for many centuries. The few available model results that go beyond 2100 indicate global mean sea level rise above the pre-industrial level by 2300 to be less than 1 m for a radiative forcing that corresponds to CO₂ concentrations that peak and decline and remain below 500 ppm, as in the scenario RCP2.6 (see Figure 12). For a radiative forcing that corresponds to a CO₂ concentration that is above 700 ppm but below 1500 ppm, as in the scenario RCP8.5, the projected rise is 1 m to more than 3 m. (IPCC, 2013).

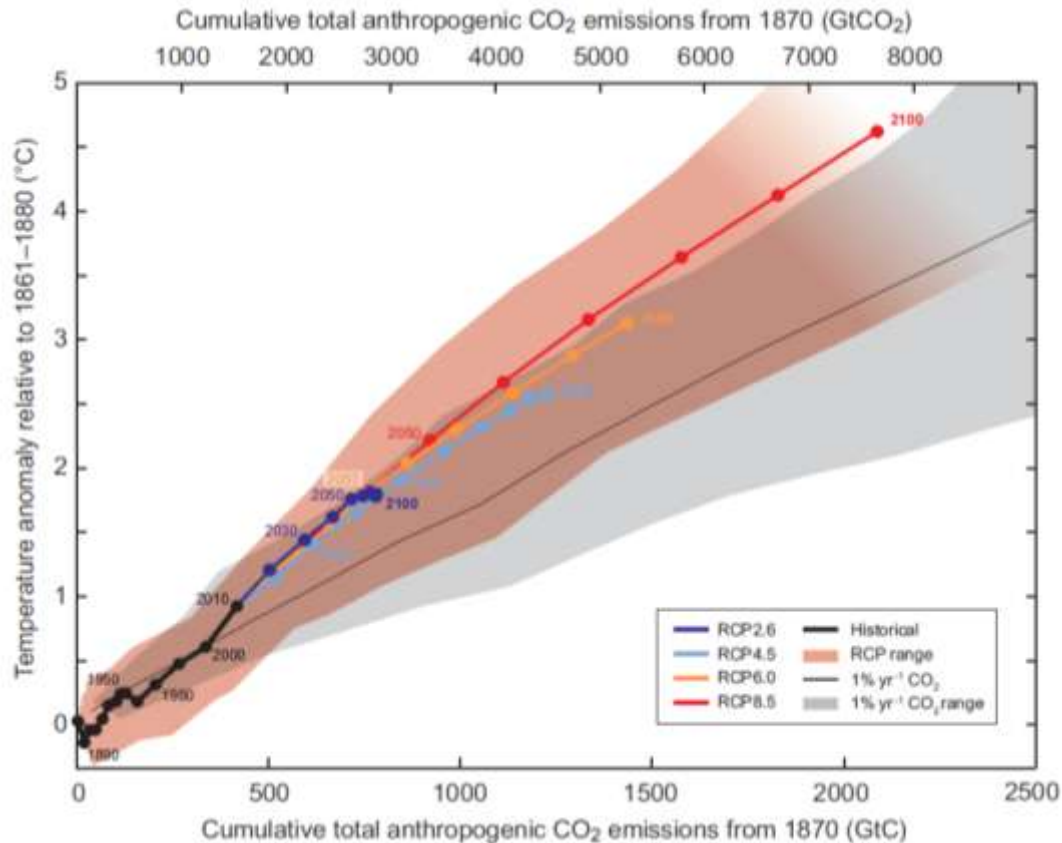


Figure 12 - Total Anthropogenic CO₂ Emissions (IPCC, 2013)

Sustained mass loss by ice sheets would cause larger sea level rise, and some part of the mass loss might be irreversible. There is high confidence that sustained warming greater than some threshold would lead to the near-complete loss of the Greenland ice sheet over a millennium or more, causing a global mean sea level rise of up to 7 m. (IPCC, 2013).

Methods that aim to deliberately alter the climate system to counter climate change, termed geoengineering, have been proposed. Limited evidence precludes a comprehensive quantitative assessment of both Solar Radiation Management (SRM) and Carbon Dioxide Removal (CDR) and their impact on the climate system. CDR methods have biogeochemical and technological limitations to their potential on a global scale. There is insufficient knowledge to quantify how much CO₂ emissions could be partially offset by CDR on a century timescale. Modelling indicates that SRM methods, if realizable, have the potential to substantially offset a global temperature rise, but they

would also modify the global water cycle, and would not reduce ocean acidification. If SRM were terminated for any reason, there is high confidence that global surface temperatures would rise very rapidly to values consistent with the greenhouse gas forcing. CDR and SRM methods carry side effects and long-term consequences on a global scale (IPCC, 2013).

1.1.4 Is CO₂ a driver of Climate Change?

Natural and anthropogenic substances and processes that alter the Earth's energy budget are drivers of climate change. Radiative forcing (RF) quantifies the change in energy fluxes caused by changes in these drivers for 2011 relative to 1750, unless otherwise indicated. Positive RF leads to surface warming, negative RF leads to surface cooling. RF is estimated based on in-situ and remote observations, properties of greenhouse gases and aerosols, and calculations using numerical models representing observed processes. Some emitted compounds affect the atmospheric concentration of other substances. The RF can be reported based on the concentration changes of each substance. Alternatively, the emission-based RF of a compound can be reported, which provides a more direct link to human activities. It includes contributions from all substances affected by that emission. The total anthropogenic RF of the two approaches are identical when considering all drivers (IPCC, 2013).

Some of the assessments derived from the data are the following (also see Figure 13):

- The total radiative forcing has led to an uptake of energy by the climate system. The largest contribution to total radiative forcing is caused by the increase in the atmospheric concentration of CO₂ since 1750 (IPCC, 2013).
- The total anthropogenic RF for 2011 relative to 1750 is $\sim 2.29 \text{ W/m}^2$ ¹ and it has increased more rapidly since the 1970s in comparison to prior decades. The total anthropogenic RF best estimate for 2011 is 43% higher than that reported in IPCC's Fourth Assessment Report for the year 2005. This is sourced by a combination of accelerated growth in most greenhouse gas concentrations and

¹ The strength of driver is quantified as Radiative Forcing (RF) in units watts per square meter (W/m^2)

improved estimates of RF by aerosols indicating a weaker net cooling effect (negative RF) (IPCC, 2013).

- The CH₄ and CO₂ emissions individually have caused an RF of ~0.97 W/m² and ~1.68 W/m². Including emissions of other carbon-containing gases, which also contributed to the increase in CO₂ concentrations, the RF of CO₂ is ~1.82 W/m² (IPCC, 2013).
- Carbon monoxide (CO) emissions are sure to have induced a positive RF, while emissions of nitrogen oxides (NO_x) are likely to have induced a net negative RF (IPCC, 2013).

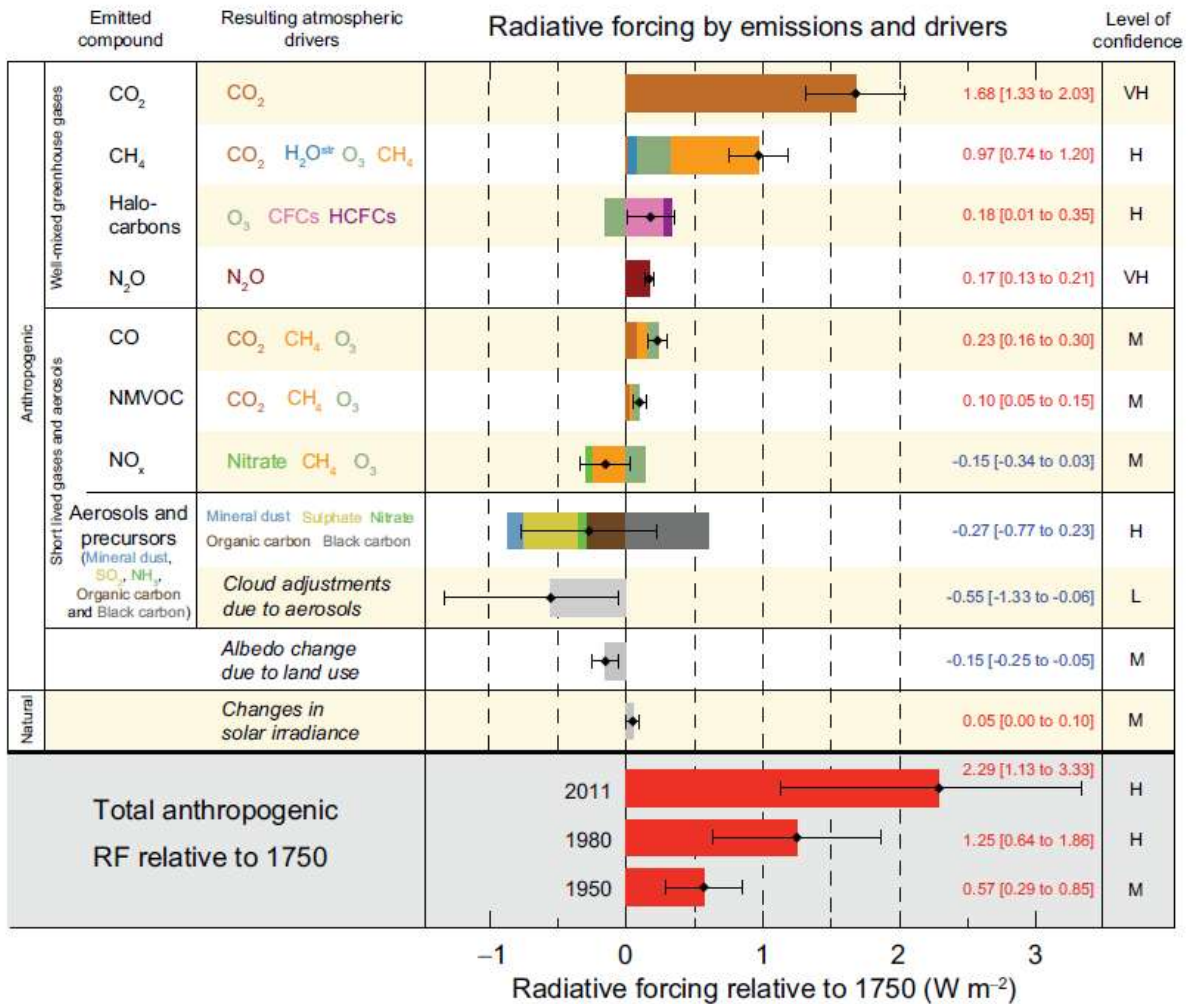


Figure 13 - Radiative force by emissions and drivers (IPCC, 2013)

1.1.5 CO₂ and Power plants in US

Public exposure to air emissions (air pollution) from a power plant is regulated by the U.S. Environmental Protection Agency (EPA) primarily through two sets of standards:

- The National Ambient Air Quality Standards (NAAQS) for major, “criteria,” air pollutants including sulfur dioxide (SO₂), nitrogen oxides (NO_x), carbon monoxide (CO), ozone (O₃), particulate matter (PM_{2.5} or PM₁₀), and lead (Pb).
- The National Emissions Standards for Hazardous Air Pollutants (NESHAP) for hazardous elements like mercury (Hg) or cadmium (Cd) and compounds like acetaldehyde (CH₃CHO) or hydrochloric acid (H₂SO₄), all often mentioned simply as HAPs.

(Wisconsin Public Service Commission, 2015)

The State governments are typically charged with enforcing the NAAQS for criteria pollutants and NESHAP for HAPs. The state government air pollution control permit program has permits for two kinds of scenarios: new and existing facilities. For a proposed new power plant, the objective is to ensure through a “construction permit” and “air dispersion modeling” that the plant can meet air pollution standards before it is built and operating. Existing plants receive operation permits that set emission limits and establish monitoring and reporting requirements (Wisconsin Public Service Commission, 2015).

SO₂ has been a cause of acid precipitation, commonly known as “acid rain,” which can damage vegetation and acidify lakes. Species vulnerable to acidic conditions have trouble reproducing and, in some cases, die. NO_x and volatile organic compounds (VOCs) are components of ozone formation. Ozone is a principal component of smog and can result in respiratory health and other environmental effects. Particulate matter (PM) includes dust and smaller particles with a maximum particle diameter of 10 microns (PM₁₀). It takes 1,000 microns to equal 1 millimeter. In addition to PM₁₀ emission standards, there are federal standards for PM_{2.5}, extremely small particles with a diameter between 2.5 and 10 microns. Small particulates have been shown to cause respiratory problems because they can penetrate deeper into the lungs than the larger particulates. The agencies have been monitoring PM_{2.5} statewide since 1999. Only a relatively small amounts of fine particulates are directly emitted from combustion

sources. A more significant concern is the NO_x and SO₂ emissions from power plants that burn coal or natural gas. These compounds are part of a complex chemical reaction in the atmosphere that creates nitrate- and sulfate-based fine particulates. Most of the States' efforts to reduce fine particulate pollution are based on year-round control of NO_x and SO₂ contaminants (Wisconsin Public Service Commission, 2015).

Mercury (Hg) is naturally present in small quantities in the environment. Human activities have greatly increased the concentration of this pollutant in the air and water. Coal-fired power plants are the biggest category of mercury emitters. Mercury is very volatile and can travel around the world in the atmosphere, repeatedly being deposited and re-emitted into the atmosphere. Mercury is deposited in lakes and rivers by rain, snow and surface runoff. While mercury is a pollutant with global consequences, the local impacts of mercury emissions from power plants also remain a serious concern. Once deposited in waterways, bacteria can convert mercury into methyl mercury that can be easily absorbed by fish and other organisms. Eating contaminated fish is the primary pathway for human exposure to mercury. Ingested mercury can damage the nervous system, especially in children and fetuses. Currently, most of the lakes and streams have DNR fish consumption "safe-eating" guidelines for mercury. Some Wisconsin lakes and streams or stream segments have fish consumption "special advice" because of higher levels of mercury in certain sport fish which can be found on the public website (Wisconsin Public Service Commission, 2015).

It is also important to know about the presence of sensitive environmental resources in the area that would be affected by the power plant's emissions. For example, the plant should be located far from any designated wilderness such as national forests whose ecology, public use and enjoyment could be adversely affected by air pollution.

Federal emissions standards are based on health effects research. In an effort to minimize pollutants released to the air, best-achieving emission control technologies are often made a requirement for plant operation. Even though a power plant's emissions are required to meet air emission standards, more sensitive individuals might not be adequately protected. When air pollution levels increase in an area, more vulnerable individuals like the elderly, the sick, and the very young might experience health problems (Wisconsin Public Service Commission, 2015).

1.2 Reducing Emissions by Carbon dioxide (CO₂) capture and sequestration (CCS)

There are several possible approaches to reduce CO₂ emissions. These include energy efficiency improvements, adoption of alternative fuels, Nuclear Power, renewable energy, changes in lifestyle, choosing investment, policy maker's engagement, etc. One of the ways to do so is by CO₂ Capture and Sequestration.

Carbon dioxide (CO₂) capture and sequestration (CCS) is a set of technologies that can greatly reduce CO₂ emissions from new and existing coal- and gas-fired power plants and large industrial sources. CCS is a three-step process that includes:

1. Capturing CO₂ from the gasses vented from power plants or industrial processes.
2. Transporting the captured and compressed CO₂ (via pipelines and storage tanks).
3. Injecting/Geologically sequestering with the intent to store, or pressure replenishment in oil & gas extraction reservoirs, which is typically in deep underground rock formations. These formations are often a mile or more beneath the surface and consist of porous rock that holds the CO₂. Overlying these formations are impermeable, non-porous layers of rock that trap the CO₂ and prevent it from migrating upward (Environmental Protection Agency, 2015).

CCS can significantly reduce CO₂ emissions from large stationary sources from the commercial sector, which include coal- and natural-gas-fired power plants, and chemical processing plants. EPA has setup Greenhouse Gas Reporting Program that includes facilities that capture CO₂ for the purpose of supplying the CO₂ for industrial use or injecting it underground. According to the 2011 EPA report, CO₂ capture was occurring at over 120 facilities in the United States, mainly on industrial processes and it is used for a wide range of applications. Applications include enhanced oil recovery (EOR), food and beverage manufacturing, pulp and paper manufacturing, and metal fabrication. As CCS becomes more widespread, it is expected that the portion of CO₂ captured in the United States from power generation and industrial processes will increase. Figure 14 below shows the portion of CO₂ that is currently being captured from power plants and other industrial facilities and the portion that is extracted by production wells from natural CO₂ bearing formations in the United States. Figure 14

also shows the various domestic applications of captured and extracted CO₂ (Environmental Protection Agency, 2015).

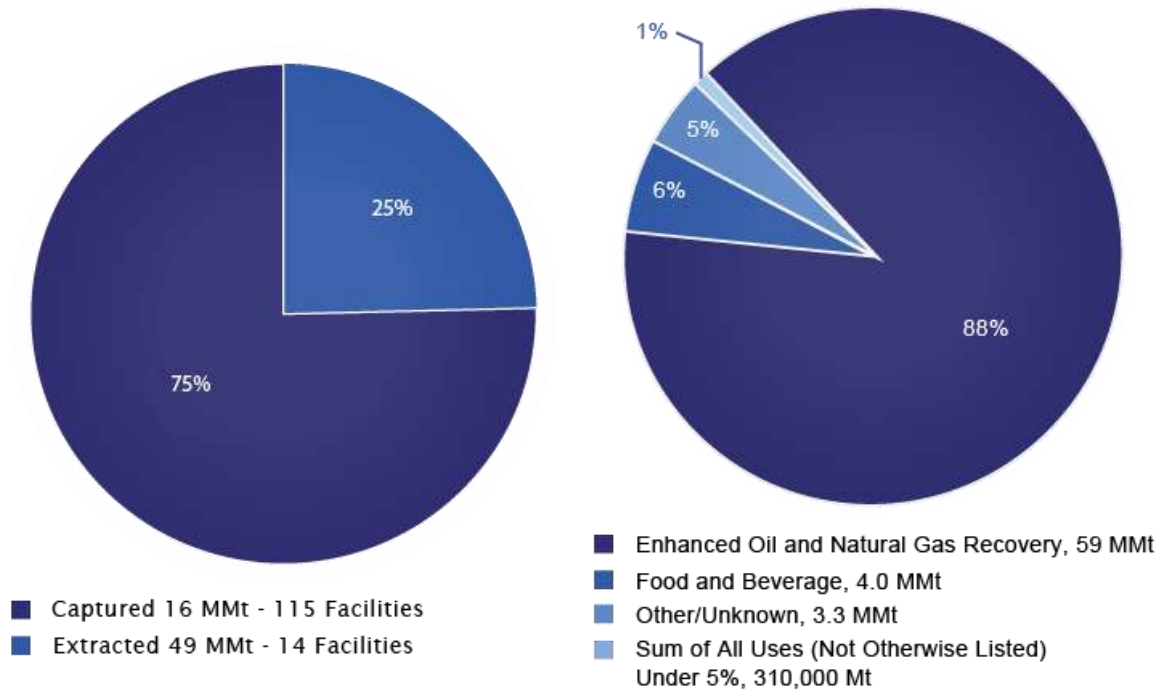


Figure 14 - CO₂ Capture & Extraction Facilities and Sources (Environmental Protection Agency, 2011)

**Note that natural sources of CO₂ are not considered in the total CO₂ applied figure.

For storage, CO₂ is compressed after capturing and then transported to a site where it is injected underground for permanent deposition, also known as “sequestration”. CO₂ is commonly transported by pipeline, but it can also be transported by train, truck, or ship. Figure 15 shows suitable formations for sequestration that include depleted oil and gas fields, deep coal seams, and saline formations. The U.S. Department of Energy estimates that anywhere from 1,800 to 20,000 billion metric tons of CO₂ could be stored underground in the United States. That is equivalent to 600 to 6,700 years of current level emissions from large stationary sources in the United States (Environmental Protection Agency, 2015).

All potential sequestration sites must undergo appropriate site characterization to ensure that the site can safely and securely store CO₂. After being transported to the

sequestration site, the compressed CO₂ is injected deep underground into solid, but porous rock, such as sandstone, shale, dolomite, basalt, or deep coal seams. Suitable formations for CO₂ sequestration are located under one or more layers of cap rock, which trap the CO₂ and prevent upward migration. These sites are then rigorously monitored to ensure that the CO₂ remains permanently underground. The safety and security of CO₂ geologic sequestration is a priority for Industry and the government agencies that has the oversight (Environmental Protection Agency, 2015).

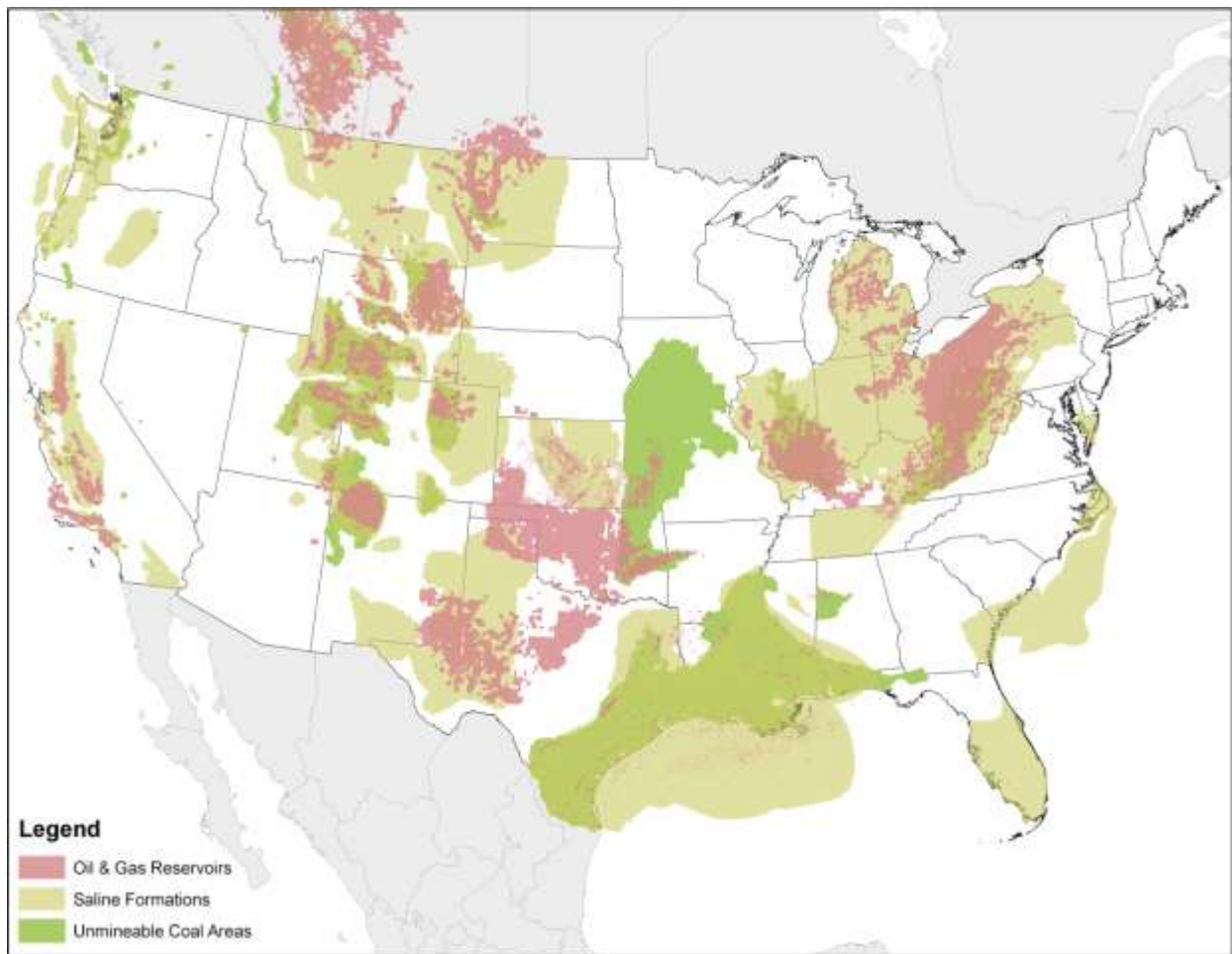
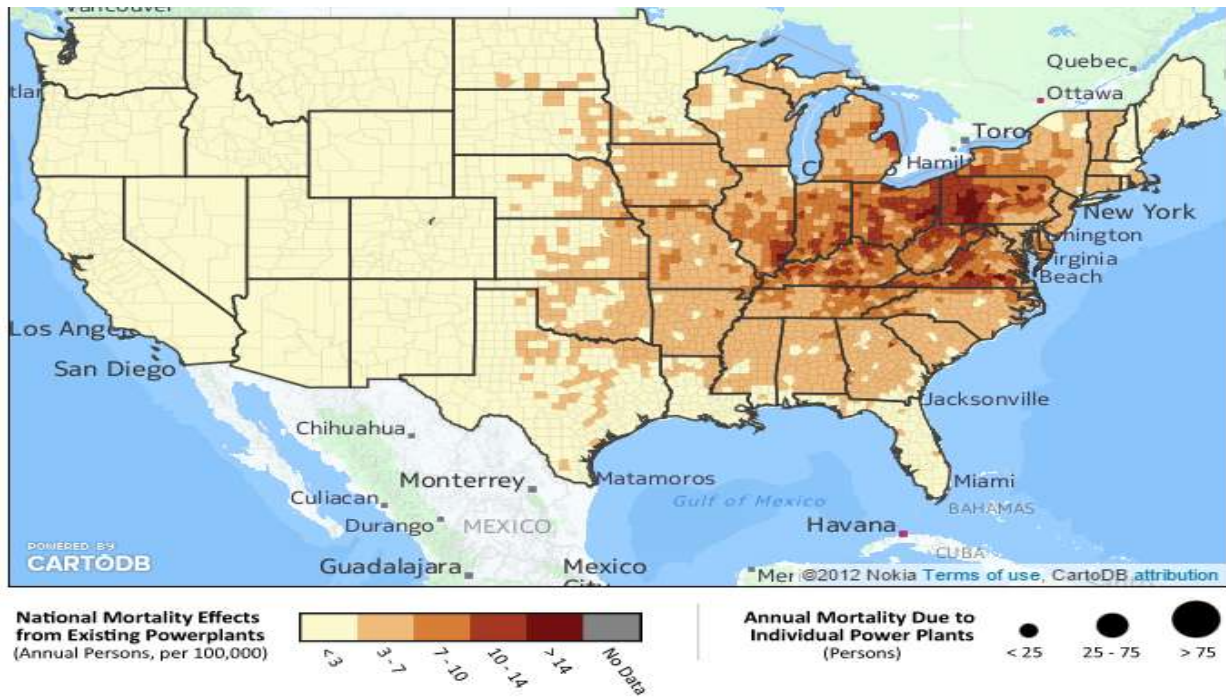


Figure 15 - Geologic Storage Potential in the United States (Environmental Protection Agency, 2015)

1.3 CO₂ sequestration application in limited space

Power plants that burn coal, oil, or natural gas emit air pollutants into the atmosphere and are required to be fitted with pollution control equipment to reduce emissions. Many of the power plant's air pollutants have been identified and are regulated by federal and state environmental regulatory agencies. But yet there is a high risk of death and disease in areas of high concentration power plants. (Figure 16 and 17)



* The results shown represent a specific year's plant operations. Plant operating levels change from year to year, and can be higher or lower than represented in our data. However, for the most part, power plant health impacts have dropped significantly in recent years. Data is estimated 2012 impacts. All monetary values are expressed in thousands of dollars.
County level data is health impacts/100,000 persons.

Figure 16 - National Mortality Effects from Existing Power plants (Clean Air Task Force, 2010)

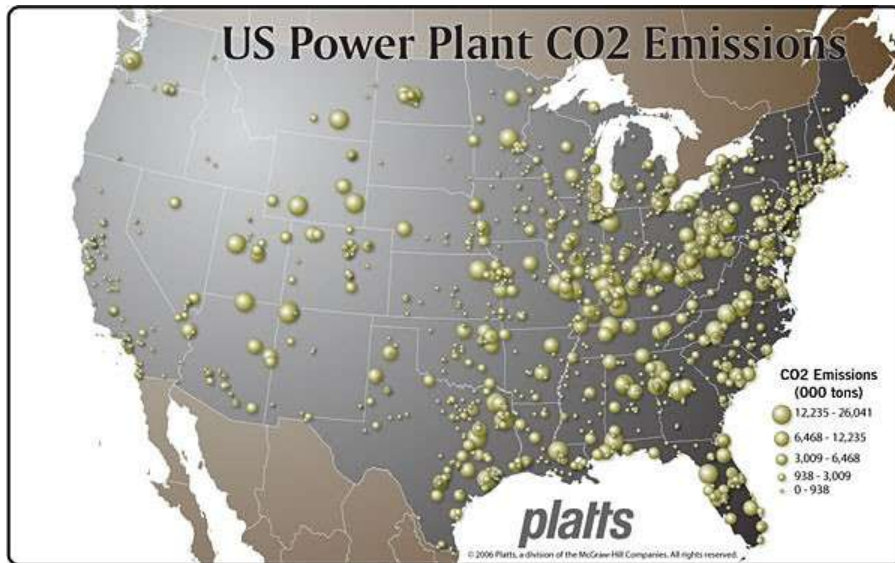


Figure 17 - US Power Plant CO₂ Emissions (Huttenbach, 2009)

When applying CCS in areas where there is a high concentration of power plants, there is a risk for possibly over pressurizing the injected geologic formation. In this case, CO₂ sequestration must be designed in a way where pressure is reduced by placing production well as close as possible to the injection well, calling this approach pressure management. Focusing on the distance to production well is typically called well spacing in reservoir engineering.

2 Literature Review

CO₂ sequestration is extensively studied due to vast interest in public, government, and industry.

2.1 CO₂ plume monitoring technologies

Technology for monitoring CO₂ are available for various applications. According to Lawrence Berkeley National Laboratory every storage project would be composed of four distinct phases: pre-operational, operational, closure and post-closure (Figure 18).

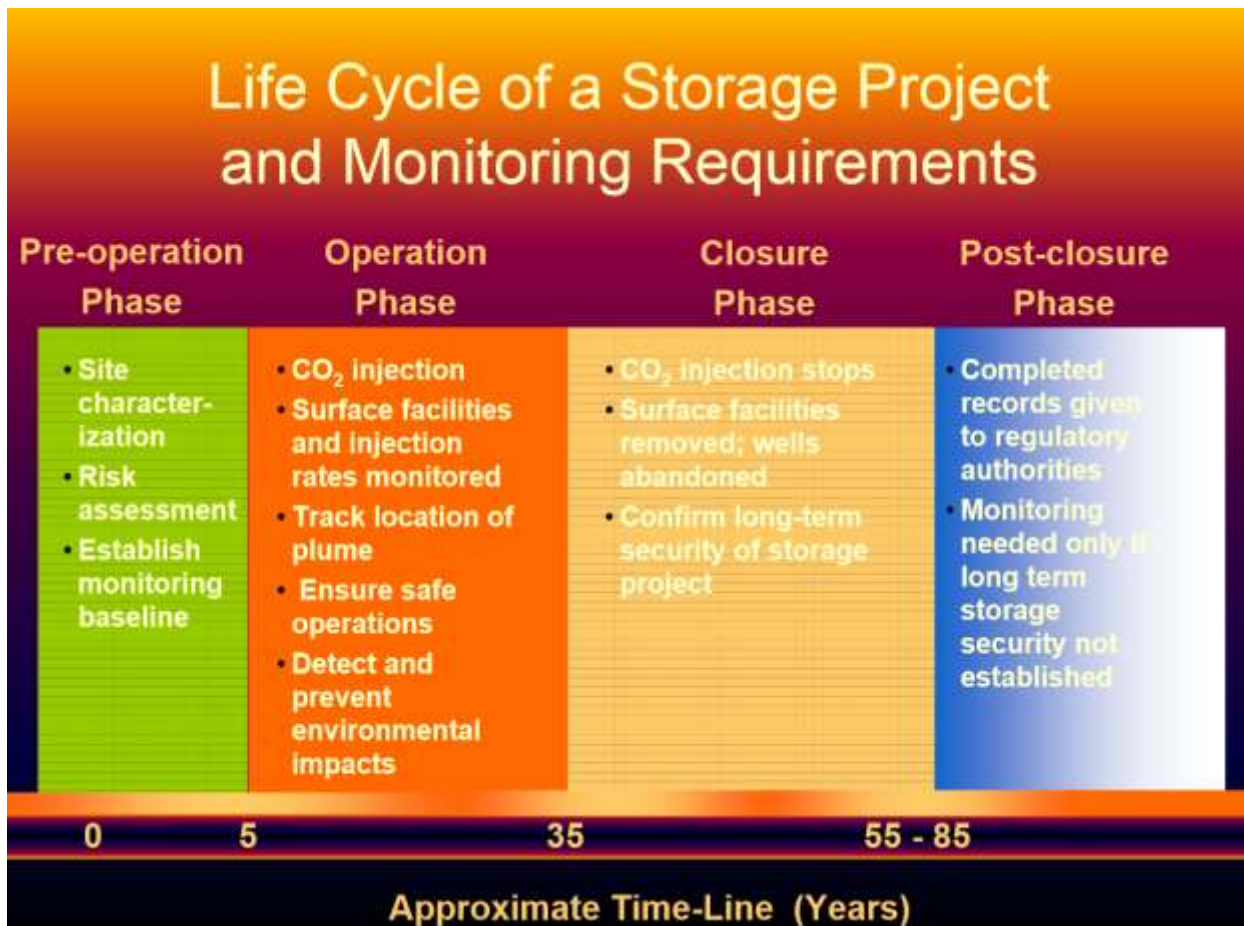


Figure 18 - Life cycle of a storage project and monitoring requirements (Office Fossil Energy, Dept of Energy)

During pre-operational phase, the operator could utilize well logs, wellhead pressure, formation pressure, injection and production rate testing, seismic survey, gravity survey, electromagnetic survey, and pressure and water quality about the storage formation.

During operations phase, the operator could utilize wellhead pressure, injection and production rates, micro-seismicity, produced brine's CO₂ ratio and pre-operational tools. When operations are completed, then operator could perform seismic surveys, wellhead pressure monitoring of the storage zone and aquifer zones above. Lawrence Berkeley National Laboratory recommends the use of computer modeling in all phases for comparing field results, and project planning (Office Fossil Energy, Dept of Energy)

2.2 CO₂ absorption reduces pressure buildup

During CO₂ injection into brine aquifers-containing residual and/or dissolved CH₄, three distinct regions develop: (1) a single-phase, dry-out region around the well-bore filled with pure supercritical CO₂; (2) a two-phase, two-component system containing CO₂ and brine; and (3) a two-phase, two-component system containing CH₄, and brine (Hosseini, Mathias, & Javadpour, 2012). An existing analytical solution was extended for pressure buildup during CO₂ injection into brine aquifers, by incorporating dissolved and/or residual CH₄. In this way, the solution additionally accounts for partial miscibility of the CO₂-CH₄-brine system and the relative permeability hysteresis associated with historic imbibition of brine and current drainage due to CO₂ injection and CH₄ bank development. Comparison of the analytical solution results with commercial simulator, CMG-GEM, shows excellent agreement among a range of different scenarios. The presence of residual CH₄ in a brine aquifer summons two competing phenomena, (1) reduction in relative permeability (phase interference), which increases pressure buildup by reducing total mobility, and (2) increase in bulk compressibility which decreases pressure buildup of the system. If initial CH₄ is dissolved (no free CH₄), these effects are not as important as they are in the residual gas scenario. Relative permeability hysteresis increased the CH₄ bank length (compared to non-hysteretic relative permeability), which led to further reduction in pressure buildup. The nature of relative permeability functions controls whether residual CH₄ is beneficial or disadvantageous to CO₂ storage capacity and injectivity in a candid brine aquifer.

2.3 Long term CO₂ storage possibility

Disposal and long-term sequestration of anthropogenic "greenhouse gases" such as CO₂ is a proposed approach to reducing global warming. Deep, regional-scale aquifers in sedimentary basins are possible sites for sequestration, given their ubiquitous nature. A mathematical sedimentary basin model, including multiphase flow of CO₂, groundwater, and brine, was used to evaluate residence times in possible aquifer storage sites and migration patterns and rates away from such sites in the Powder River Basin of Wyoming (McPerson & Lichtner, 2001). The model was also used to simulate CO₂ flow through fractures, to evaluate partitioning between fracture and rock matrix. These simulations provided insight regarding the ultimate propensity of permeability reductions versus permeability increases in the fracture zone associated with carbonate reactions. Regional-scale hydrologic properties, including the presence of fracture zones, were calibrated using surface heat flow data. The results suggest that, in general, long-term (~1000 years or more) sequestration in deep aquifers is possible, if subsurface structure and permeability are well characterized. However, additional risks are involved. In addition to CO₂ escape from sequestration aquifers into other aquifers or to the land surface, another environmental threat posed by subsurface sequestration is contamination by brines. The potential was evaluated for such unintended aquifer contamination by displacement of brines out of adjacent sealing layers such as marine shales. Results suggest that sustained injection of CO₂ may incur wide-scale brine displacement out of adjacent sealing layers, depending on the injection history, initial brine composition, and hydrologic properties of both aquifers and seals.

2.4 Pressure management scheme mitigated for large scale pressure build up

Carbon dioxide injection into deep saline formations may induce large-scale pressure increases and migration of native fluid (Cihan, Birkholzer, & Zhou, 2013). Local high-conductivity features, such as improperly abandoned wells or conductive faults, could act as conduits for focused leakage of brine into shallow groundwater resources.

Pressurized brine can also be pushed into overlying/underlying formations because of

diffuse leakage through low-permeability aquitards, which occur over large areas and may allow for effective pressure bleed-off in the storage reservoirs. Their study presents the application of a recently developed analytical solution for pressure buildup and leakage rates in a multilayered aquifer-aquitard system with focused and diffused brine leakage. The accuracy of this single-phase analytical solution for estimating far-field flow processes was verified by comparison with a numerical simulation study that considers the details of two-phase flow. They presented several example applications for a hypothetical CO₂ injection scenario (without consideration of two-phase flow) to demonstrate that the new solution is an efficient tool for analyzing regional pressure buildup in a multilayered system, as well as for gaining insights into the leakage processes of flow through aquitards, leaky wells, and/or leaky faults. This solution may be particularly useful when a large number of calculations needs to be performed for uncertainty quantification, for parameter estimation, or for the optimization of pressure-management schemes.

Figure 19 is an example of a typical CO₂ plume. The label on Figure 19 shows gas saturation and the high pressure zone where gas accumulates (on top of the reservoir).

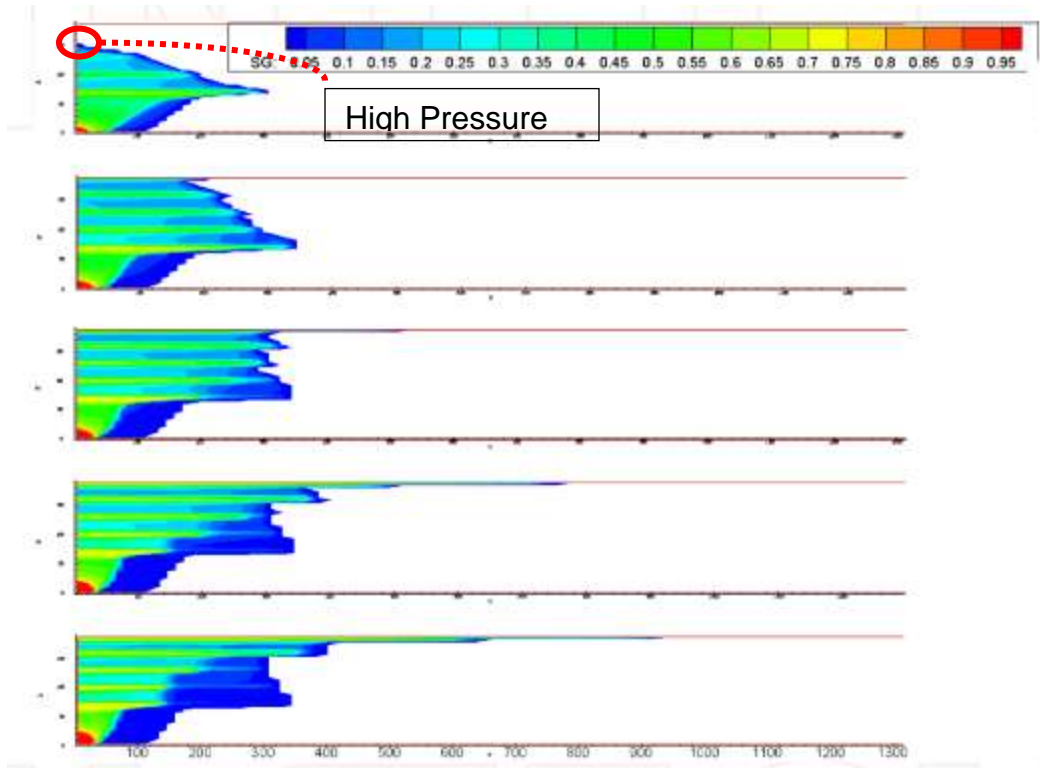


Figure 19 - Example of CO₂ Plume in Brine Aquifer (Water Saturation) (Agarwal & Zhang, 2014)

2.5 Maximum injection capacity

As the amount of CO₂ present in the atmospheres is increasing due to combustion emission, it is becoming more and more important to find ways to reduce greenhouse gas emissions. One of the ways to do that is through carbon sequestration. Saline formations (aquifers) provide viable destination for carbon sequestration. The storage potential in these reservoirs is estimated at several thousands of Giga Tons (Gt) of CO₂. Even though the capacity is substantial, the process of filling this capacity has a lot of challenges. Injection of large volumes within short period of time increases the formation pressure (which should be below fracture pressure) very fast. For each particular reservoir, injection capacity should be identified based on which CO₂ can be injected within a particular injection area and time. In order to achieve this, an in-depth sensitivity study needs to be done on the various reservoir parameters such as thickness, rock compressibility, permeability, porosity, reservoir temperature and pressure, aquifer fracture pressure, number and placement of injection's wells.

Injection in a limited drainage area has a risk of pore pressure increase. (Joshi, 2014)

The brine property for CO₂ dissolution is a utility to overcome spatial challenge. A limited drainage area also referred as a closed system could be modeled using no-flow outer boundaries depending on geological settings. Consequently, any pressurization of closed aquifer extends farther in the aquifer, leading to greater risk. (Anchliya, 2009) (Oruganti & Bryant, 2008).

Studies on the limit of storage were conducted by Anchliya (2009), van Engelenburg (1993), Schembre-McCabe et al. (2007), van der Meer and van Wees (2006), and Anchliya et al. (2012) where they have showed reservoir pressurization limitations in a limited aquifer. Figure 20 is an example of a study by Anchliya (2009), where it illustrates a difference between a model with limited aquifer volume (using a no-flow boundary) and a model for an open aquifer (using a constant-pressure boundary). The pressure upper limit was maintained by not letting injection pressure exceed the fracture pressure.

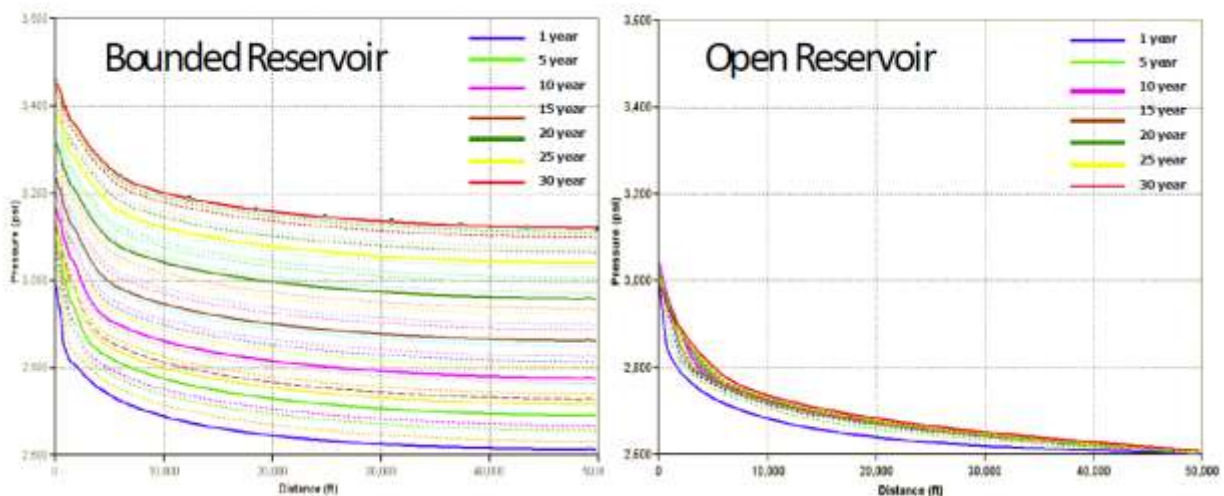


Figure 20 - Bounded vs Open Reservoir (Anchliya, 2009)

2.6 Modelling CO₂ plume behavior

Studies show that bottom injection of CO₂ at high rates for a slight dipping aquifer has a significant impact on the total amount of CO₂ injected, dissolved and trapped in the aquifer. (Lam, 2010) Bottom completion and high rate injection allow more CO₂ to be injected and the plume to come into contact with larger amounts of brine due to buoyancy effect and larger distribution of the plume, which will enhance solubility and residual trapping mechanisms. Temperature and pressure have a slight impact on the solubility of CO₂. The results also show that reservoir permeability has a large impact on the dissolved and trapped CO₂, as it facilitates the lateral migration of CO₂ enhancing dissolution into the brine.

2.7 Using modeling to verify feasibility of CO₂ Storage

Studies by Lam (2010), Moreno (2013), and Burton (2008) used a commercial reservoir simulator, CMG, to model the feasibility of CO₂ sequestration in areas of interest.

Utilization of a variety of geological formations has been identified as an alternative to counter the impact of the emissions. CO₂ sequestration refers to the capture and long term storage of CO₂. In order to properly assess the viability of CO₂ sequestration in a geological formation as a “safe” and long term solution, several questions have to be answered: Is this formation capable of trapping the amount of CO₂ to be injected? Does the seal of this formation (the cap rock) have the proper characteristics to ensure a low risk structural trapping? Which trapping mechanisms are present and what kind of interactions (geochemical, geomechanical, etc.) are expected as the CO₂ is injected? These questions are addressed and evaluated in the CO₂ storage project for a deep saline aquifer located in the Citronelle field in Mobile, Alabama. A full field reservoir model was built using information from the actual field site and reservoir scale simulations are performed. Initially, they evaluated different trapping mechanisms (residual or capillary trapping, solubility, mineral and structural trapping) and their contribution to the storage process. Quality and integrity of the cap rock, representing the ability to trap “mobile” CO₂ structurally, was studied to assess the potential risk of leakage. Additionally, impact of the nature of the edge boundary conditions on the

pressure and saturation distribution throughout the reservoir was studied. Finally, in order to ensure the long term storage of the CO₂, a Post-Injection Site Care (PISC) study was performed. Pressure stabilization time was assessed within acceptable thresholds, allowing for possible post-stabilization leakage of brine or CO₂ detection. (Moreno, 2013)

2.8 Mt. Simon Sandstone for CO₂ storage

Geological carbon storage (GCS) capacity for Cambrian Mt Simon Sandstone is in excess of 86 billion metric tons of CO₂, according to DOE/NETL Carbon Sequestration Atlas of the US and Canada (CSAUS&C). There are many studies focusing on estimates in the Mt Simon and the feasibility of GCS for a large, stationary emissions source. Initial estimates of GCS potential in the Mt Simon Sandstone suggests that storage capacity may exceed hundreds of years of annual stationary CO₂ emission. Since 2003, DOE collaborated a comprehensive study of the Illinois Basin CO₂ storage potential in the search for a reservoir-seal system that provides capacity, injectivity, and containment. The initial regional characterization showed that the Mt. Simon Sandstone offered sufficient depth, thickness, and porosity to contain CO₂ and the overlying rock unit, the Eau Claire Formation, provided the necessary seal for safe and effective long-term storage (Figure 21). Within the Illinois Basin, three thick shale units function as major regional seals. The lowermost and primary seal, the Eau Claire, has no known penetrating fractures. According to CSAUS&C, the Midwest Geological Sequestration Consortium's (MGSC) Illinois Basin–Decatur Project (IBDP) was a field project in collaboration of the MGSC, the Archer Daniels Midland Company (ADM), Schlumberger Carbon Services, and other subcontractors to inject 1 million metric tons of anthropogenic carbon dioxide (CO₂) into a saline reservoir, the Mt. Simon Sandstone, in Decatur, Illinois. The CO₂ injection began on November 17, 2011, at a nominal rate of 1,000 metric tons per day. After 3 years of operation, the injection goal was met in November 2014. Capacity, injectivity, and containment potential have met and/or exceeded pre-injection expectations. All three major seals are laterally extensive and from subsurface wireline correlations appear to be continuous within a 100-mile radius of the site. There were no mapped regional faults or fractures within a 25-mile radius of

the proposed site. 2-D and 3-D seismic reflection data were acquired near the site to identify the presence of faults and geologic structures in the vicinity of the injection well site.

Mt. Simon's gas storage viability has been assessed with ten different research projects, and thoroughly characterized using data collected from well logs, seismic volumes, and core analyses, and interpretation of the injection and verification wells (in the Mt. Simon and Eau Claire). The IBDP's Mt. Simon was 1,506 feet-thick in the intervals of 7,025 to 7,050 feet and 6,985 to 7,015 feet. The porosity is in the range of 18 to 25 percent and the permeability is in the range of 40 to 380 millidarcy (mD) over both intervals. (National Energy Technology Laboratory, Department of Energy, 2015) (Barnes & Bacon, 2008)

The rocks of the aquifer system are exposed in large areas of northern Wisconsin and eastern Minnesota, adjacent to the Wisconsin Dome, a topographic high on crystalline Precambrian rocks. From this high area, the rocks slope southward into the Forest City Basin in southwestern Iowa and northwestern Missouri, southeastward into the Illinois Basin in southern Illinois, and eastward toward the Michigan Basin, a circular low area centered on the Lower Peninsula of Michigan. The configuration of the top of the Mount Simon sandstone (that forms the Mount Simon aquifer) is shown in Figure 21. (U.S.

Geological Survey, 2009)

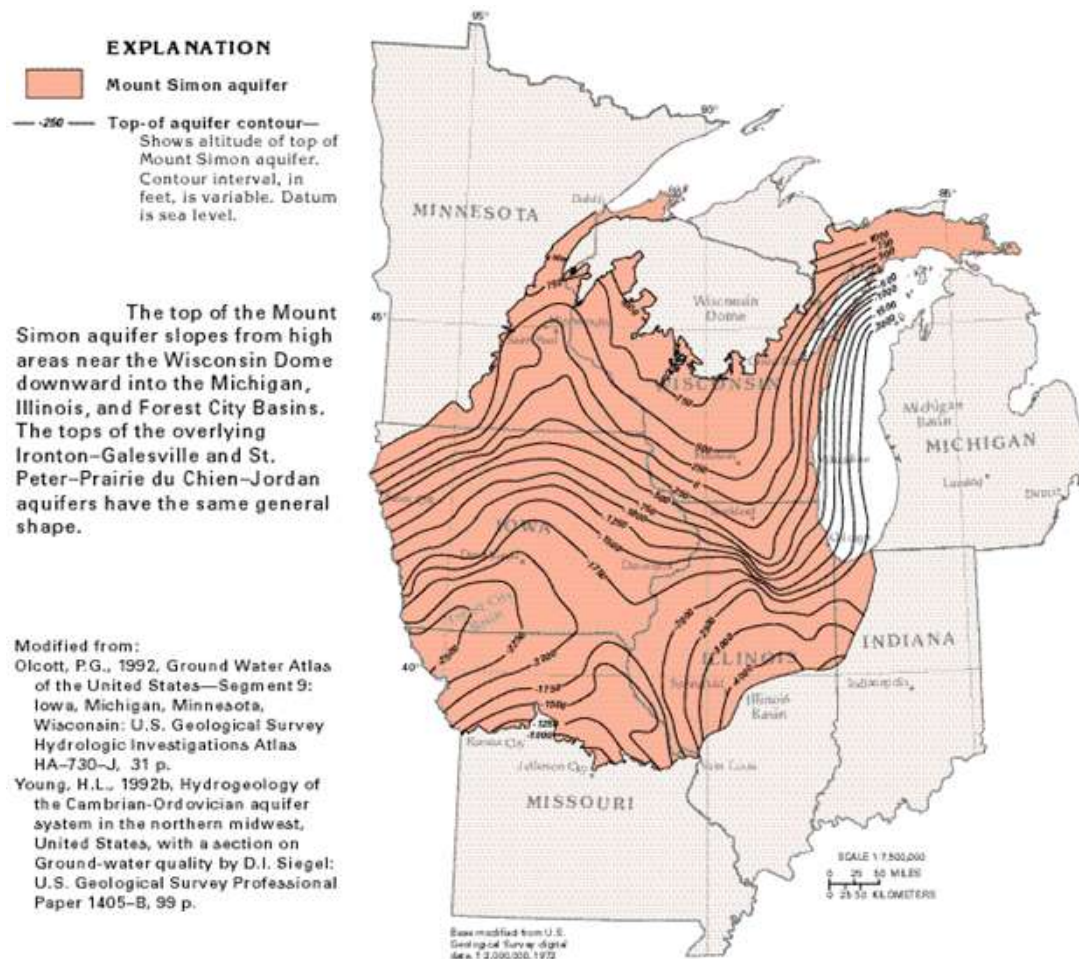


Figure 21 - Mount Simon Aquifer - Contour Map (U.S. Geological Survey, 2009)

Figure 21 shows that the aquifer representing the lower part of the Cambrian-Ordovician aquifer system is buried to depths of 2,000 to 3,500 feet below sea level in the structural basins. Also, there are configurations of two overlying aquifers (Ironton-Galesville and St. Peter-Prairie du Chien-Jordan) that are similar to that of the Mount Simon aquifer. The deeply buried parts of the aquifer system contain saline water (which are ideal for CO₂ storage).

The chemical quality of the water in large parts of the aquifer system is suitable for most uses. The water is not highly mineralized in areas where the aquifers crop out or are buried to shallow depths, but mineralization generally increases as the water moves downgradient toward the structural basins. The distribution of dissolved-solids

concentrations in the St. Peter-Prairie du Chien-Jordan aquifer shows this increase (Figure 22).

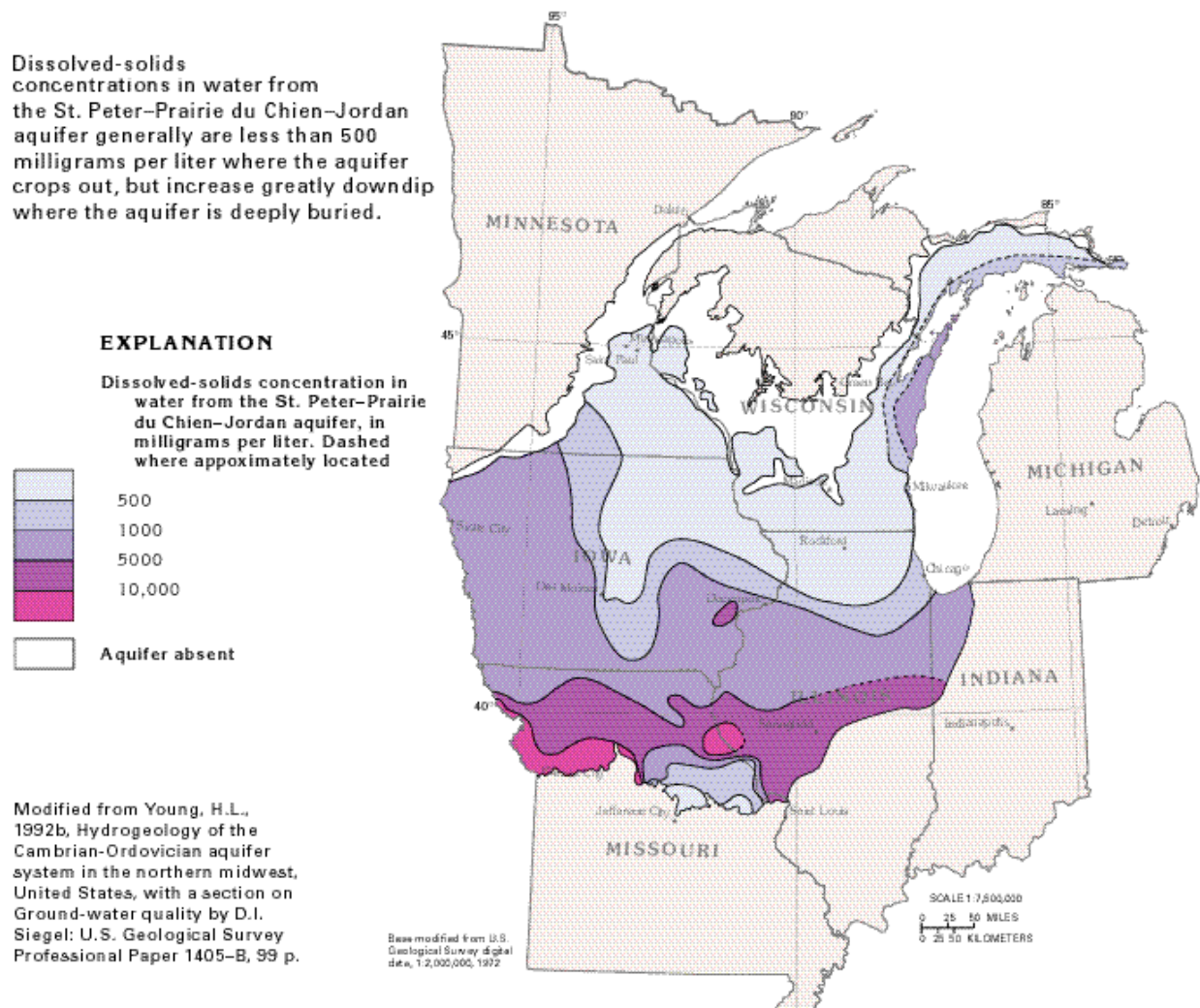


Figure 22 - Contour map showing dissolved-solids concentrations of St. Peter-Prairie du Chien-Jordan Aquifer (U.S. Geological Survey, 2009)

In Figure 22, the St. Peter-Prairie du Chien-Jordan Aquifer is at or near the land surface in southeastern Minnesota, northeastern Iowa, southern Wisconsin, the Upper Peninsula of Michigan, and central Missouri. It contains water with dissolved-solids concentrations of less than 500 milligrams per liter, the limit recommended for drinking water by the U.S. Environmental Protection Agency. In the deeper portions of the aquifer, the dissolved solids concentrations increase to more than 1,000 milligrams per

liter in western and southern Iowa, north-central Illinois, and along the northwestern shore of Lake Michigan. In parts of Missouri, where concentrations are greater than 10,000 milligrams per liter the ground-water movement is almost stagnant. The data for dissolved solids in water from the Mount Simon aquifer shows the same trends as those in water from the St. Peter-Prairie du Chien-Jordan aquifer.

(U.S. Geological Survey, 2009).

2.9 Application for a Power Plant

A modern commercial 500-MW coal power plant generates about 3 million metric tons of CO₂ per year. This project assumes of the emission captured will be refined/produced to CO₂ and will be utilized to with the intent for storage as a mitigation placed under conditional approval under the EPA permit. This type of study will focus on the aquifer pore volume required to store the CO₂, the needs for surface area and number of wells if the plant life is assumed to be 50 years.

As indicated in the literature search U.S. Department of Energy (2011) atlas CO₂ storage proposes a large variety of brine aquifers as CO₂ storage candidates, along with few field projects. In a situation where a power plant taking advantage of aquifer like Mt. Simon with characteristics like porosity greater than 10%, permeability greater than 20 md, and thickness more than 100 ft. A CO₂ injector well could store more than 39 million bbl. in a 50-year period, with volumetric injection rate of 2,000 BPD or more. The details to determine the aquifer area to inject depends on many characteristics, but this study leads to develop understanding in making judgement on how to manage pressure at a local level in a sweep like pattern with four producers and one injector. Experience with managing pressure in natural gas storage indicates that it is not possible to recover all of the stored gas if the reservoir is pressurized well above the initial reservoir pressure. This has been interpreted as an indication that some of the stored gas has leaked out or trapped within the reservoir. This trapping may occur for CO₂ storage in an aquifer as indicated by Shen et. al. (2015).

Some of the elements that could improve storage viability will be overburden thickness, greater aquifer thickness reduces the required aquifer area by increasing both injectivity and storage potential per unit area, water salinity.

2.9.1 Handling Produced Brine

When assessing environmental impact from produced brine, handling and utilization is a great problem to have yet to be addressed by conventional technology. Currently all modern methods to dispose or utilization has created environmental hazards that can't be addresses. There are some design concepts that look into alternatives but none of them are utilized on a large industrial scale.

Produced water treatment would be costly when utilizing conventional methods (like desalination and treatment technologies). There may be new alternatives available, like solar-driven technology for freshwater production (Khatib & Verbeek, 2002), advanced vapor-compression desalination technology (Ruiz, 2005), and coupling carbon dioxide sequestration and extracted water for treatment and use in a power plant (National Energy Technology Laboratory, U.S. Dept of Energy, 2008) may be feasible. (Anchliya, 2009) As sources of fresh water depletes (like North America), then the treated water from brine could help with the demand for water needs commercial and residential use.

2.9.2 Permitting availability & costs and tax relief

With substantial costs from field operations (well development), CO₂ and brine management, many people look over main challenges: the difficulty for permitting new sites or maintaining existing sites, overcoming minimizing environmental impact and air quality issues which helps the operators in attaining social license from regulators and local communities (along with economic benefits).

Since now global warming has reached the public and regulators awareness or vigilance, by placing such mitigations on permits could allow convenience in permitting, and allow economic benefits from tax reliefs and incentives. By pursuing infrastructure to store CO₂, the operator could utilize local/domestic oil and gas industry when the economic incentive allows, to execute simultaneously joint venture opportunities with less effort. By leading new initiatives in this field, there may research funds available, and new sources of funds could be created from other government bodies that support green initiatives.

2.9.3 Handling of CO₂

Handling of CO₂ can be expensive, but the indirect incentives are available as discussed in the last section. One of the considerations for CO₂ handling costs are that higher injection pressure could induce higher costs making an unnecessary operational risks. This will be indirectly considered when seeking for final recommendations.

2.10 CO₂ Behavior and it's Formulation

This section presents formulas that for modeling CO₂ behavior.

2.10.1 Brine & CO₂ solubility behavior

The methodology selected for the study incorporates both mobile and immobile supercritical CO₂ to change into aqueous phase via the dissolution process. When denser CO₂-saturated water forms then it should sink to the bottom of the formation (Shen et. al., 2015). The convection effect will force the fresh water to replace the CO₂-saturated water with high solubility dissolution, forming large impact.

CO₂ solubility in brine is calculated by solving the equality of fugacities of CO₂ in the gas and aqueous phase (Nghiem L. S., 2009). Upon injection, CO₂ dissolves in the aqueous phase, and it can be represented by the following chemical reaction:

$$f_{CO_2,g} = f_{CO_2,aq} \text{ -----(1)}$$

In equation 1, $f_{CO_2,g}$ is the gas fugacity calculated from Peng and Robinson's cubic equation of state (Peng & Robinson, 1976) and $f_{CO_2,aq}$ is the aqueous phase fugacity calculated from Henry's law.

$$f_{CO_2,aq} = y_{CO_2,aq} \times H_{CO_2,aq} \text{(2)}$$

In equation 2, $H_{CO_2,aq}$ is Henry's constant for CO₂ solubility in brine and $y_{CO_2,aq}$ is the mole fraction of CO₂ in brine.

To calculate the Henry's law constant, correlations are derived using formulas (by (Harvey, 1996), (Garcia, 2001), and (Bakker, 2003)) to predict accurate CO₂ solubility ((Nghiem L. S., 2009) (Nghiem, et al., 2009), (CMG (Computer Modelling Group), 2011), & (Shen et. al., 2015)). The following paragraphs discusses the Harvey (1996), Garcia (2001), and Bakker (2003) formulas.

Gas solubility depends on the salinity of the aqueous phase. Gas solubility increases as pressure increases and decreases as temperature or salinity increases (Nghiem L. S., 2009) (Nghiem, et al., 2009). Harvey (1996) published correlations for Henry's constant of many gaseous components including CO₂. The solubility of light gases normally decreases with increasing salinity; this phenomenon is referred to as the salting-out process.

$$\ln(H_i^S) = \ln(p_{H_2O}^S) + A(T_{r,H_2O})^{-1} + B(1 - T_{r,H_2O})^{.355} (T_{r,H_2O})^{-1} + C[\exp(1 - T_{r,H_2O})](T_{r,H_2O})^{-0.41} \dots\dots\dots(3)$$

The followings are definitions for equation 3.

H_i^S = Henry's constant for component i at the saturation pressure of H_2O * $p_{H_2O}^S$
 H_2O in MPa at T(K)

T_{c,H_2O} = Critical temperature of H_2O (°K)

T_{r,H_2O} = Reduced temperature of H_2O (°K)

$A = -9.4234$

$B = 4.0087$

$C = 10.3199$

The saturation pressure of H₂O at T is calculated from the Saul and Wagner (1987) correlation. The Henry's law constant at p and T is then given by:

$$\ln(H_i) = \ln(H_i^S) + \frac{1}{RT} \int_{p_{H_2O}^s}^p \bar{V}_i dP \quad \dots\dots\dots(4)$$

Where \bar{V}_i is the partial molar volume of component i in the aqueous phase. For CO_2 , the correlation by Garcia (2001) is used:

$$\bar{V}_{CO_2} \left(\frac{cm^3}{mol} \right) = 37.51 - 9.585 * 10^{-2}T + 8.740 * 10^{-2}T^2 \quad \dots\dots\dots(5)$$

The salting-out coefficient is defined by the following relation between Henry's constant in pure water and in brine:

$$\ln \left(\frac{H_{salt,i}}{H_i} \right) = k_{salt,i} * m_{salt} \quad \dots\dots\dots(6)$$

In the equation above, $H_{salt,i}$ is Henry's constant in brine solution at i , H_i is Henry's constant at zero salinity at i , $k_{salt,i}$ is salting-out coefficient at i , m_{salt} is molality of the dissolved salt (mol/kg)

Additionally, for CO_2 and CH_4 , Bakker (2003) gives the following correlations for the salting-out coefficients:

$$k_{salt,CO_2} = 0.11572 - (6.0293 * 10^{-4}T) + (3.5817 * 10^{-5}T^2) - (3.7772 * 10^{-9}T^3) \quad \dots(7)$$

2.10.2 Structural trapping

The critical pressure and critical temperature of CO_2 are 1070 psi and 87.8 °F, respectively. When CO_2 is injected into an aquifer deeper than 2625 feet, it is in supercritical state (Bachu, 2003). The density of the injected supercritical CO_2 is less than half of lower than saline formation water at reservoir conditions of approx. 3077 psi and 150 °F. Thus the injected CO_2 's buoyancy will drive the fluid upwards behavior

similar to supercritical CO₂ in an aquifer (Nghiem L. S., 2009) (Nghiem, et al., 2009). In order to develop a storage reservoir a caprock is needed on top of the aquifer to serve as a structural trapping mechanism to prevent mobile CO₂ from leaking out (Bachu, 2003).

2.10.3 Residual Gas Trapping

One of the important process of trapping CO₂ is Residual Gas Trapping. This mechanism converts CO₂ into an immobile phase in the pores via the capillary effect and increasing wetting-phase saturation (imbibition). The imbibition usually occurs at the back of the plume's supercritical CO₂ after enough molecules accumulate (top of the plume). The Land's model (Land 1968) was used in this study to calculate the residual gas (CO₂) saturation, as follows (Nghiem L. S., 2009) (Nghiem, et al., 2009):

$$S_{gt}(S_{gi}) = \frac{S_{gi}}{1 + CS_{gi}} \dots\dots\dots(8)$$

$$C = \frac{1}{S_{gt,max}} - \frac{1}{S_{g,max}} \dots\dots\dots(9)$$

In equations 8 and 9, S_{gt} is residual gas saturation corresponding to S_{gi} , S_{gi} is the gas saturation value (S_g) when the shift to wetting-phase saturation occurs, C is Land's coefficient, $S_{g,max}$ is the maximum gas saturation, $S_{gt,max}$ is the maximum residual gas saturation.

Figure 23 is a graph of gas saturation - S_g vs. Gas relative permeability - k_{rg} . where drainage gas saturation curve reverses and decreases. (Shen et. al., 2015)

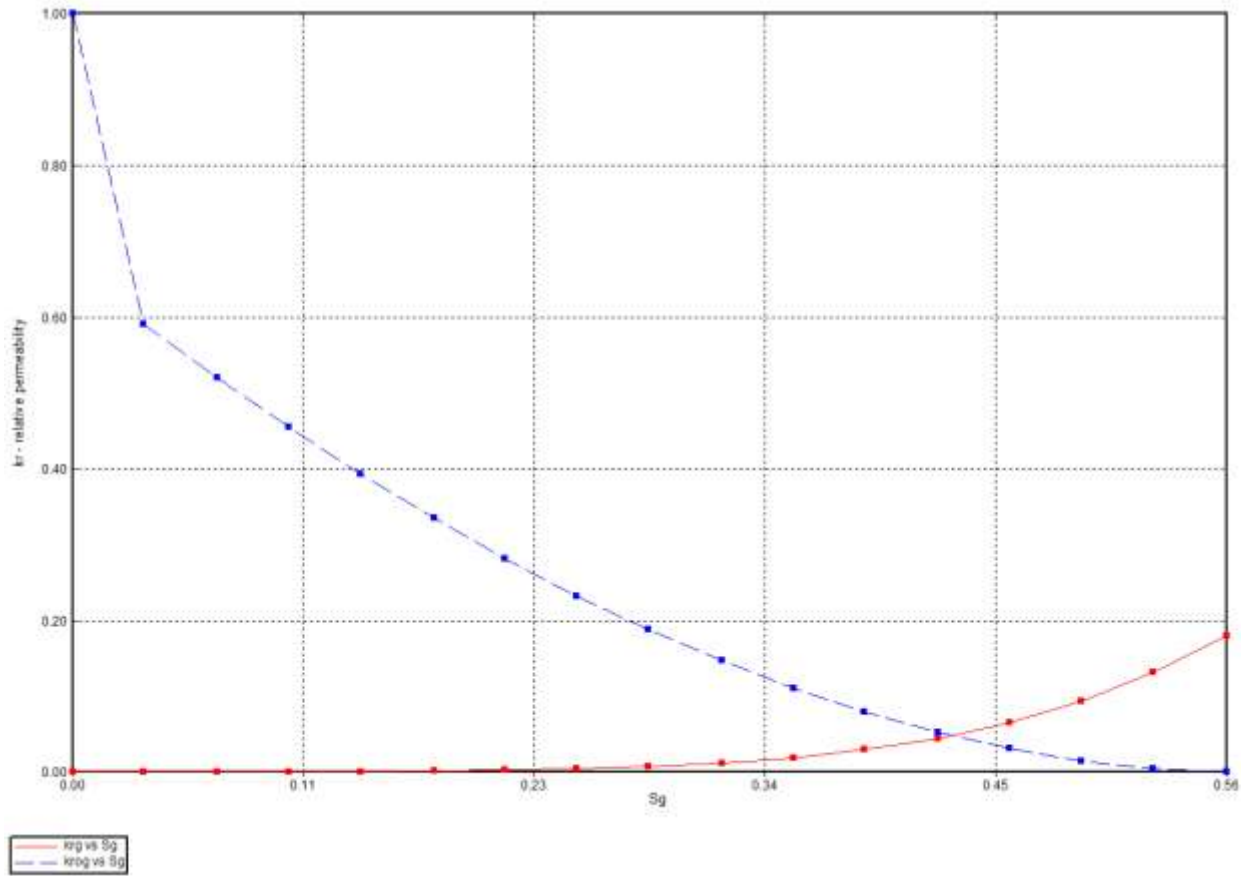


Figure 23 - Gas Saturation vs. Gas Relative Permeability (Shen et al. 2015)

2.10.4 Chemical reactions

When CO₂ mixes with water, it creates H⁺ and HCO₃⁻ or HCO₃²⁻ ions as a chemical reaction. Chemical equilibrium reactions were used in this study to model the fast and reversible intra-aqueous chemical reaction (ionic trapping mechanism) (Nghiem L. S., 2009) (Nghiem, et al., 2009). The chemical equilibrium reactions were governed by chemical equilibrium constants ((Bethke, 1996); (Nghiem L. S., 2009), & (Nghiem, et al., 2009)), as shown here:



When $CO_{2(aq)}$ gets dissolved, then it is formulated to equation 5.

$$Q_\alpha - K_{eq,\alpha} = 0, \alpha = 1, \dots, R_{aq} \dots\dots\dots(12)$$

In equation 12, the R_{aq} is the constant for intra-aqueous chemical equilibrium reactions, the $K_{eq,\alpha}$ is the chemical equilibrium constant for the aqueous reaction α , and the Q_α is the activity product for the aqueous reaction α .

The constant, $K_{eq,\alpha}$ is studied by Kharaka et al. (1988) and Delany and Lundeen (1990) for several aqueous reactions. The activity product Q_α is calculated by (Nghiem L. S., 2009) (Nghiem, et al., 2009):

$$Q_\alpha = \prod_{k=1}^{n_{aq}} a_k^{v_{k,\alpha}} \dots\dots\dots(13)$$

In the equation above, the n_{aq} is the number of aqueous components, the a_k is the activity for variable k , and the $v_{k,\alpha}$ is the stoichiometry coefficients of the chemical equilibrium reactions.

The variable a_k is the product of the molality and the activity coefficient of variable k . The *B-dot* models utilized to calculate the ionic activity coefficients performed by Bethke (1996) and Pitzer (1987) (Nghiem L. S., 2009) (Nghiem, et al., 2009)).

Geochemical reaction occurs between minerals and aqueous components, and are reversible. The changes in the moles of minerals through dissolution or precipitation can be estimated after the geochemical reaction occurs (Shen et. al., 2015). The dissolution or precipitation of minerals follows the Nghiem et al. (2009) method adoption of Bethke (1996) study and given as:

$$r_\beta = \widehat{A}_\beta k_\beta \left(1 - \frac{Q_\beta}{K_{eq,\beta}} \right), \beta = 1, \dots, R_{mn} \dots\dots\dots(14)$$

In the equation above, the r_β is the reaction rate for a given mineral β , the R_{mn} is number of mineral reactions, the \widehat{A}_β is reactive surface area, the k_β is rate constant of mineral reaction, and the Q_β is activity product of the mineral reaction.

2.11 Comparison with other studies

Most of the modeling work has assumed infinite capacity of the target aquifer and that injected CO₂ will displace the water in the pore space. Various authors [(Baklid, 1996); (Xu et. al., 2003); (Kumar, 2004); (Nghiem L., 2004); (Sengul, 2006); (Izpec, 2006); (Burton, 2008); (Oruganti & Bryant, 2008)] have simulated the multiphase physics and thermodynamics of CO₂ injection using a constant-pressure outer boundary on their models. Generally, when developing a field wide study a constant-pressure boundary exists only if the aquifer outcrops to the atmosphere, or at the bottom of a surface water body (ocean, river, lake). Such systems are frequently referred to as “Open” systems. Authors like Pruess et al. (2003) tried to model the aquifer as effectively infinite, because aquifers are known to extend from several acres to thousands of miles wide and from a few feet to hundreds of feet thick. Orr (2004) and Noh et al. (2007) emphasize the analogies of sequestration operation with EOR, thus treating CO₂ injection as a steady-state displacement process. (Anchliya, 2009)

However, these modeling approaches neglect to optimize pressure management the fact that commercial scale sequestration projects, and will have multiple injectors sequestering CO₂ at constant injection rates. And in some cases could be adjacent to other power plants in the area. Even in the case of an effectively infinite or an open aquifer, the drainage area will be limited by feedback from the nearest injectors and water will not move out of the limited drainage area. Hence, the drainage area available to each well will be limited and the claim that the pore water will be pushed away to create space for the injected CO₂ may not be applicable in that case. Therefore, the conclusions drawn from constant-pressure boundary modeling approaches may not be very practical and applicable for large distance injector-producer sequestration projects.

3 Objective:

The objective of this thesis work was finding ways to increase the storage injection capacity of a brine aquifer based on reservoir parameters and to optimize the well placement by identifying and developing analytical and numerical tools. The research also focused on conducting a sensitivity analysis on these parameters in order to find out the optimal injection scenario to obtain the amount of maximum CO₂ sequestration in a reservoir. This study can help the CO₂ sequestration capacity predictions and screening of suitable reservoirs based on technical and economic criteria. In order to derive the injection capacity of a reservoir based on the reservoir parameters, two analytical models of multiple well injections were studied: i) Single-phase (Brine injection in a brine reservoir and ii) Two phase model (CO₂ injection in a brine reservoir). In both cases, the aim was to analyze the pressure build-up and discuss and compare results based on numerical simulations. Although analytical modeling is less accurate (compare to numerical) and restricted to vertical well injection it allows large number of realizations for sensitivity analysis to find significant patterns of the process and reduces the number of numerical simulations needed at final stages of optimization. Analysis was done by considering infinite acting, homogenous, isotropic and isothermal reservoir condition. The Ei-function approximation method was used to simulate results on pressure profile across the reservoir. Once a validated model was obtained, the CO₂ injection capacity of saline aquifers was increased by applying the multiple well injection strategy. This was done by determining the well interferences based on superposition principle and mapping the pressure build-up profile in the reservoir. Various approaches were used to get maximum injection capacity.

In this study, the injected pressure was an independent variable selected to find minimum distance required to displace the CO₂. It was a good constituent to consider when leading a recommendation for a minimal pressure increase above hydrostatic pressure so that the injection could be robust, avoiding unwanted reservoir damage. If additional CO₂ needs to be stored then additional injection wells could be drilled along with four production wells.

The objective of this research was also to study the impact of the aquifer properties and operational parameters to understand the CO₂ plume behavior and their contribution to various trapping mechanisms. Such study will help minimize uncertainty in estimates of the capacity and injectivity of CO₂. In order to accomplish these objectives, selection of a set of representative characteristics for an aquifer as base case was first modeled. Next variation of injection schemes and rates were modeled to evaluate CO₂ plume behavior and the potential of CO₂ storage volume. In addition, this study demonstrated the influence of different trapping mechanisms due to variation of reservoir properties and dip angle.

4 Methodology

The performance of the reservoir was investigated using CMG software. CMG's GEM greenhouse gases (GEM GHG) option was applied to set up the base case simulation parameters used throughout this study. GHG, the new additional module from CMG, is an adaptive tool for carrying out compositional simulation for sequestration of CO₂ and other greenhouse gases in saline aquifers. The modeling of CO₂ storage in saline aquifers involves the solution of the component transport equations, the equations for thermodynamic equilibrium between the gas and aqueous phases, and the equations for geochemistry. The latter involve reactions between the aqueous species and mineral precipitation and dissolution. They are based on an adaptive implicit formulation, which helps in deciding for each grid and each time step whether to use fully implicit or explicit solution methods. During subsequent simulation runs, blocks may be switched to explicit if an adaptive/implicit formulation and a stability-switching criterion is used. Consistent of the usual capability of other simulators, CMG's GHG simulator support modeling with mass transfer of components into different phases (solubility) and aqueous phase density and viscosity correlations.

4.1 Model Design

A 3D homogeneous aquifer with a constant-pressure injector and constant-rate producer was simulated as the base case. The GEM simulator was used for prediction of reservoir behavior when CO₂ was injected for 50 years.

4.2 Grid description

The model dimensions were 50550x50550x650 feet for a Cartesian grid system consisting of 170X170X13 blocks as shown in Figure 24. The aquifer boundary conditions were no flow as an open boundary with a caprock on top with a 50 feet thickness.

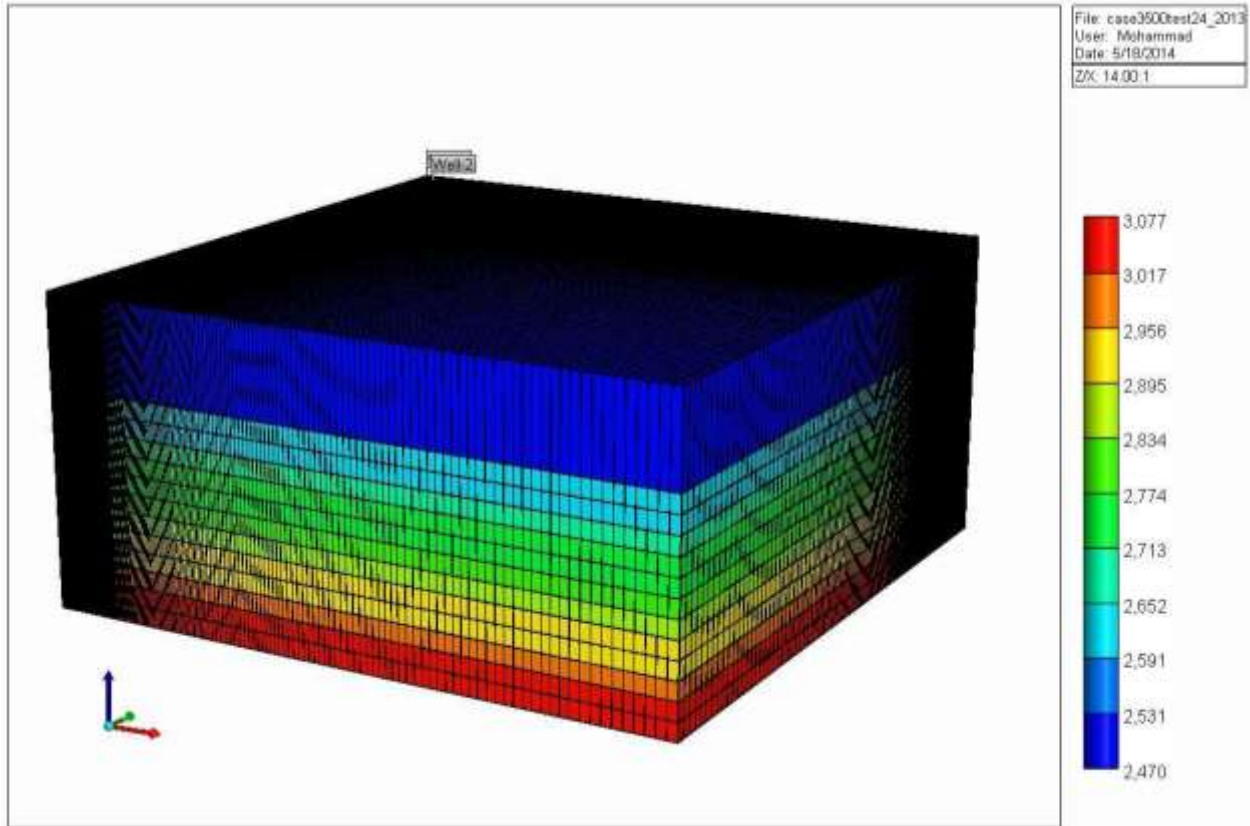


Figure 24 - 3D Grid used in the model

Figure 24 shows a 3-D image of the grid generated for the simulation study. The grid was generated with higher resolution near the zone of interest, where sequestration was taking place. In horizontal direction, the length and width were assigned for every 10 cubes, in the following order: 50', 60', 75', 90', 105', 125', 150', 180', 215', 255', 305', 365', 435', 520', 625', 700', 800'. In vertical direction, the reservoir has a height of 600 feet that are divided into 12 layers, with additional layer of 50 ft. of sealing caprock.

4.3 Description of the reservoir characteristics

This research utilized CMG modeling software throughout the study. In modeling, as a baseline to mimic the conditions, an initial first cube was created with no boundary effect. In order to assess the system closely, the model was designed with higher resolution (higher number of blocks) at the zone of interest than towards the outskirts.

The design of the model was setup based on the assumption of 5-spot spacing pattern (Figure 25), as an ideal for field applications. This technique was represented by selecting a quadrant area, where injector well was placed at a corner block, and producer well's spacing were resulted based on the injected volume. Due to symmetry, the quadrant represents a mirror image for the rest of the field.

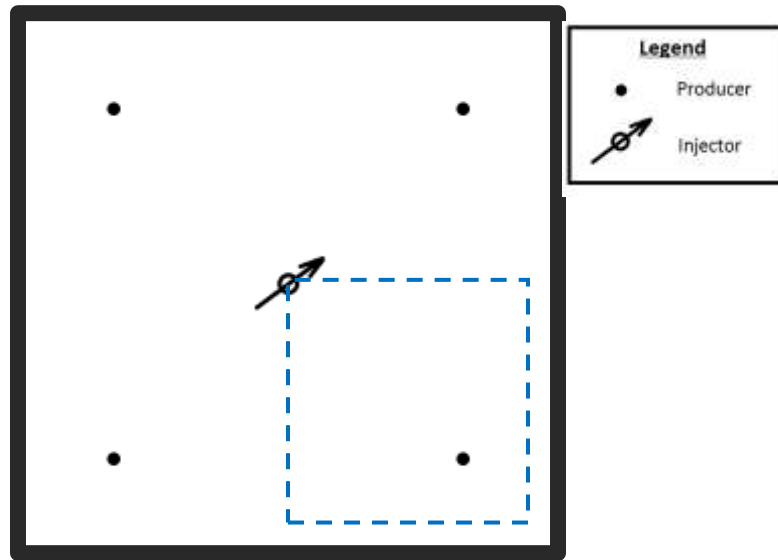


Figure 25 - 5-spot spacing

The reservoir characteristics utilized for developing the model are listed in Table 1 below.

Table 1 - Reservoir Characteristics

| | |
|-----------------------------|--------------------------------------|
| Porosity | 10 % |
| Permeability | 20 md |
| Rock Compressibility | $3e^{-6}$ 1/psi |
| Pressure at top of the seal | 2700 psi |
| Reservoir temperature | 132°F @ 6000 ft. thru 150°F 7500 ft. |
| Water Compressibility | $2.99e^{-006}$ 1/psi |

4.4 Well location selections

In order to determine the optimum location of injection and production wells, the following approach was used:

4.4.1 Vertical location

Three scenarios were considered in terms of location of bottom hole for injection and production wells. Option one and two considered both wells at the same level as either at the top or at the bottom. In these two cases where wells are placed at the same level, there was a short distance between two wells that reduced the breakthrough time during the simulations. In the third case scenario, injection well was considered at the bottom and the producing well at the top layer which provided greater distance between two wells. Additionally, injection at the bottom layer required high injection pressures and helped to inject more volumes of CO₂ due to its compressibility. This also minimized single phase of CO₂ horizontal area, and swept out enough brine before plume expands vertically in a pancake shape.

4.4.2 Optimizing well location horizontally

Horizontally, the injector well was selected at block #1 on the x-plane, and block #1 on the y-plane calling the x-y plane as a horizontal location. The injector location was noted as 1,1 in the model's image. While the injector location stayed the same for all of the runs, the production well moved closer or farther away in X, Y direction. For all locations of production well, x was equal to y. The production well's desired location was at a distance where only brine was produced while having the location as close as possible to the injector. For example, Figure 26 shows the top view of locations for injection and production wells where block #40 represented production well at (40, 40) on the x-y plane.

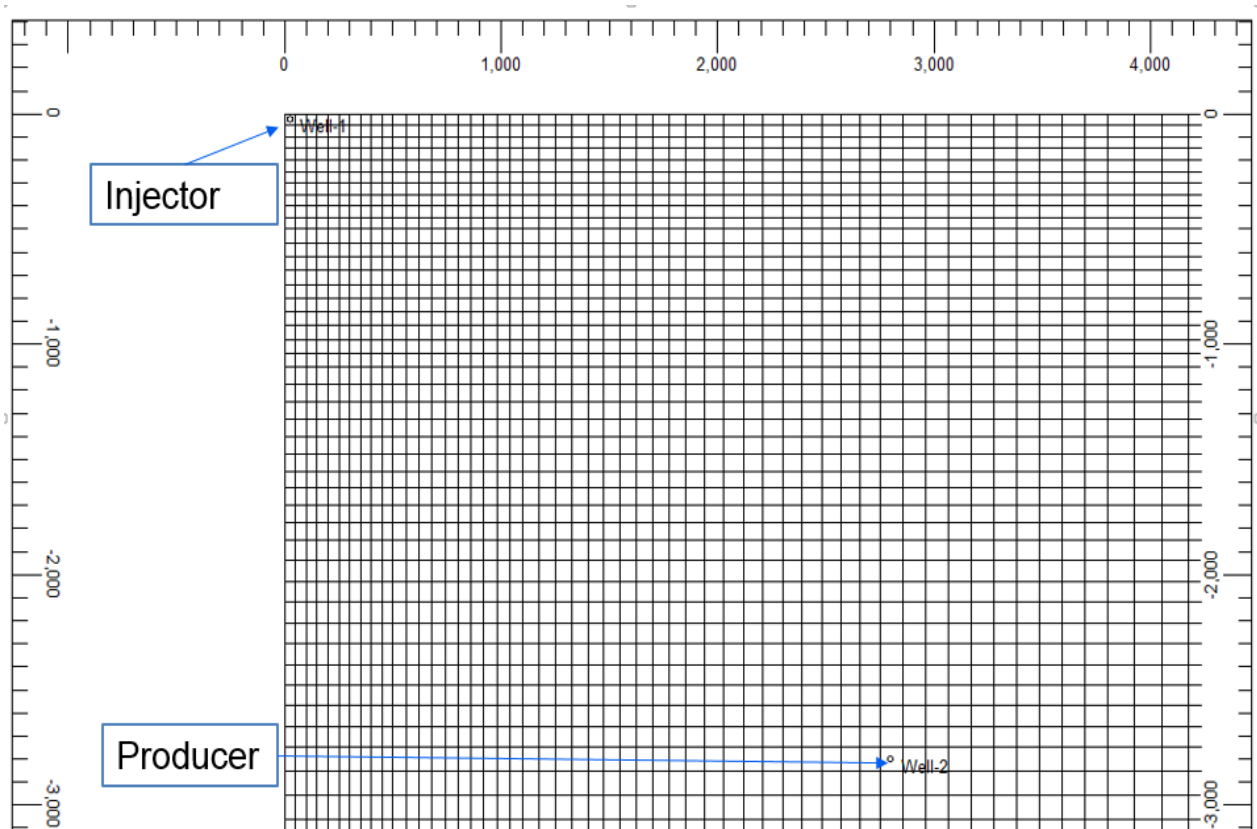


Figure 26 - 2-D image of the x-y plane.

4.5 Injection Pressures

The lower limit of the injection pressure was based on the pressure value that exceeded slightly the formation pressure at the depth of injection. The upper limit of the injection pressure was bounded by the fracture gradient at the same depth. However, the injection pressure was used as a parameter to determine an optimum value that provides long term injection regardless of the selected brine production for a project life of 50 years with no CO₂ production.

4.6 Local Production Management

It was not within the scope of the study to investigate ideal brine production rate, but model indicated the following findings. Production can't be too high or too low. When brine production was too low, the pressure reduction was insignificant at the top of the

reservoir to create a drawdown. When the brine production rate was too high, it generated large pressure decline with earlier breakthrough for the CO₂. Some of the things to consider for lower brine production that it should not displace fluid with matching injection quantity (or not displace enough fluid). Also, minimizing the risk of high pressure concentration at the top of plume and maintaining the single phase CO₂ area were challenging in order to prevent fingering and coning of CO₂. As a result, a brine production rate of 500 bbl/day was selected for the quarter of five-spot pattern. Once the well was close enough then it produced high quantities of CO₂ (Figure 27). Since the goal was not to produce CO₂, the run was repeated using next (X,Y) block over & away as the location of production well until there was no gas found.

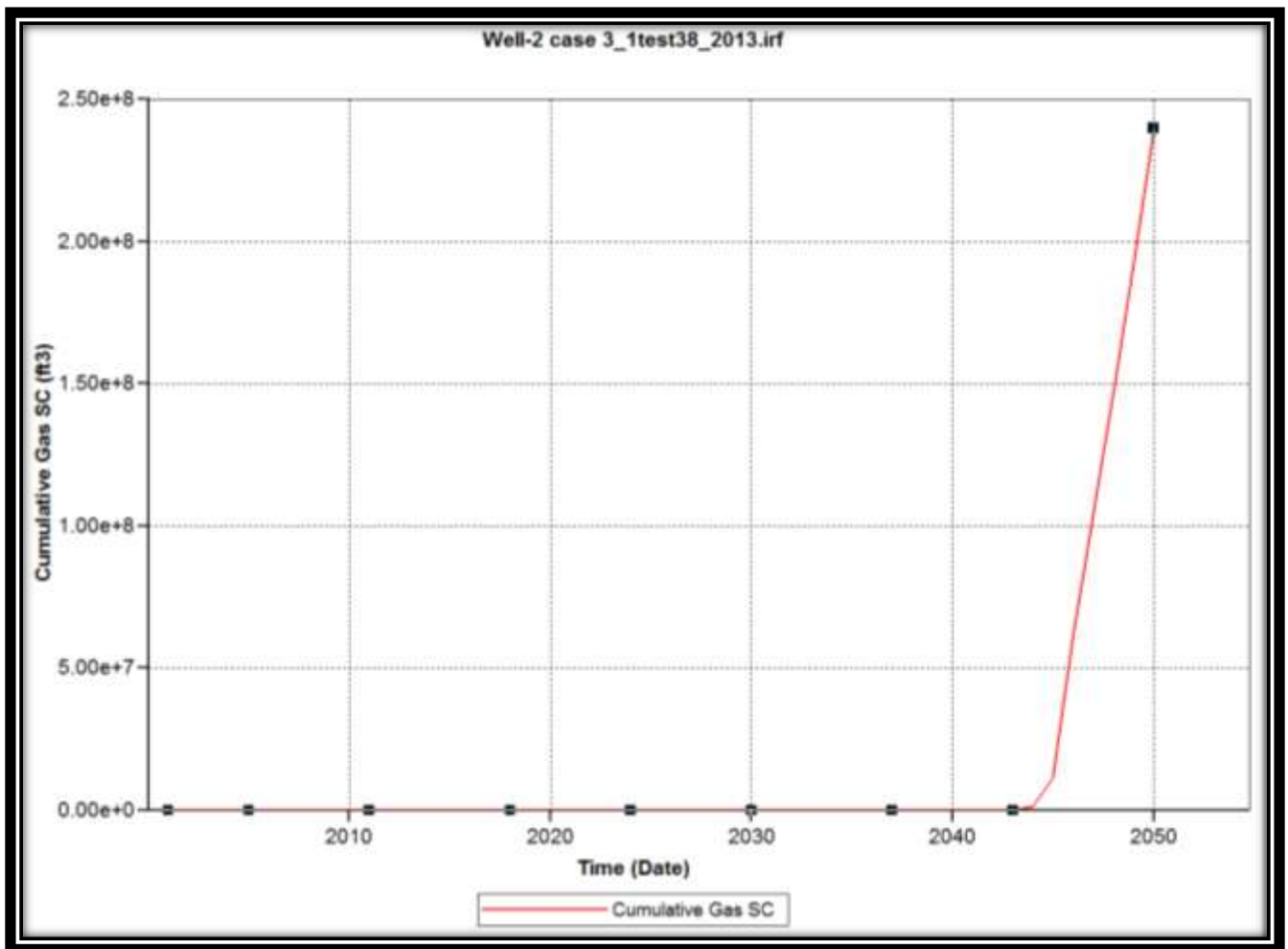


Figure 27 – Cumulative production as a function of time [for production well when it gets close to the plume]

5 Discussion of Results

This section presents all the results collected in varying different injection pressures and distances of the production well. Table 2 is the summary of results, where the columns represent run number, injection pressure, production well's block # (where the injection well is on block 1 is (1,1) on (x, y) direction block and the vertical block does not change), and the average injection rate for the injection well that was resulted from the model's calculations.

Table 2 - Summary of Runs

| Run No. | Injection Well's Pressure, psi | Production well Location Block # (X,Y) | Avg. Injection Rate (bbl/day) |
|---------|--------------------------------|--|-------------------------------|
| 1 | 3500 | 24 | 1119.8 |
| 2 | | 25 | 1117.7 |
| 3 | | 26 | 1115.7 |
| 4 | 4000 | 30 | 2148.6 |
| 5 | | 31 | 2147.4 |
| 6 | 4500 | 34 | 3087.9 |
| 7 | | 35 | 3086.8 |
| 8 | | 36 | 3085.6 |
| 9 | 5000 | 37 | 3957.2 |
| 10 | | 38 | 3956.3 |
| 11 | 5500 | 30 | 4775.5 |
| 12 | | 34 | 4773.7 |
| 13 | | 36 | 4772.0 |
| 14 | | 38 | 4770.4 |
| 15 | | 39 | 4769.5 |
| 16 | | 40 | 4768.9 |
| 17 | 6000 | 41 | 5532.7 |
| 18 | | 42 | 5532.0 |
| 19 | | 43 | 5531.1 |

5.1 Run #1

Figure 28 shows bottom hole fluid rates and bottom-hole pressures for production and injection wells, and gas water ratio for an injection pressure of 3500 psi versus time. The production well located at block #24 produced at 500 bbl/day. Well number 1 represents injection well, and Well number 2 represents brine co-production well. The bottom-hole fluid rate represents the CO₂ injection rate. The results show that the production well started to produce CO₂ after 30 years of production, thus the production well should be located further away.

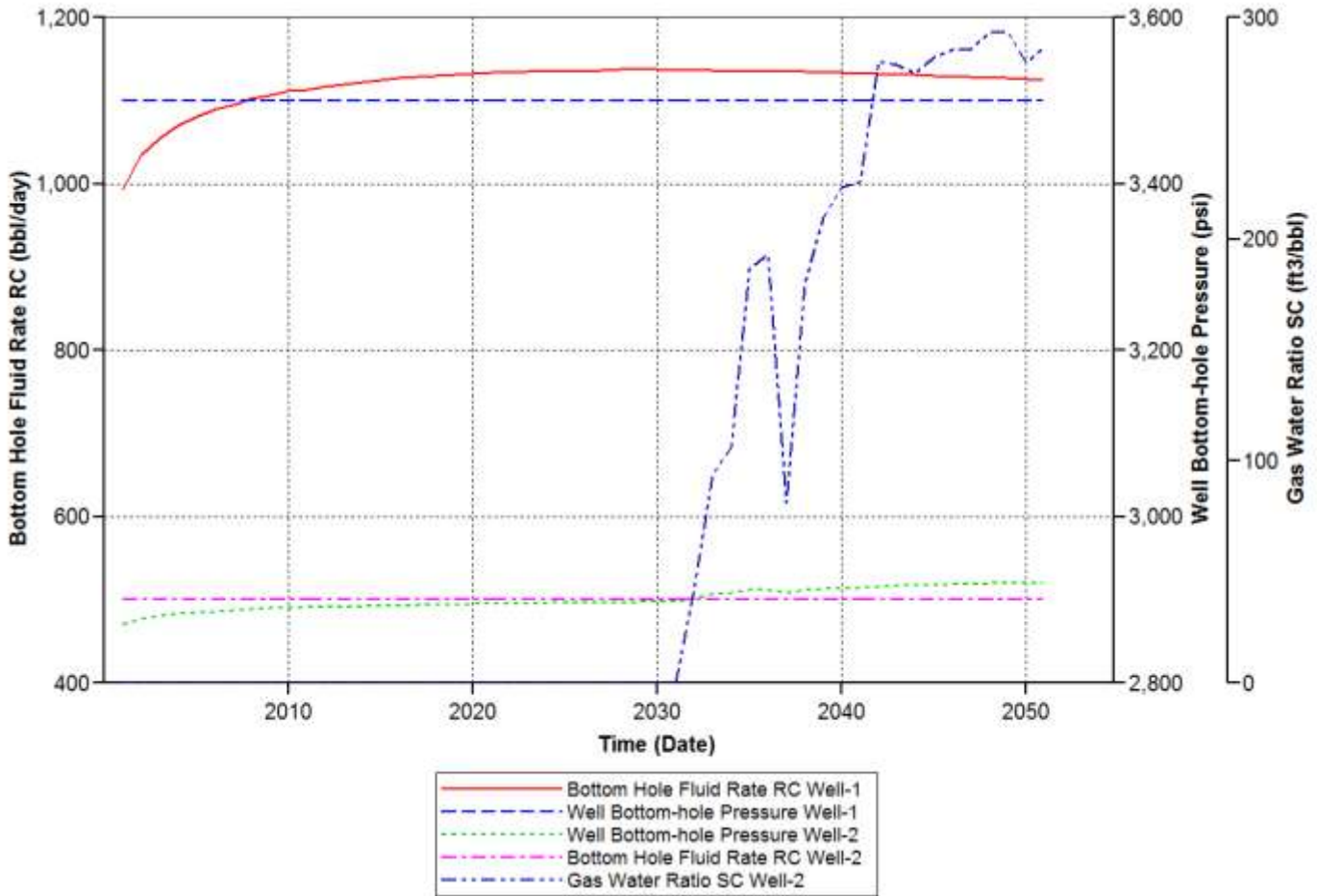


Figure 28 – Results for Run #1

5.2 Run #2

Figure 29 shows bottom hole fluid rates and bottom-hole pressures for production and injection wells, and gas water ratio for an injection pressure of 3500 psi versus time. The production well located at block #25 produced at 500 bbl/day. Well number 1 represents injection well, and Well number 2 represents brine co-production well. The bottom-hole fluid rate represents the CO₂ injection rate. The results show that CO₂ is produced 40+ years after production, so the production well could be located further away.

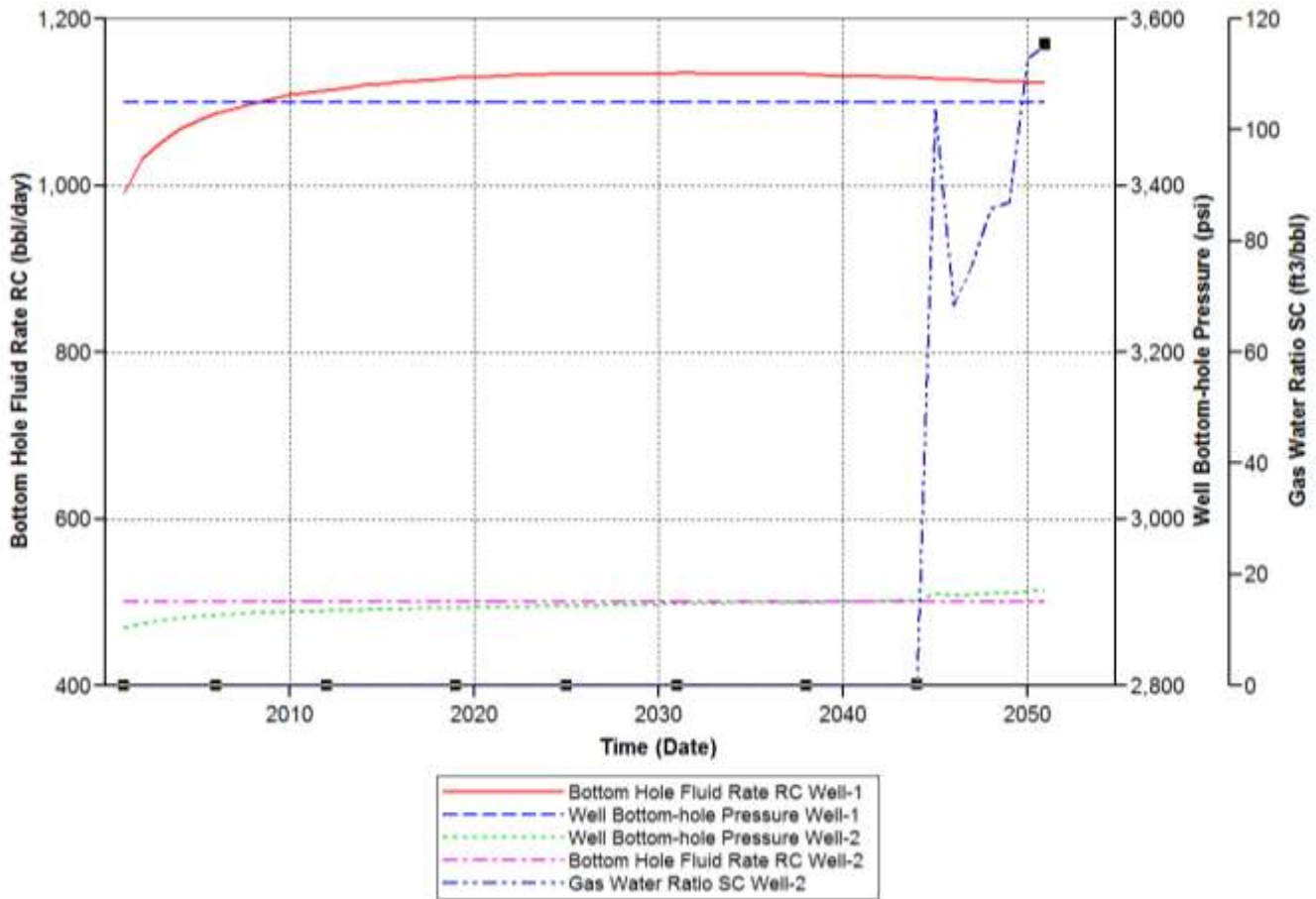


Figure 29 - Results for Run #2

5.3 Run #3

Figure 30 shows bottom hole fluid rates and bottom-hole pressures for production and injection wells, and gas water ratio for an injection pressure of 3500 psi versus time. The production well located at block #26 produced at 500 bbl/day. Well number 1 represents injection well, and Well number 2

represents brine co-production well. The bottom-hole fluid rate represents the CO₂ injection rate. The results show that no CO₂ is produced, so the production well has reached the optimum distance.

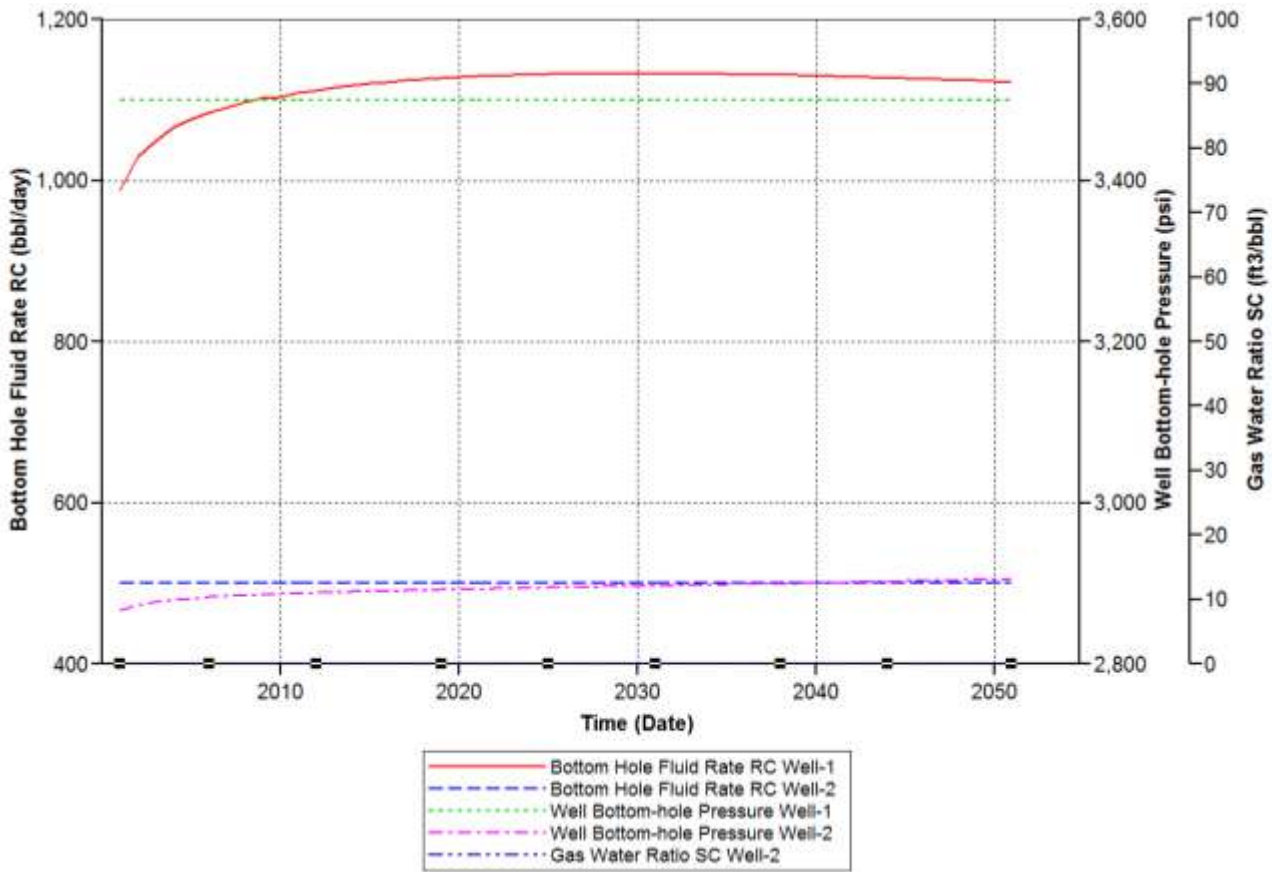


Figure 30 – Results for Run #3

5.4 Run #4

Figure 31 shows bottom hole fluid rates and bottom-hole pressures for production and injection wells, and gas water ratio for an injection pressure of 4000 psi versus time. The production well located at block #30 produced at 500 bbl/day. Well number 1 represents injection well, and Well number 2 represents brine co-production well. The bottom-hole fluid rate represents the CO₂ injection rate. The results show that CO₂ is produced 40+ years after production, so the production well could be located further away.

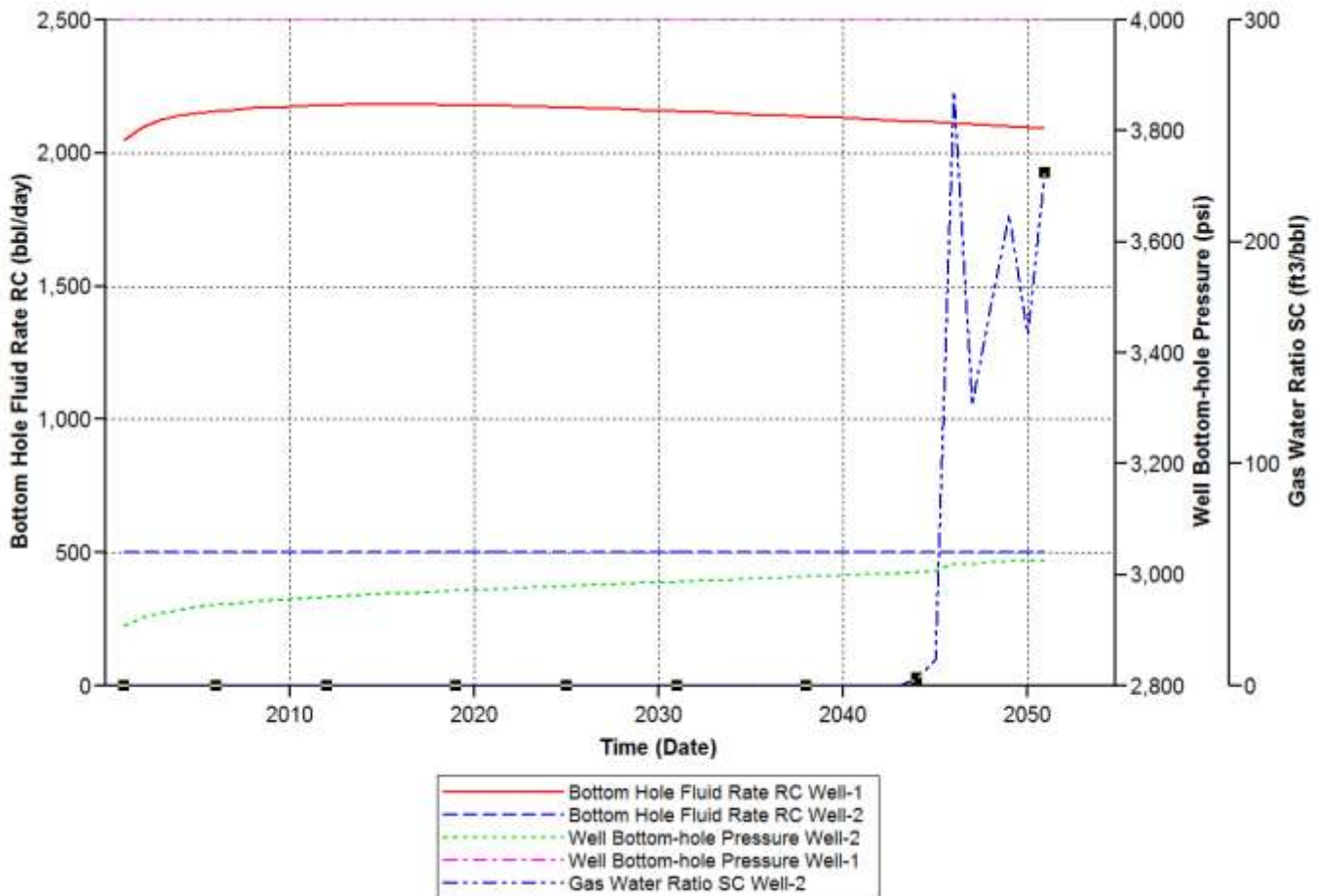


Figure 31 - Results for Run #4

5.5 Run #5

Figure 32 shows bottom hole fluid rates and bottom-hole pressures for production and injection wells, and gas water ratio for an injection pressure of 4000 psi versus time. The production well located at block #31 produced at 500 bbl/day. Well number 1 represents injection well, and Well number 2 represents brine co-production well. The bottom-hole fluid rate represents the CO₂ injection rate. The results show that no CO₂ is produced, so the production well has reached the optimum distance.

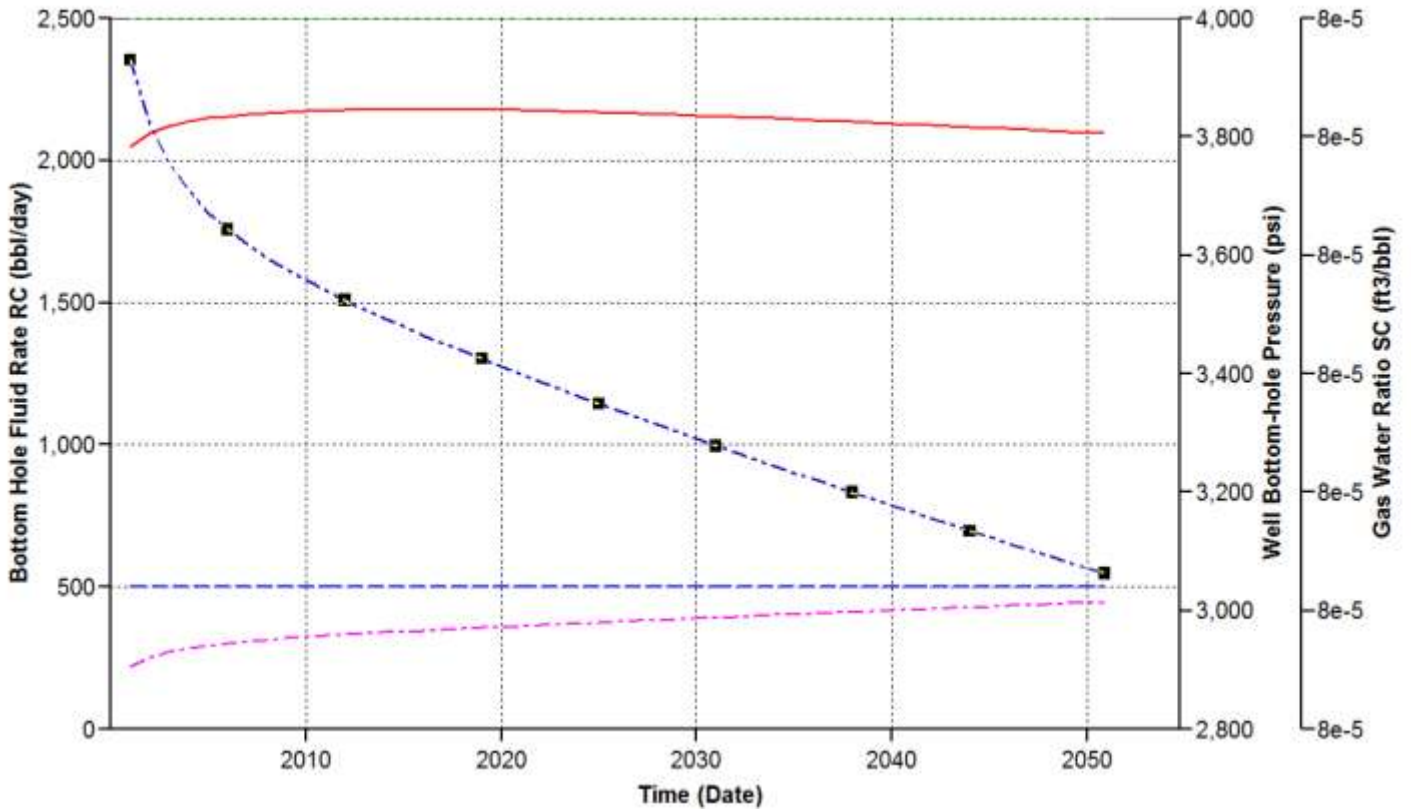


Figure 32 - Results for Run #5

5.6 Run #6

Figure 33 shows bottom hole fluid rates and bottom-hole pressures for production and injection wells, and gas water ratio for an injection pressure of 4500 psi versus time. The production well located at block #34 produced at 500 bbl/day. Well number 1 represents injection well, and Well number 2 represents brine co-production well. The bottom-hole fluid rate represents the CO₂ injection rate. The results show that CO₂ is produced slightly before 50 years after production, so the production well could be located slightly further away.

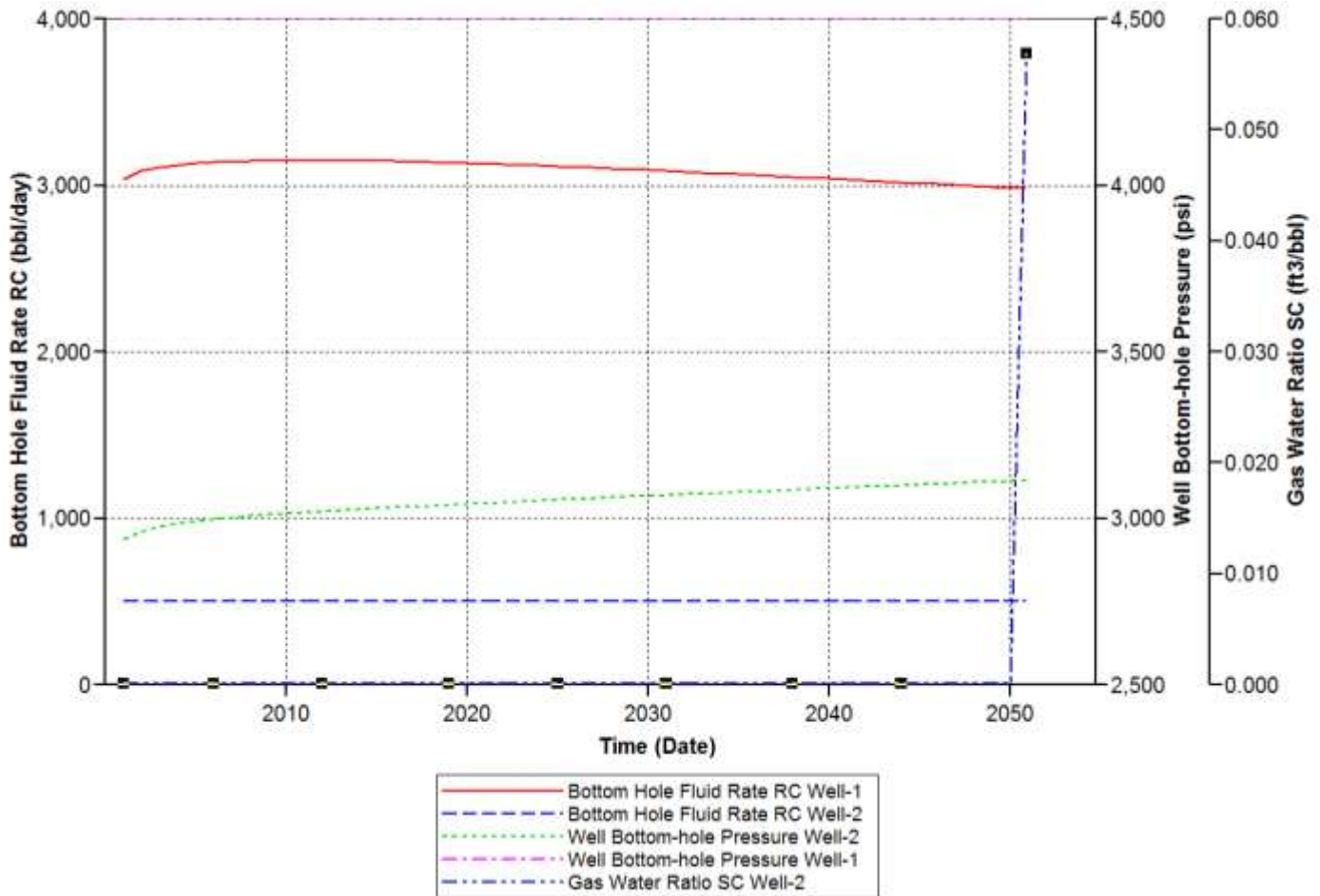


Figure 33 - Results for Run #6

5.7 Run #7

Figure 34 shows bottom hole fluid rates and bottom-hole pressures for production and injection wells, and gas water ratio for an injection pressure of 4500 psi versus time. The production well located at block #35 produced at 500 bbl/day. Well number 1 represents injection well, and Well number 2 represents brine co-production well. The bottom-hole fluid rate represents the CO₂ injection rate. The results show that no CO₂ is produced throughout its projected time, so the production well has reached the optimum distance.

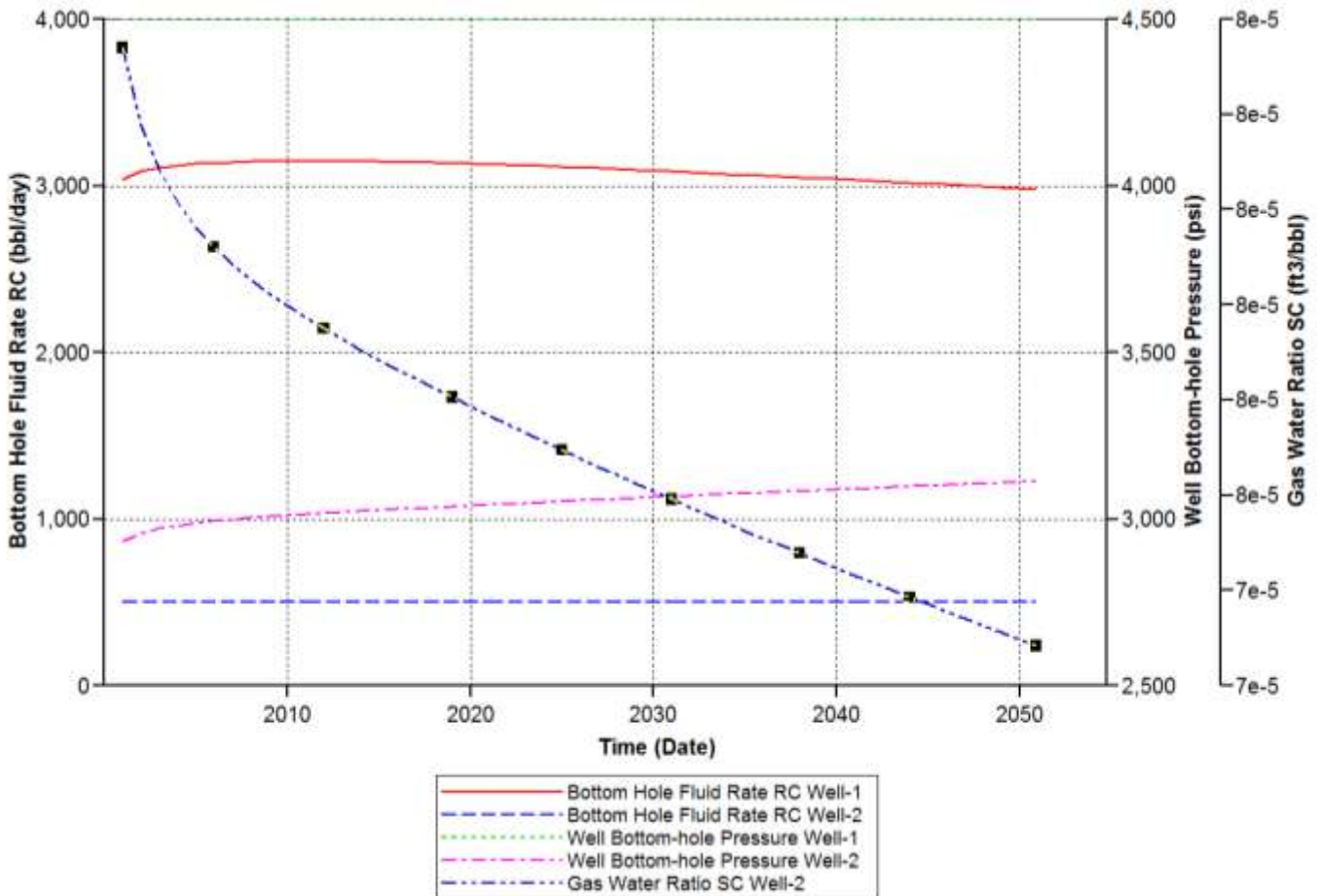


Figure 34 - Results for Run #7

5.8 Run #8

Figure 35 shows bottom hole fluid rates and bottom-hole pressures for production and injection wells, and gas water ratio for an injection pressure of 4500 psi versus time. The production well located at block #36 produced at 500 bbl/day. Well number 1 represents injection well, and Well number 2 represents brine co-production well. The bottom-hole fluid rate represents the CO₂ injection rate. The results show that no CO₂ is produced throughout its projected time.

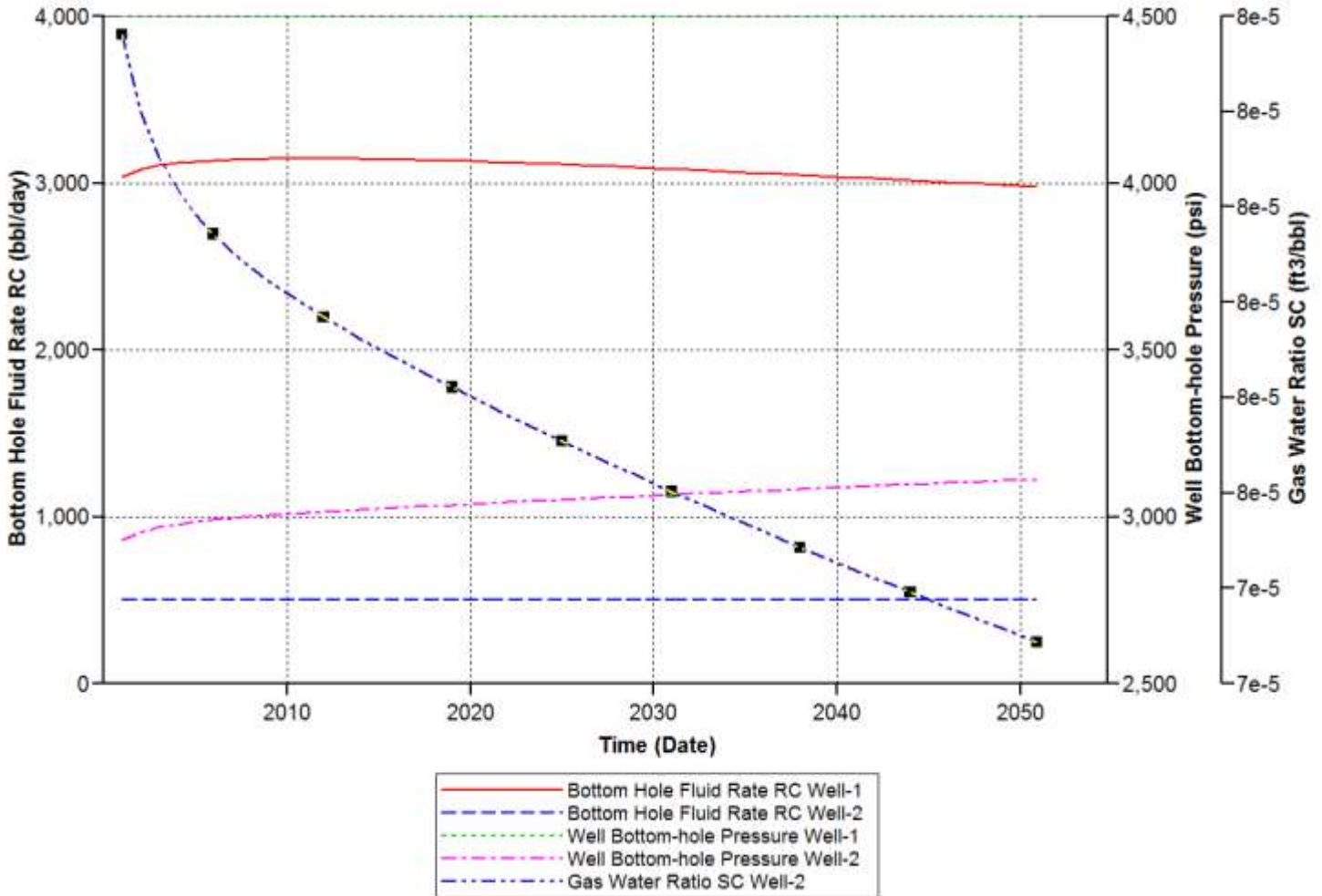


Figure 35 - Results for Run #8

5.9 Run #9

Figure 36 shows bottom hole fluid rates and bottom-hole pressures for production and injection wells, and gas water ratio for an injection pressure of 5000 psi versus time. The production well located at block #37 produced at 500 bbl/day. Well number 1 represents injection well, and Well number 2 represents brine co-production well. The bottom-hole fluid rate represents the CO₂ injection rate. The results show that no CO₂ is produced throughout its projected time, so the production well is located at an optimum distance.

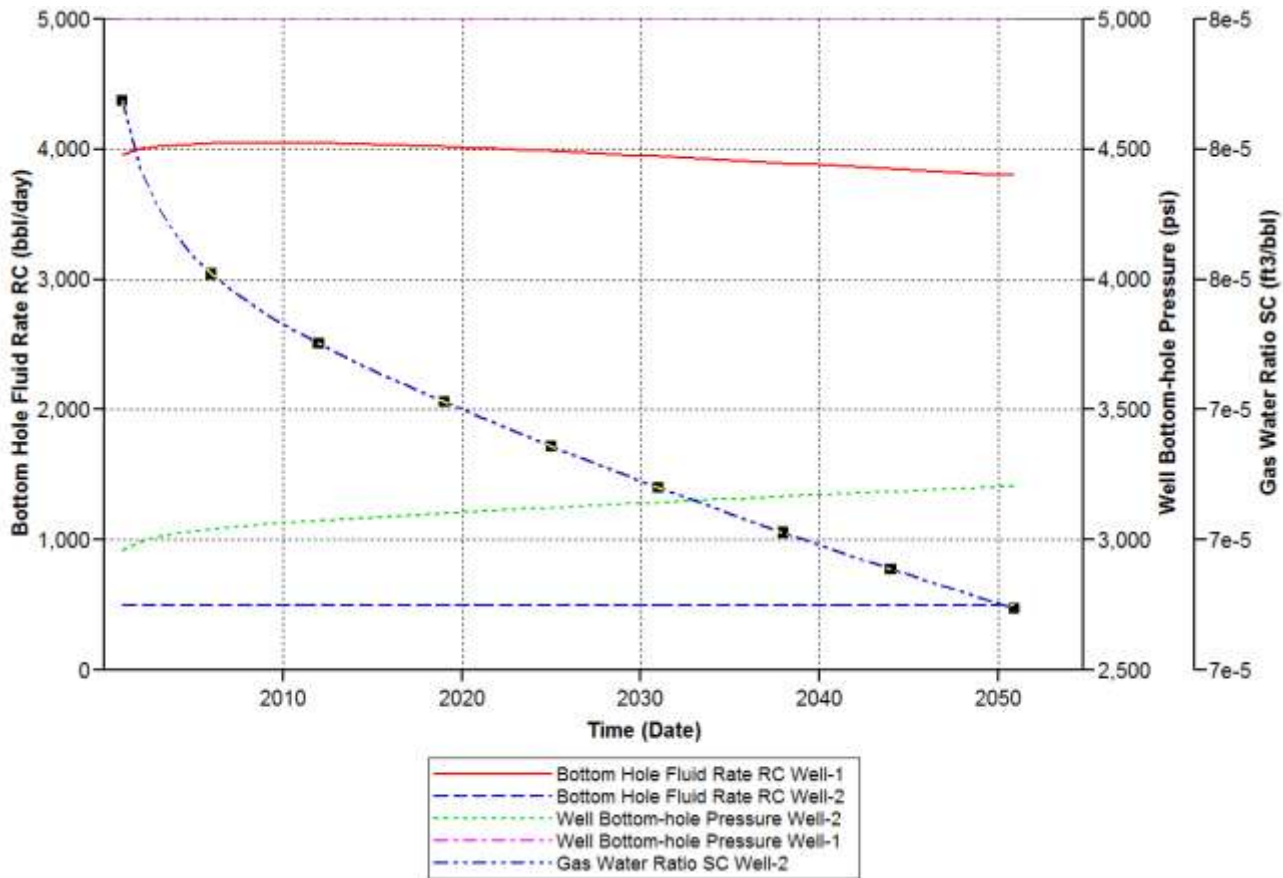


Figure 36 – Results for Run #9

5.10 Run #10

Figure 37 shows bottom hole fluid rates and bottom-hole pressures for production and injection wells, and gas water ratio for an injection pressure of 5000 psi versus time. The production well located at block #38 produced at 500 bbl/day. Well number 1 represents injection well, and Well number 2 represents brine co-production well. The bottom-hole fluid rate represents the CO₂ injection rate. The results show that no CO₂ is produced throughout its projected time.

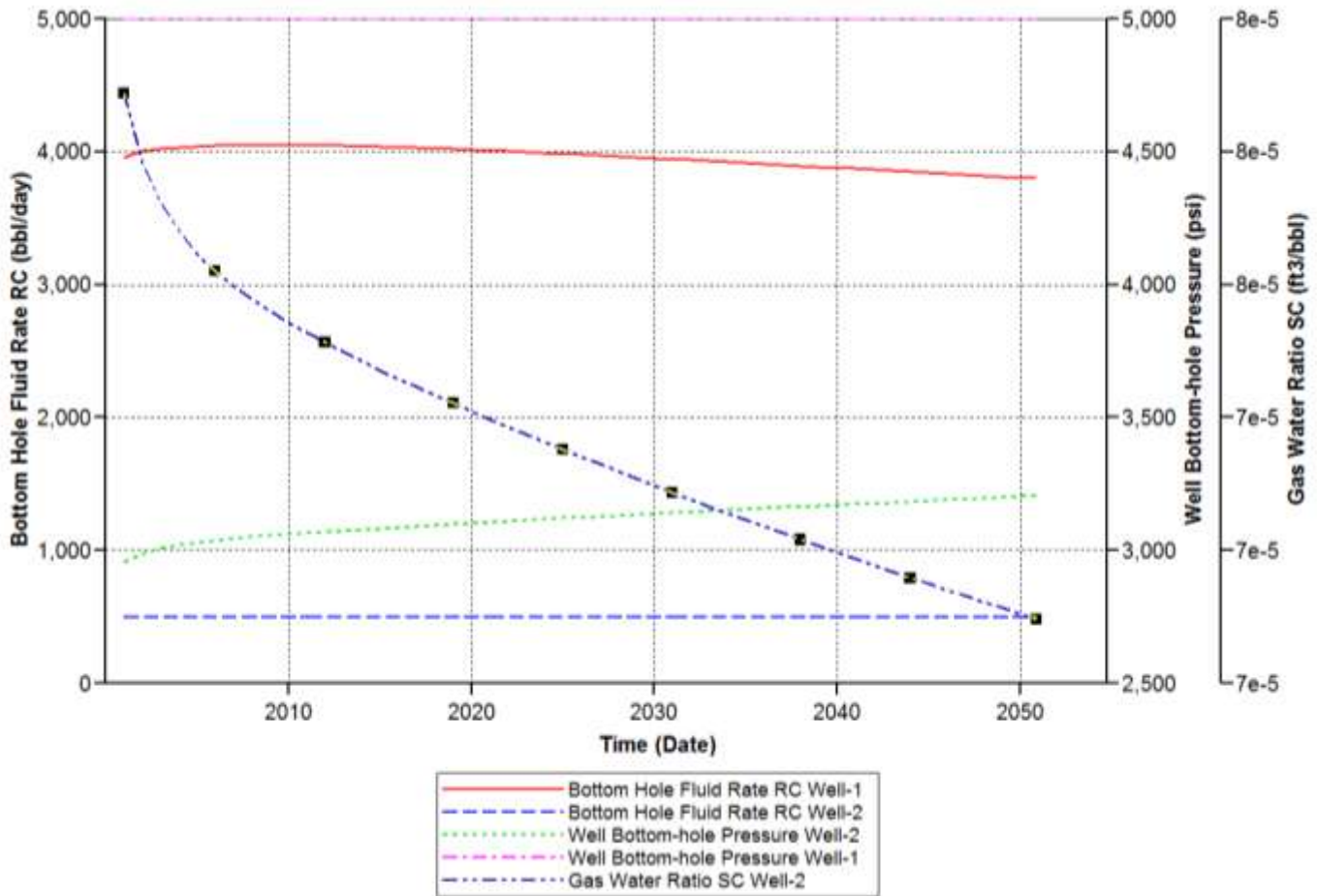


Figure 37 - Results for Run #10

5.11 Run #11

Figure 38 shows bottom hole fluid rates and bottom-hole pressures for production and injection wells, and gas water ratio for an injection pressure of 5500 psi versus time. The production well located at block #30 produced at 500 bbl/day. Well number 1 represents injection well, and Well number 2 represents brine co-production well. The bottom-hole fluid rate represents the CO₂ injection rate. The results show that CO₂ is produced approximately 17 years after production, so the production well could be located further away.

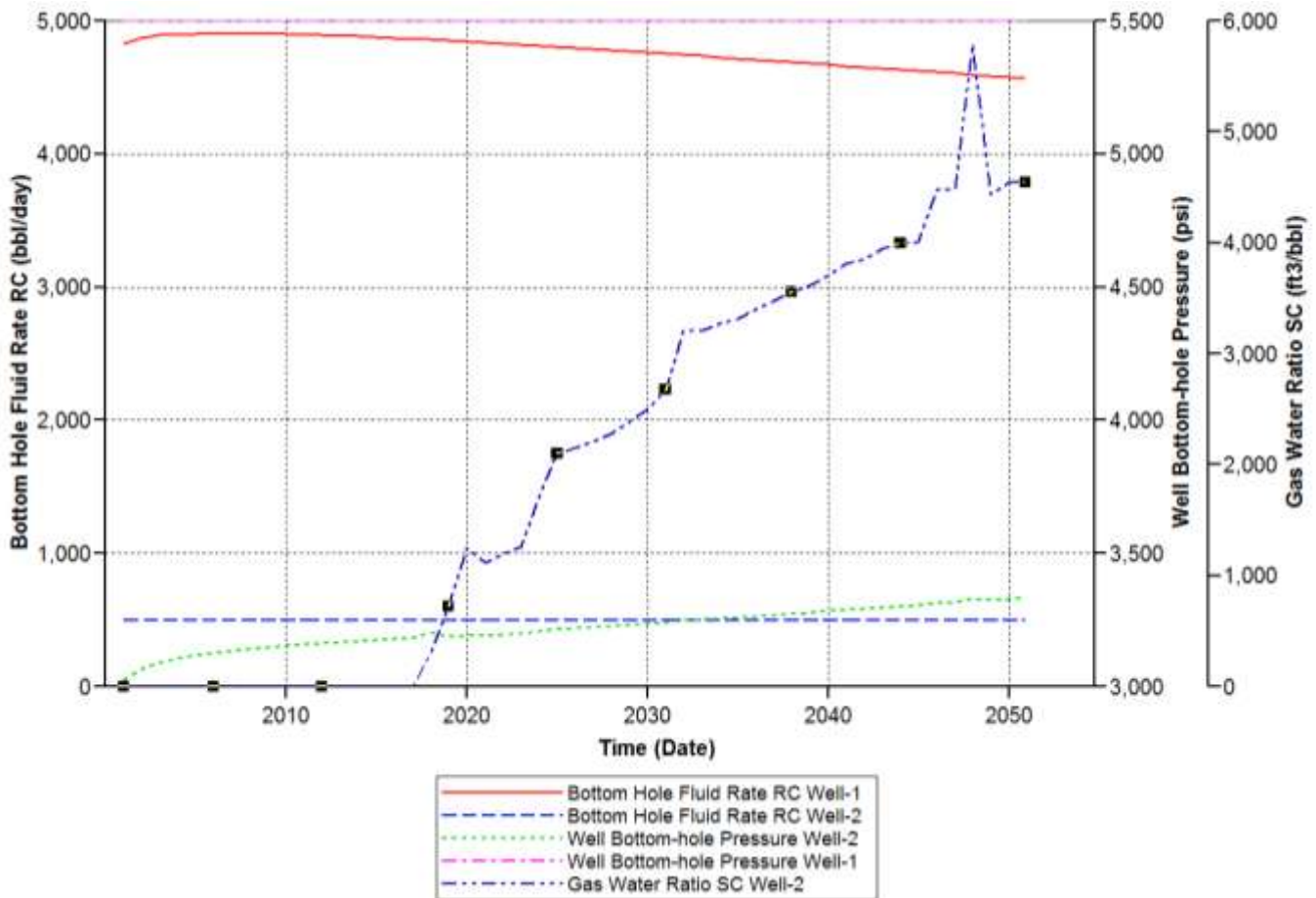


Figure 38 - Results for Run #11

5.12 Run #12

Figure 39 shows bottom hole fluid rates and bottom-hole pressures for production and injection wells, and gas water ratio for an injection pressure of 5500 psi versus time. The production well located at block #34 produced at 500 bbl/day. Well number 1 represents injection well, and Well number 2 represents brine co-production well. The bottom-hole fluid rate represents the CO₂ injection rate. The results show that CO₂ is produced approximately 24 years after production, so the production well could be located further away.

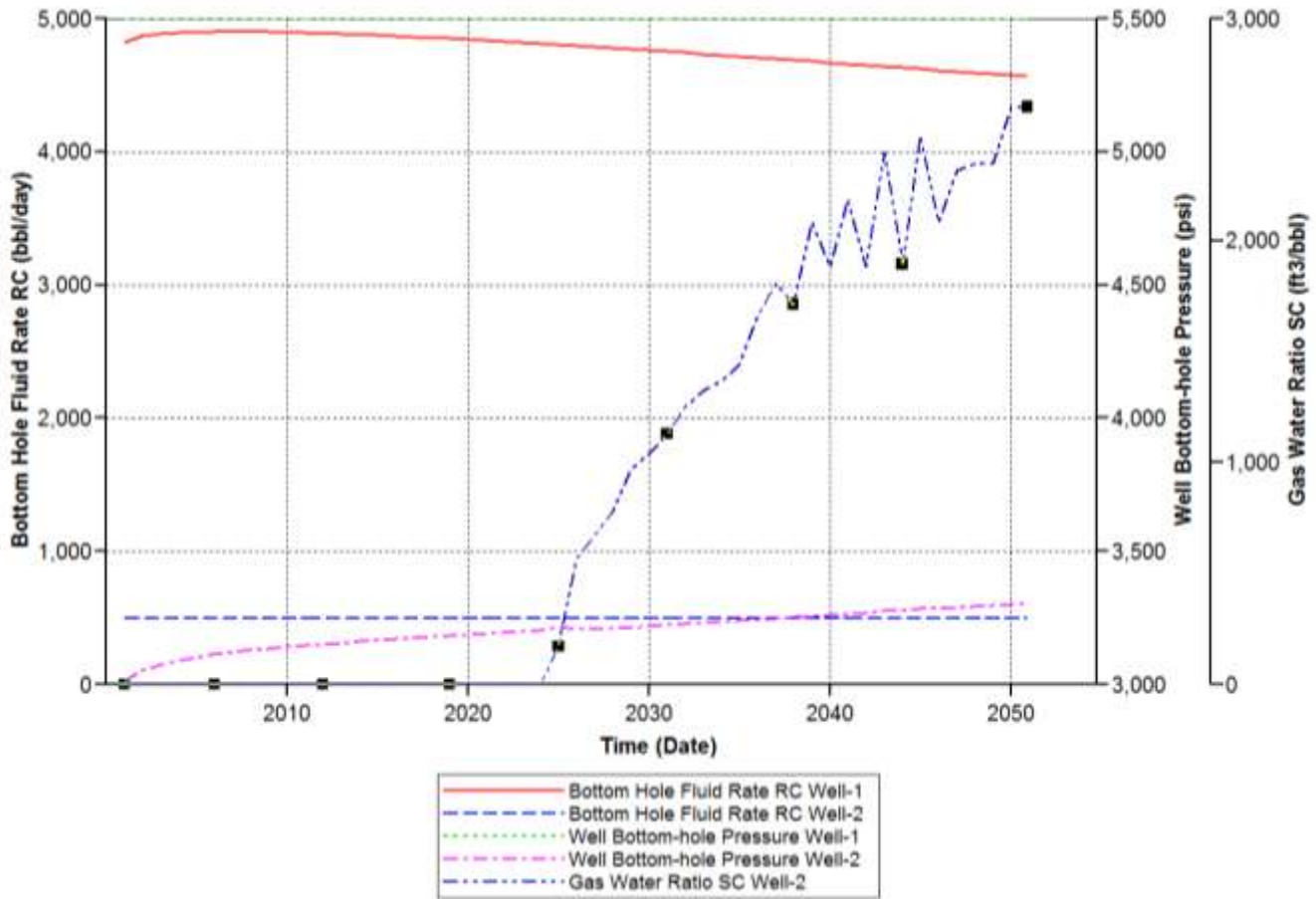


Figure 39 – Results for Run #12

5.13 Run #13

Figure 40 shows bottom hole fluid rates and bottom-hole pressures for production and injection wells, and gas water ratio for an injection pressure of 5500 psi versus time. The production well located at block #36 produced at 500 bbl/day. Well number 1 represents injection well, and Well number 2 represents brine co-production well. The bottom-hole fluid rate represents the CO₂ injection rate. The results show that CO₂ is produced approximately 32 years after production, so the production well could be located further away.

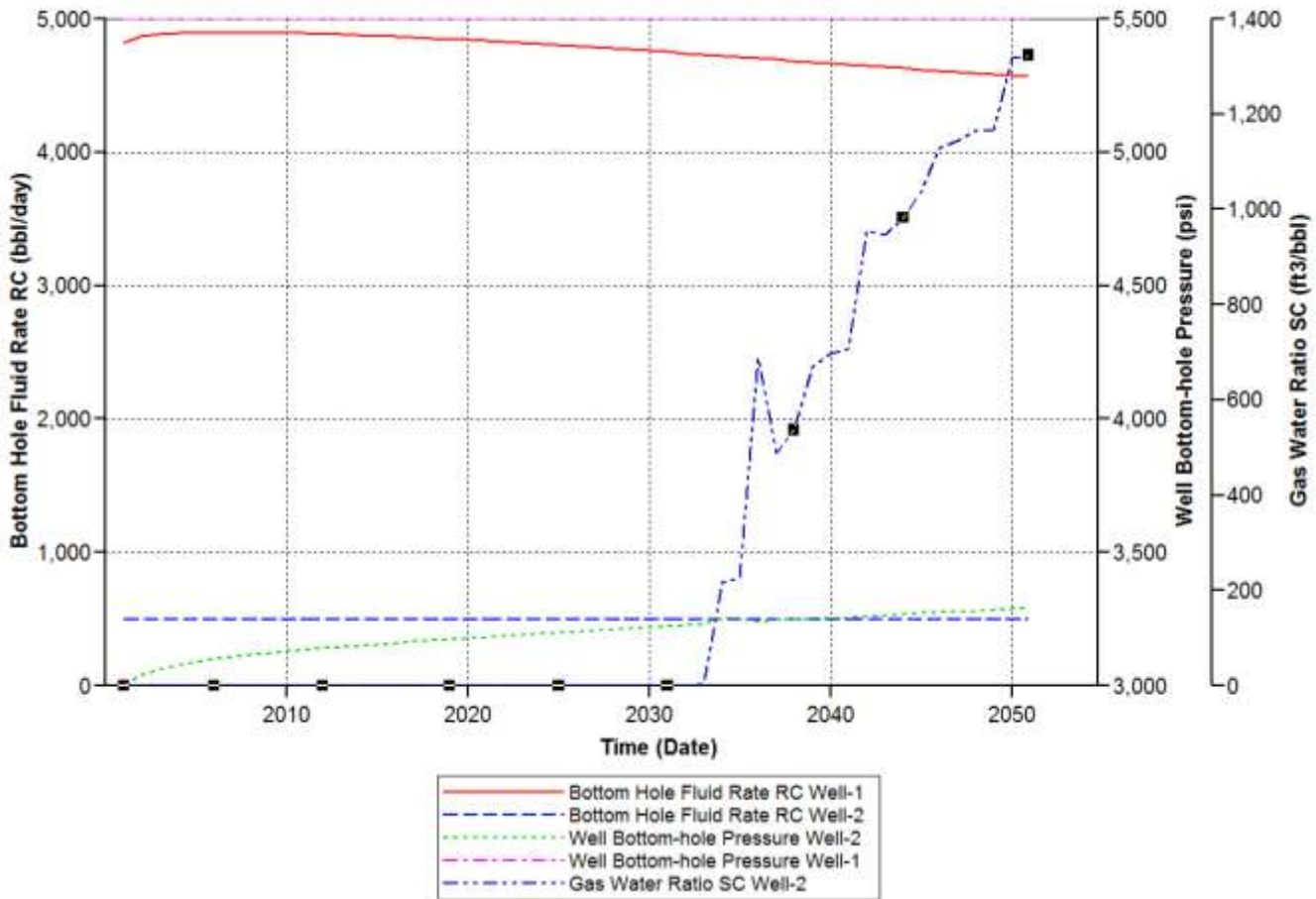


Figure 40 - Results for Run #13

5.14 Run #14

Figure 41 shows bottom hole fluid rates and bottom-hole pressures for production and injection wells, and gas water ratio for an injection pressure of 5500 psi versus time. The production well located at block #38 produced at 500 bbl/day. Well number 1 represents injection well, and Well number 2 represents brine co-production well. The bottom-hole fluid rate represents the CO₂ injection rate. The results show that CO₂ is produced approximately 43 years after production, so the production well could be located further away.

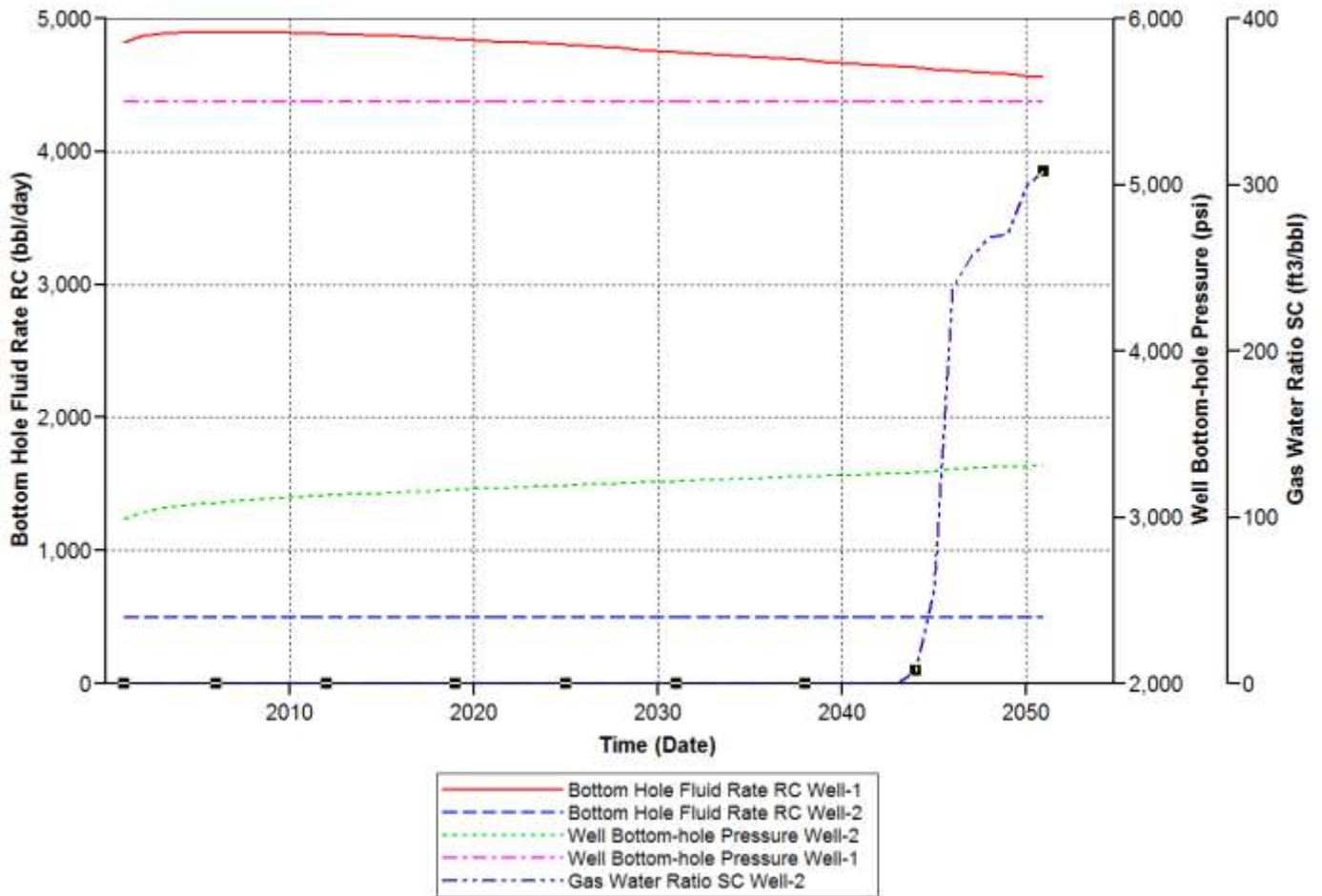


Figure 41 - Results for Run #14

5.15 Run #15

Figure 42 shows bottom hole fluid rates and bottom-hole pressures for production and injection wells, and gas water ratio for an injection pressure of 5500 psi versus time. The production well located at block #39 produced at 500 bbl/day. Well number 1 represents injection well, and Well number 2 represents brine co-production well. The bottom-hole fluid rate represents the CO₂ injection rate. The results show that CO₂ is produced slightly before 50 years after production, so the production well could be located slightly further away.

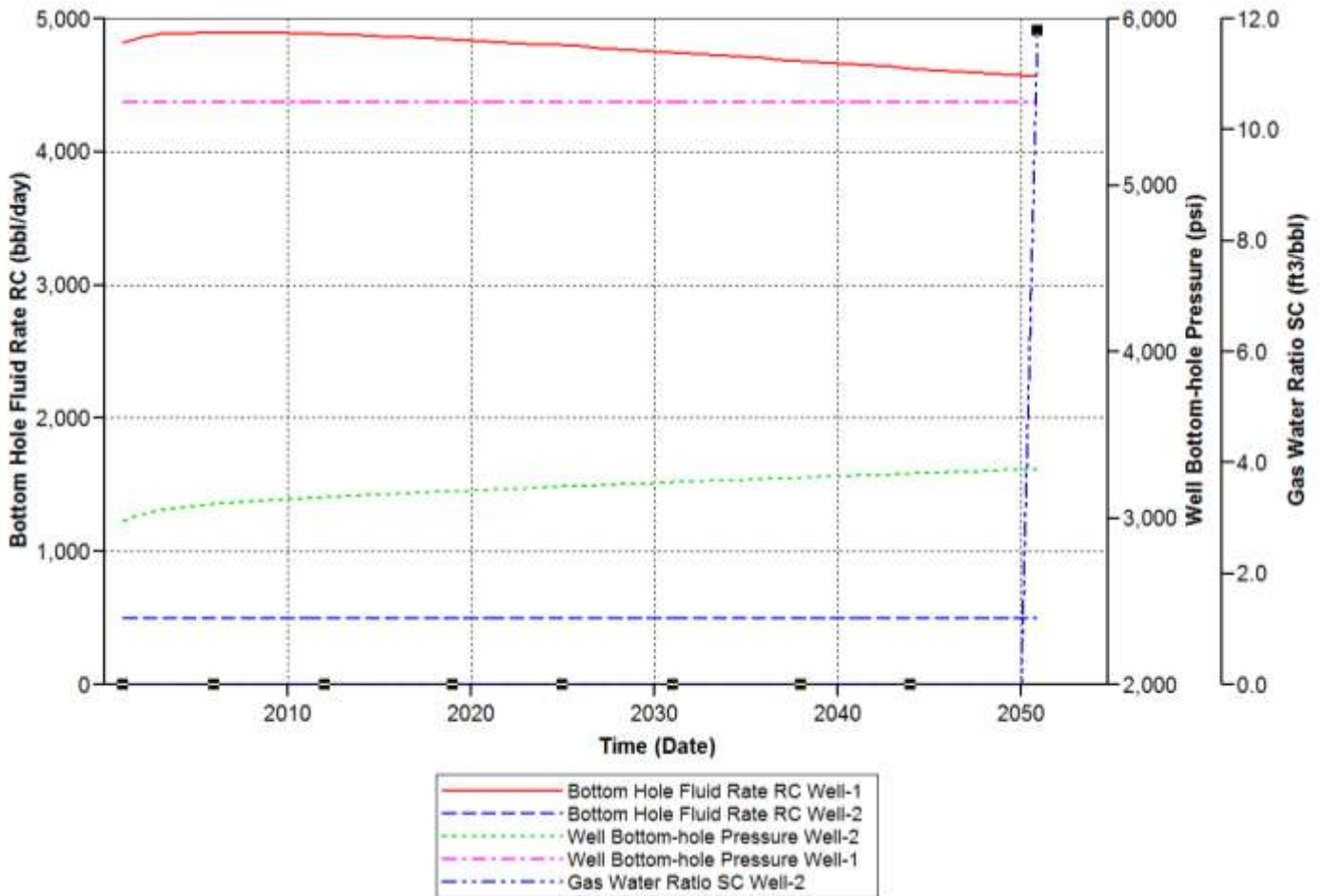


Figure 42 - Results for Run #15

5.16 Run #16

Figure 43 shows bottom hole fluid rates and bottom-hole pressures for production and injection wells, and gas water ratio for an injection pressure of 5000 psi versus time. The production well located at block #40 produced at 500 bbl/day. Well number 1 represents injection well, and Well number 2 represents brine co-production well. The bottom-hole fluid rate represents the CO₂ injection rate. The results show that no CO₂ is produced throughout its projected time of 50 years, so the production well is located at an optimum distance.

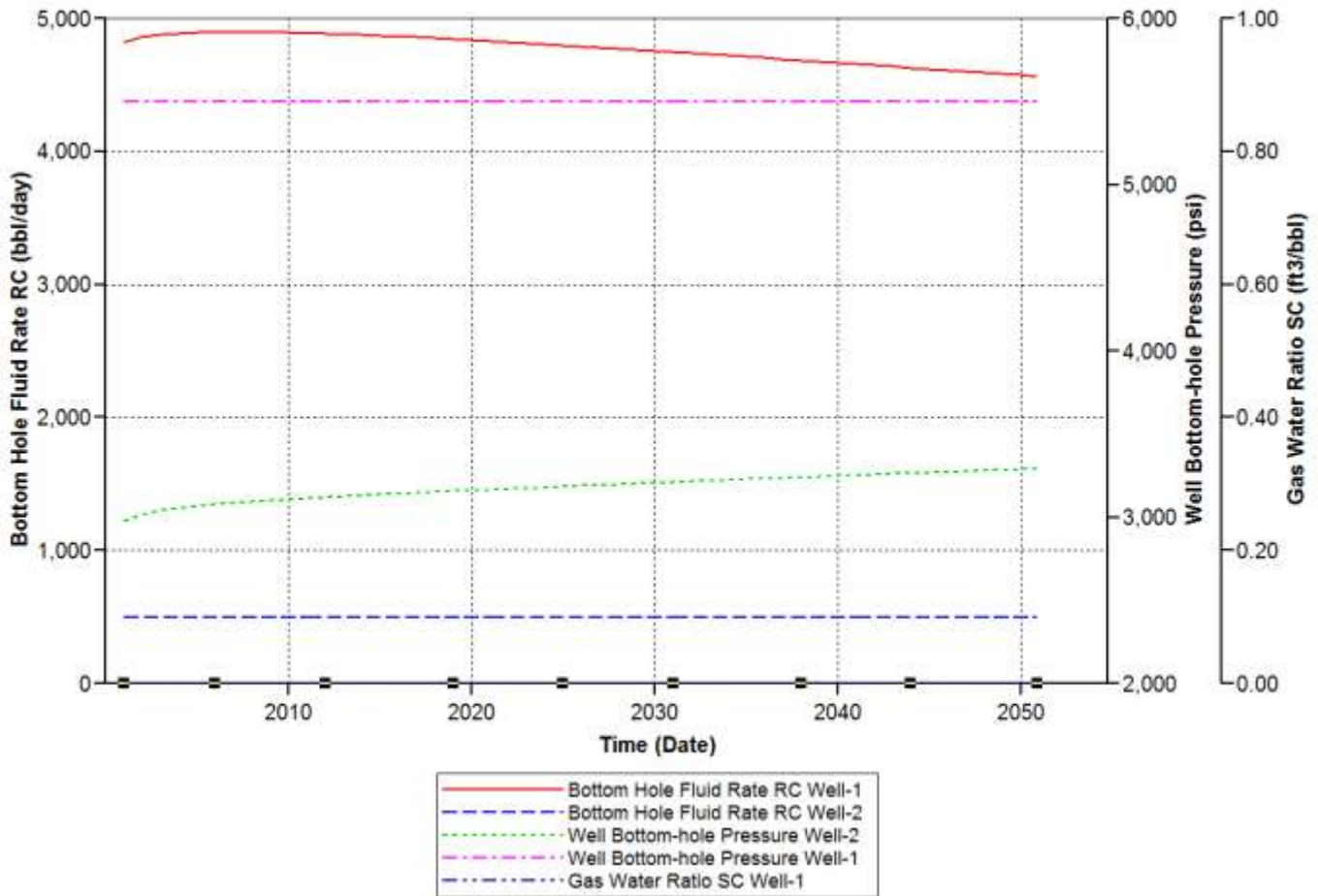


Figure 43 - Results for Run #16

5.17 Run #17

Figure 44 shows bottom hole fluid rates and bottom-hole pressures for production and injection wells, and gas water ratio for an injection pressure of 6000 psi versus time. The production well located at block #41 produced at 500 bbl/day. Well number 1 represents injection well, and Well number 2 represents brine co-production well. The bottom-hole fluid rate represents the CO₂ injection rate. The results show that CO₂ is produced almost at the end of 50 years after production, so the production well could be located slightly further away.

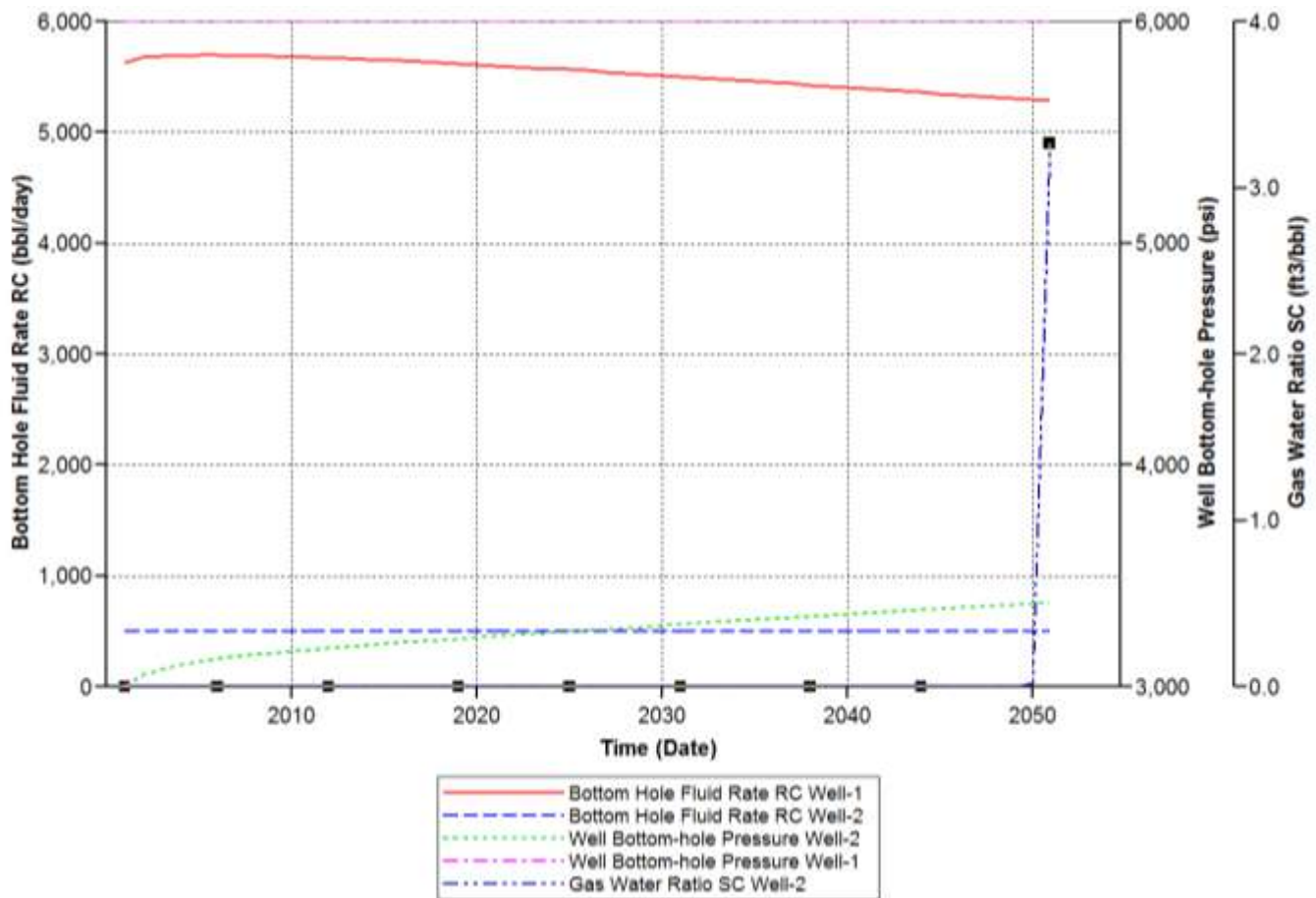


Figure 44 – Results for Run #17

5.18 Run #18

Figure 45 shows bottom hole fluid rates and bottom-hole pressures for production and injection wells, and gas water ratio for an injection pressure of 6000 psi versus time. The production well located at block #42 produced at 500 bbl/day. Well number 1 represents injection well, and Well number 2 represents brine co-production well. The bottom-hole fluid rate represents the CO₂ injection rate. The results show that no CO₂ is produced throughout its projected time of 50 years, so the production well is located at an optimum distance.

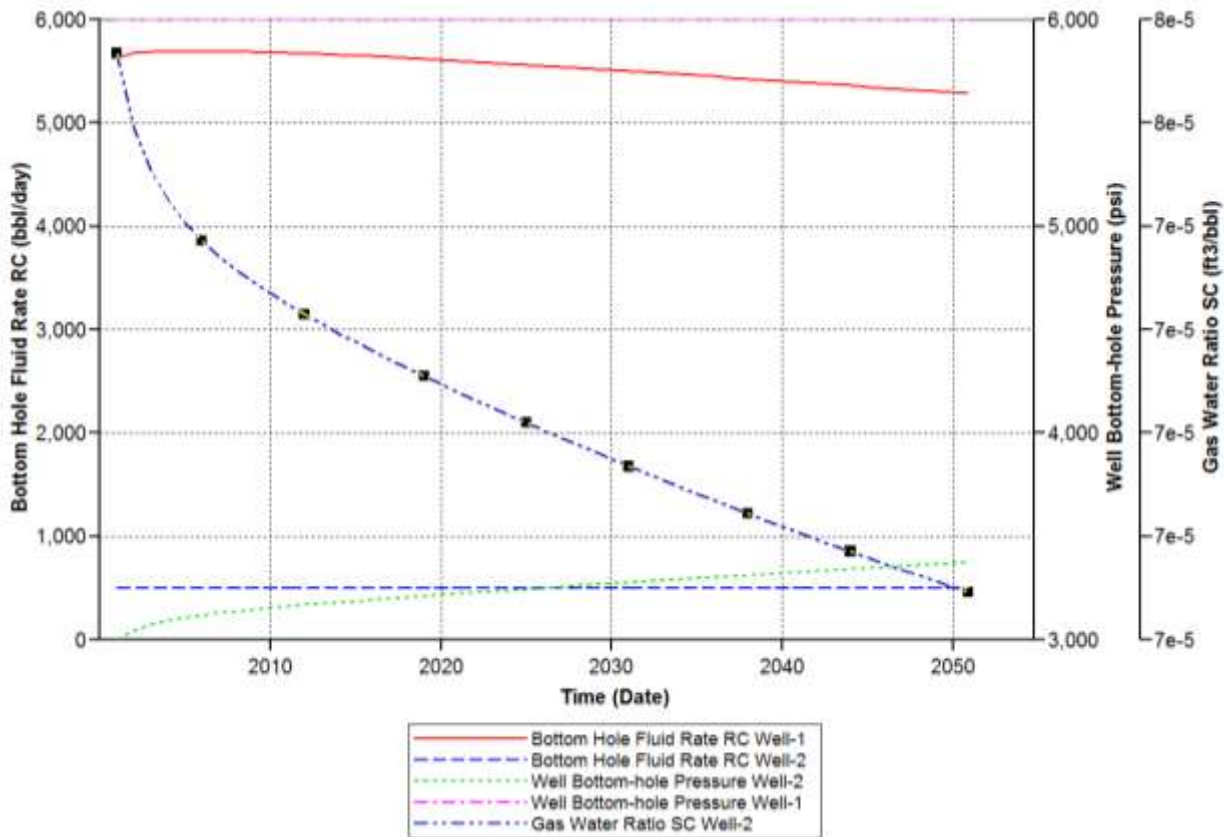


Figure 45 - Results for Run #18

5.19 Run #19

Figure 46 shows bottom hole fluid rates and bottom-hole pressures for production and injection wells, and gas water ratio for an injection pressure of 6000 psi versus time. The production well located at block #43 produced at 500 bbl/day. Well number 1 represents injection well, and Well number 2 represents brine co-production well. The bottom-hole fluid rate represents the CO₂ injection rate. The results show that no CO₂ is produced throughout its projected time of 50 years, so the production well is located further than its optimum distance.

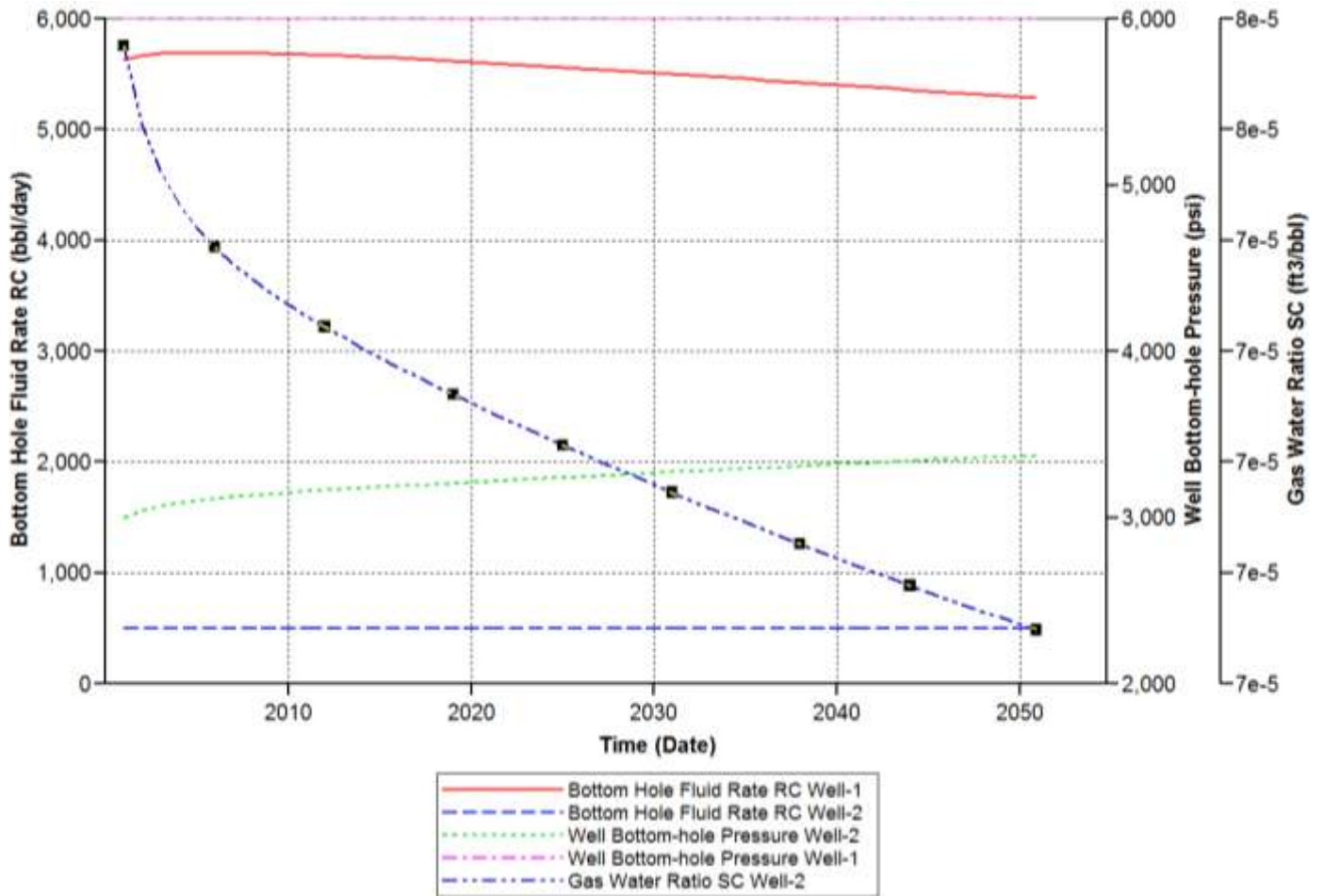


Figure 46 - Results for Run #19

5.20 Additional discussion

In this study, an interesting observation was the case when the producing well located far away, the pressure near injection well had little or no impact on high pressure zone. When the producing well was closer to injection well, CO₂ channeled over like coning or fingering reservoir behavior. Figure 47 shows the initial reservoir pressure distribution for the top layer.

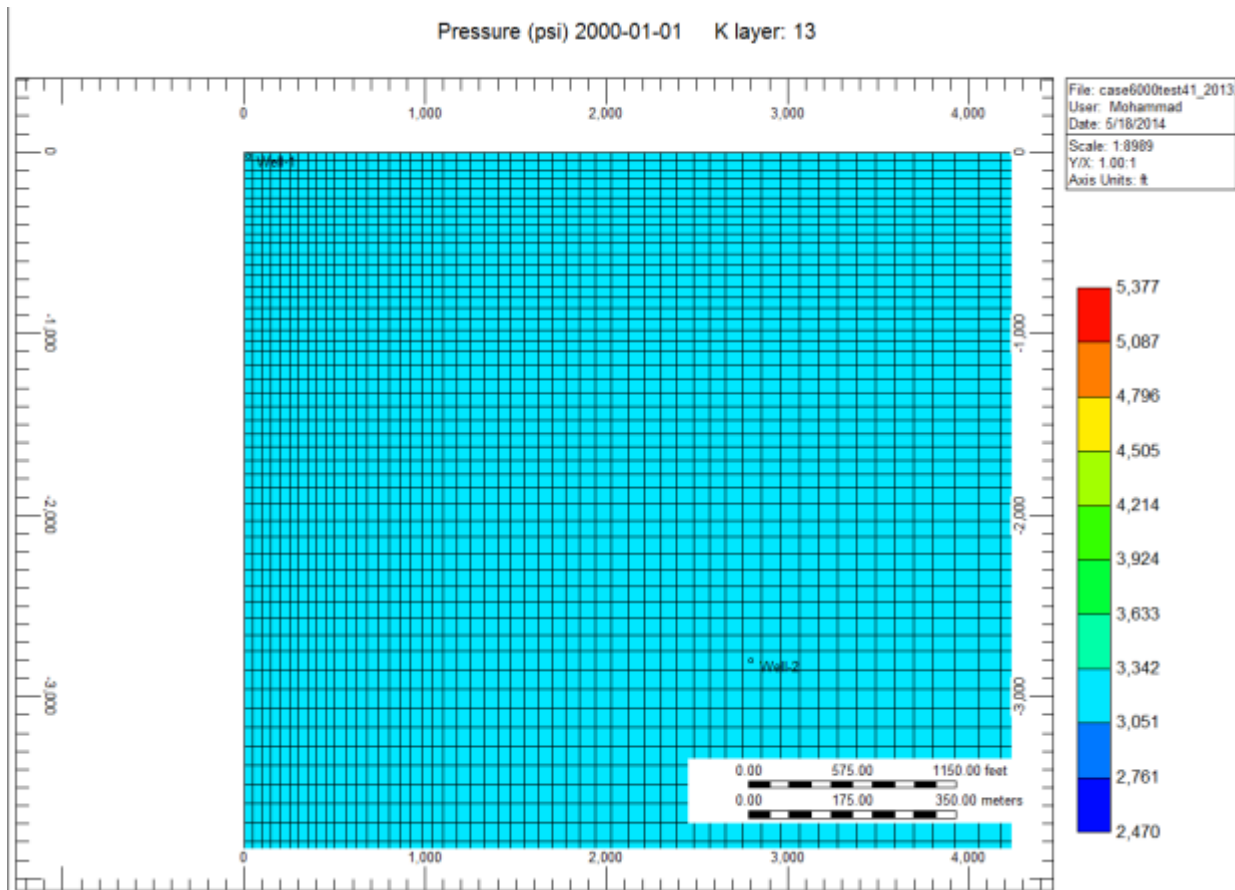


Figure 47 – Initial pressure distribution.

Reservoir pressure and CO₂ gas saturation distributions at the end of 50 years with 6,000 psi injection pressure are given in Figure 48 and Figure 49, respectively, for the top layer.

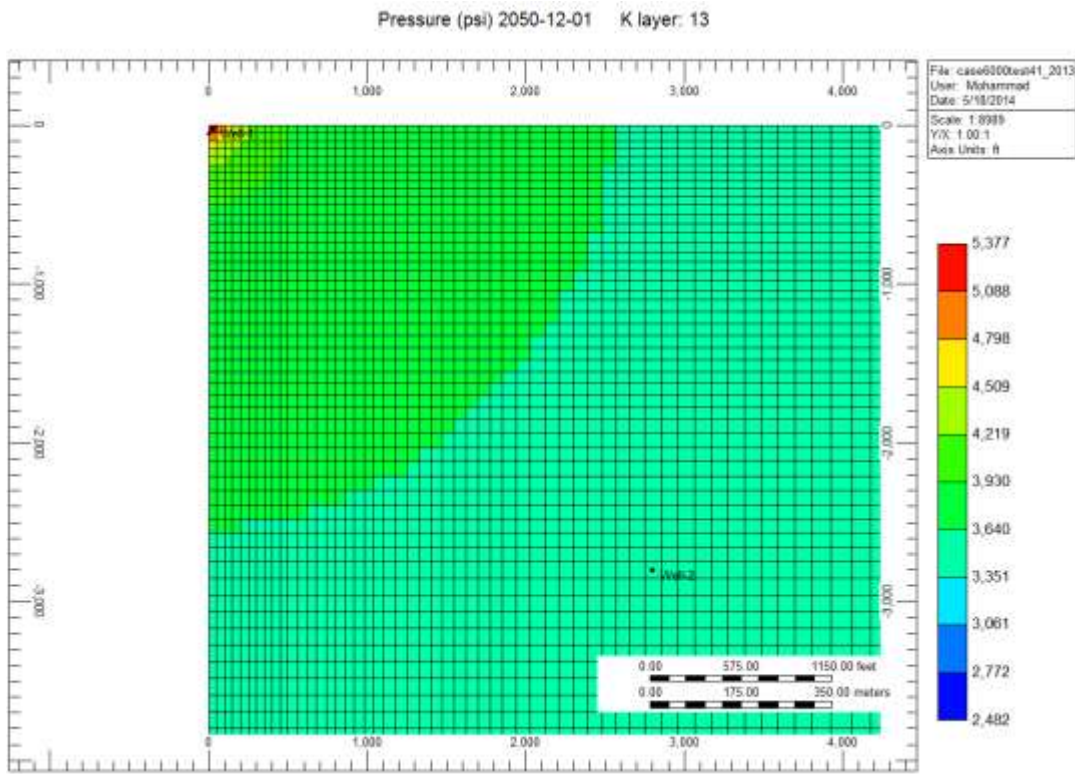


Figure 48 – Pressure distribution at the end of 50 years for injection pressure of 6000 psi

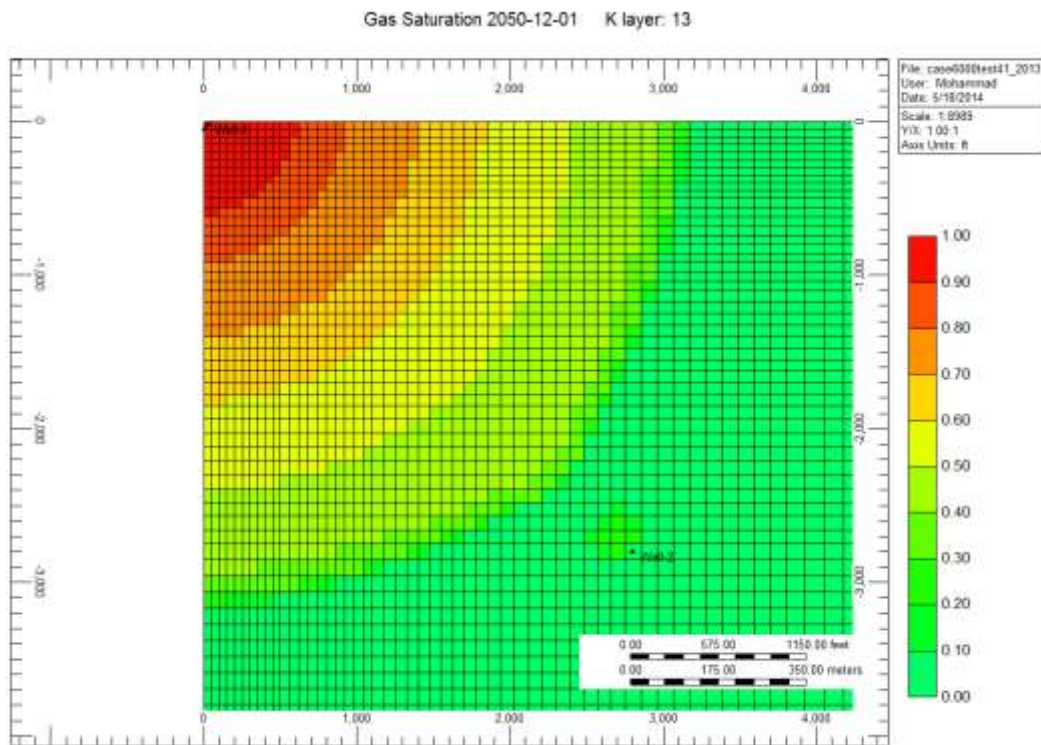


Figure 49 – Gas saturations at the end of 50 years for injection pressure of 6000 psi

Figure 50 shows the pressure distribution at the top layer at the end of 50 years when an injection pressure of 3,500 psi was used without production. Reservoir volume was not utilized under the lowest injection pressure used in the study.

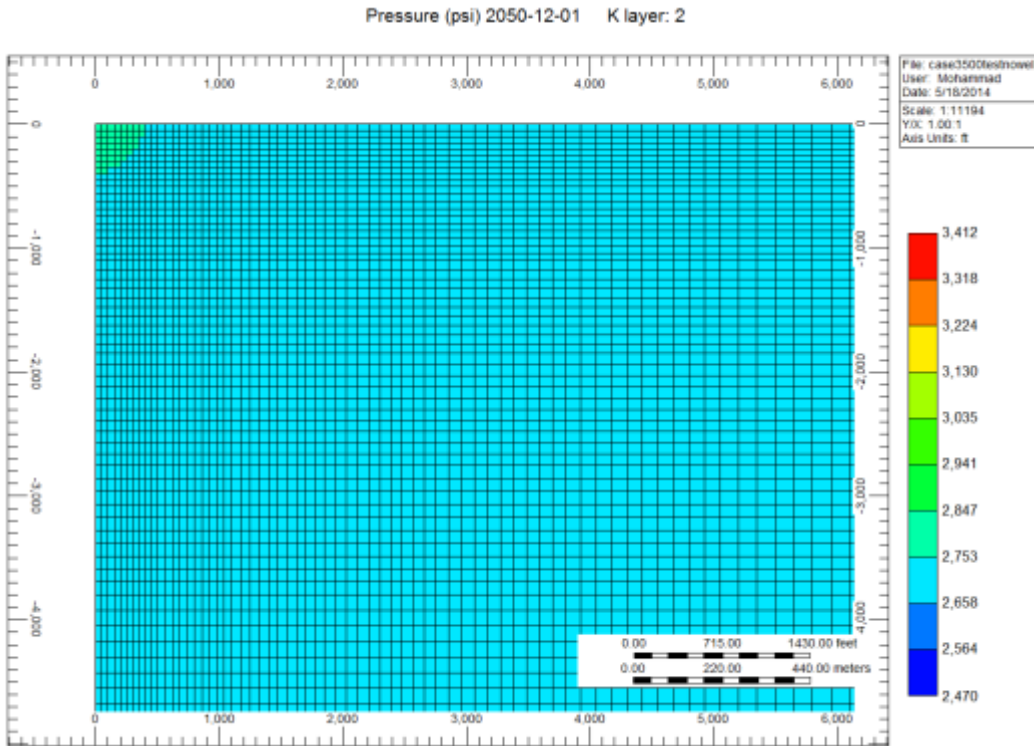


Figure 50 - Gas saturations at the end of 50 years for an injection pressure of 3500 psi without production well

5.21 Summary of results

The optimum conditions for each injection pressure are presented in Table 3. The use of higher injection pressures provided higher injection potential, however, given the reservoir conditions, it is not recommended to exceed 4500 psi injection pressure.

Table 3 – Optimum results for injection pressure used in this study

| Injection Pressure (Downhole) | Distance (Block #) | Distance (Feet) | Avg. Injection Rate (bbl/day) | Avg. Production Rate (bbl/day) |
|-------------------------------|--------------------|-----------------|-------------------------------|--------------------------------|
| 6000 | 42 | 2900 | 5532.0 | 2000 |
| 5500 | 40 | 2700 | 4768.9 | |
| 5000 | 37 | 2435 | 3957.2 | |
| 4500 | 35 | 2255 | 3086.8 | |
| 4000 | 31 | 1900 | 2147.4 | |
| 3500 | 26 | 1515 | 1115.7 | |

6 Conclusions

Based on the results of this study following conclusions are presented:

1. For 3500 psi injection pressure, the produced fluid exceeded the amount of fluid drawn out then the injected volume, lacking utilization of the storage potential.
2. The higher pressures may have a higher risk, even though the model didn't exhibit any signs of intrusion for the cases studied.
3. It is recommended to store CO₂ with 4000 – 4500 psi injection pressure range for optimum storage and production conditions.
4. The method presented in this study can be applied to perform high level assessment of CO₂ injection before committing more investment and time.

7 References

Agarwal, R. K., & Zhang, Z. (2014). *Optimization of CO₂ Sequestration in Saline Aquifers*. Intech. doi:<http://dx.doi.org/10.5772/57066>

- Anchliya, A. (2009). *Aquifer Management for CO2 Sequestration*. College Station, Texas: Texas A & M University.
- Anchliya, A., Economides, C. A., & Jafarpour, B. (2012). Aquifer Management To Accelerate CO2 Dissolution and Trapping. *Society of Petroleum Engineers Journal*, 805-816.
doi:<http://dx.doi.org/10.2118/126688-PA>
- Bachu, S. (2003). Screening and ranking of sedimentary basins for sequestration of CO2 in geological media in response to climate change. *Environmental Geology*, 277-289.
- Bakker, R. J. (2003). Computer programs for analysis of fluid inclusion data and for modelling bulk fluid properties. *Chemical Geology*, 3-23. doi:10.1016/S0009-2541(02)00268-1
- Baklid, A. K. (1996). Sleipner Vest CO2 Disposal, CO2 Injection into a Shallow Underground Aquifer. *SPE Annual Technical Conference and Exhibition*. Denver, Colorado: Society of Petroleum Engineers. doi:DOI: 10.2118/36600-MS
- Barnes, D. A., & Bacon, D. H. (2008). Geological Carbon Storage in the Cambrian Mt Simon Sandstone. *American Association of Petroleum Geologists*.
- Bennet, J. (n.d.). *Ocean Acidification*. Retrieved July 19, 2015, from <http://ocean.si.edu/ocean-acidification>
- Bethke, C. M. (1996). *Geochemical Reaction Modeling*. New York, NY: Oxford University Press.
- Burton, M. K. (2008). Time-Dependent Injectivity During CO2 Storage in Aquifers. *SPE/DOE Improved Oil*. Tulsa, Oklahoma: Society of Petroleum Engineers.
doi:<http://dx.doi.org/10.2118/113937-MS>
- Cihan, A., Birkholzer, J. T., & Zhou, Q. (2013). Pressure buildup and brine migration during CO2 storage in multilayered aquifers. *Groundwater*, 252 - 267. Retrieved from <http://www.ncbi.nlm.nih.gov/pubmed/22880722>
- Clean Air Task Force. (2010). *Death and Disease from Power Plants*. Retrieved from Clean Air Task Force Web site: http://www.catf.us/fossil/problems/power_plants/
- CMG (Computer Modelling Group). (2011). GEM Advanced Compositional and GHG Reservoir Simulator, User's Guide. Calgary, Alberta, Canada.
- D. S. Arndt, M. O. (2010, July). State of the Climate in 2009. *Bull. Amer. Meteor. Soc.*, 91(7), s1-s222.
doi:<http://dx.doi.org/10.1175/BAMS-91-7-StateoftheClimate>
- Delany, J., & Lundeen, S. (1991). *The LLNL thermochemical data base*. Livermore, CA: Lawrence Livermore National Lab., U.S. Department of Energy. Retrieved from <http://www.osti.gov/scitech/biblio/138193>

- Dustin Crandall, U., Neal Sams, U., & John Landis, O. (2011, July 13). CMG Data. *DOE R & D*. Morgantown, WV, USA: DOE NETL.
- Dustin Crandall, U., Neal Sams, U., & John Landis, O. (2011, July 13). CMG Notes. *DOE R & D*. Morgantown, WV, USA: DOE NETL.
- Dustin Crandall, U., Neal Sams, U., & John Landis, O. (2011, July 13). CMG Presentation and Notes. *DOE Presentations*. Morgantown, WV, USA: DOE NETL.
- Economides, M. a.-E. (2009). Sequestering Carbon Dioxide in Closed Underground Volume. *SPE Annual Technical Conference and Exhibition*. New Orleans: Society of Petroleum Engineers. doi:<http://dx.doi.org/10.2118/124430-MS>
- Environmental Protection Agency. (2011). *Greenhouse Gas Reporting Program 2011: reported Data*. Washington, DC: Office of Atmospheric Programs (MC-6207A) - U.S. Environmental Protection Agency. Retrieved from <https://www.epa.gov/ghgreporting/ghgrp-2011-reported-data>
- Environmental Protection Agency. (2015, July). *Climate Change*. Retrieved July 2015, from <http://www.epa.gov/climatechange/ccs/index.html>
- FutureGen Alliance. (2011, February 24). FutureGen 2.0 Project. *FutureGen 2.0*, 1-3.
- Garcia, J. E. (2001). *Density of Aqueous Solutions of CO₂*. Berkeley, CA: Lawrence Berkeley National Laboratory. Retrieved from <http://escholarship.org/uc/item/6dn022hb#page-1>
- Harvey, A. H. (1996). Semiempirical correlation for Henry's constants over large temperature ranges. *AIChE Journal*, 376-387. doi:10.1002/aic.690420531
- Hosseini, S. A., Mathias, S. A., & Javadpour, F. (2012). Analytical Model for CO₂ Injection into Brine Aquifers-Containing Residual CH₄. *Transport in Porous Media*, 795 - 815. Retrieved from <http://link.springer.com/article/10.1007%2Fs11242-012-0025-x>
- Huttenbach, R. (2009, September 5). *US Power Plant Emissions and CO₂ Pipelines*. Retrieved from A Response to Climate Change: http://petrolog.typepad.com/climate_change/2009/09/us-power-plant-emissions-and-co2-pipelines.html
- International Energy Agency. (2010). *2nd CO₂ Geological Storage Modeling Network Meeting*. Salt Lake City, UT: International Energy Agency Greenhouse Gas R&D.
- IPCC. (2013, June 7). *Fifth Assessment Report (AR5): Climate Change 2013 - The Physical Science Basis*. New York: Intergovernmental Panel on Climate Change; Cambridge University Press. Retrieved from Intergovernmental Panel on Climate Change (IPCC): <http://www.ipcc.ch/index.htm>

- Izpec, O. D. (2006). Experimental and Numerical Modeling of Direct Injection of CO₂ Into Carbonate Formations. *SPE Annual Technical Conference and Exhibition*. San Antonio, Texas: Society of Petroleum Engineers. doi:<http://dx.doi.org/10.2118/100809-MS>
- Joshi, A. (2014, 9 2). Investigation of Multiple Well Injections for Carbon Dioxide Sequestration in Aquifers. *Master's Thesis*. Waterloo, Canada: University of Waterloo. Retrieved from <https://uwspace.uwaterloo.ca/handle/10012/8754>
- Kharaka, Y. K., Gunter, W. D., Aggarwal, P. K., Perkins, E. H., & DeBraal, J. D. (1988). *A Computer Program for Geochemical Modeling of Water-Rock Interactions*. U.S. Department of Interior. Menlo Park, California: U.S. Geological Survey. Retrieved from <http://pubs.usgs.gov/wri/1988/4227/report.pdf>
- Khatib, Z., & Verbeek, P. (2002). Water to Value - Produced Water Management for Sustainable Field Development of Mature and Green Fields. *SPE International Conference on Health, Safety and Environment in Oil and Gas Exploration and Production*. Kuala Lumpur, Malaysia: Society of Petroleum Engineers. doi:<http://dx.doi.org/10.2118/73853-MS>
- Kumar, A. (2004). *A Simulation Study of Carbon Sequestration in Deep Saline Aquifers'*. Austin, TX: The University of Texas at Austin.
- Lam, N. (2010). *The Impact of Formation Characteristics on CO₂ Sequestration Into An Aquifer*. Morgantown, WV, USA: West Virginia University.
- M.J. Economides, U. o.-E. (2009). Sequestering Carbon Dioxide in a Closed Underground Volume. *SPE Annual Technical Conference and Exhibition*. New Orleans, LA: Society of Petroleum Engineers.
- McPerson, B. J., & Lichtner, P. C. (2001). CO₂ Sequestration in Deep Aquifers. *First National Conference on Carbon Sequestration*. Washington, DC: National Energy Technology Laboratory.
- Moreno, D. A. (2013). *Comprehensive Analysis of an Ongoing CO₂ Storage Project*. Morgantown, WV, USA: West Virginia University.
- National Energy Technology Laboratory, Department of Energy. (2015). *Carbon Storage Atlas*. Washington, DC: Department of Energy.
- National Energy Technology Laboratory, U.S. Dept of Energy. (2008). *Study of the use of saline formation for combined thermoelectric power plant water*. Albuquerque, NM: National Energy Technology Laboratory, U.S. Dept of Energy.

- Nghiêm L., S. P. (2004). Modeling CO₂ Storage in Aquifers with a Fully-Coupled Geochemical EOS Compositional Simulator. *SPE/DOE Symposium on Improved Oil Recovery*. Tulsa, Oklahoma: Society of Petroleum Engineers. doi:<http://dx.doi.org/10.2118/89474-MS>
- Nghiêm, L. S. (2009). Simulation of Trapping Processes for CO₂ Storage in Saline Aquifers. *Canadian International Petroleum Conference*. Calgary, Alberta : Petroleum Society of Canada. doi:10.2118/2009-156
- Nghiêm, L. X., Shrivastava, V. K., Tran, D., Kohse, B. F., Hassam, M. S., & Yang, C. (2009). Simulation of CO₂ Storage in Saline Aquifers. *SPE/EAGE Reservoir Characterization and Simulation Conference*. Abu Dhabi, UAE : Society of Petroleum Engineers. doi:10.2118/125848-MS
- NOAA. (2015). *Cooperative Air Sampling Network*. Retrieved July 19, 2015, from <http://www.esrl.noaa.gov/gmd/ccgg/flask.php?active=on>
- Noh, M. H., Lake, L. W., Bryant, S. L., & Araque-Martinez, A. N. (2007). Implications of Coupling Fractional Flow and Geochemistry for CO₂ Injection in Aquifers. *Society of Petroleum Engineers*, 406-414. doi:<http://dx.doi.org/10.2118/89341-PA>
- Office Fossil Energy, Dept of Energy. (n.d.). Retrieved from http://www.cslforum.org/publications/documents/Melbourne/benson_sally_wed_Pal_AB_0915.pdf
- Orr, F. (2004). Storage of Carbon Dioxide in Geologic Formations. *Journal of Petroleum Technology*, 90-97.
- Oruganti, Y., & Bryant, S. L. (2008). Pressure Build-Up During CO₂ Storage in Partially Confined Aquifers. *9th International Conference on Greenhouse Gas Control Technologies (GHGT-9)* (pp. 3315-3322). Washington, DC: Greenhouse Gas Control Technologies. doi:10.1016/j.egypro.2009.02.118
- Peng, D.-Y., & Robinson, D. B. (1976). A New Two-Constant Equation of State. *Industrial & Engineering Chemistry Fundamentals*, 59-64. doi:10.1021/i160057a011
- Pitzer, K. S. (1987). A thermodynamic model for aqueous solutions of liquid-like density. *Reviews in Mineralogy and Geochemistry*, 97-142.
- Ruiz, J. H. (2005). *An Advanced Vapor-Compression Desalination System*. College Station, Texas: Texas A&M University.

- Sengul, M. (2006). CO2 Sequestration - A Safe Transition Technology. *SPE International Health, Safety & Environment Conference*. Abu Dhabi, UAE: Society of Petroleum Engineers. Retrieved from <https://www.onepetro.org/conference-paper/SPE-98617-MS>
- Shen, C.-H., Nghiem, L., Chen, T.-L., & Hsieh, B.-Z. (2015). Plume Migration of Different Carbon Dioxide Phases During Geological Storage in Deep Saline Aquifers. *Terrestrial Atmospheric and Oceanic Sciences*, 375-386. doi:10.3319/TAO.2015.01.05.02
- Stenhouse, N., Maibach, E., Cobb, S., Ban, R., Bleistein, A., Croft, P., . . . Leiserowitz, A. (2014). Meteorologists' Views About Global Warming: A Survey of American Meteorological Society Professional Members. *American Meteorological Society*, 123-125.
- U.S. Department of Energy. (2011). Resource Assessment Team Goals. *In-House R & D Work Proposal*. Morgantown, West Virginia, USA: NETL.
- U.S. Geological Survey. (2009, February 09). *Ground Water Atlas of the United States*. Retrieved from USGS Products: http://pubs.usgs.gov/ha/ha730/ch_a/A-text4.html
- Van der Meer, L., & Diederik van Wees, J. (2006). Limitations to Storage Pressure in Finite Saline Aquifers and the Effect of CO2 Solubility on Storage Pressure. *SPE Annual Technical Conference and Exhibition*. San Antonio: Society of Petroleum Engineers. doi:10.2118/103342-MS
- van Engelenburg, B. a. (1993). Disposal of Carbon Dioxide in Permeable Underground Layers: A Feasible Option? *Climatic Change*, 55-69.
- Wisconsin Public Service Commission. (2015). *Environmental Impacts of Power Plants*. Madison, Wisconsin: Wisconsin Public Service Commission. Retrieved from <https://psc.wi.gov/thelibrary/publications/electric/electric15.pdf>
- Xu, T., Apps, J. A., & Pruess, K. (2003). Numerical simulation of CO2 disposal by mineral trapping in deep aquifers. (Y. Kharaka, Ed.) *Elsevier - Applied Geochemistry*, 917-936. Retrieved from http://webpages.fc.ul.pt/~fbarriga/ZeroEm/Bibliografia_files/Xu+al_2004_ApplGeochem.pdf